2013-10-03

Melt-freeze crust formation and evolution in the Columbia Mountains

Buhler, Ryan

UNIVERSITY OF CALGARY

Melt-freeze crust formation and evolution in the Columbia Mountains

by

Ryan Buhler

A THESIS SUBMITTED TO THE FACULTY OF GRADUATE STUDIES IN PARTIAL FULFILLMENT OF THE REQUIREMENTS FOR THE DEGREE OF MASTER OF SCIENCE

DEPARTMENT OF CIVIL ENGINEERING

CALGARY, ALBERTA

SEPTEMBER, 2013

ABSTRACT

Melt-freeze crusts play an important role in many slab avalanches. Recent work with snowpack models has shown the need for field based research on the formation and evolution of melt-freeze crusts. This project uses historical weather and snowpack data to determine the metrological conditions during crust formation and the resulting crust properties. In addition, field measurements of the evolution of buried melt-freeze crusts were collected over the winters of 2010-11 and 2011-12. Measured properties include density, shear strength, and thin-blade resistance. A thermal imager was used to track changes to small scale temperature gradients around crusts. A new set of crust indices were developed as a simple method for tracking changes to crust internal lamination and the bonding to adjacent layers. These measurements and indices can supplement the data used for avalanche forecasting and be used to improve and validate snowpack evolution models.

ACKNOWLEDGEMENTS

I would like to thank Dr. Bruce Jamieson who made this research possible. He has been an amazing mentor, teacher, and supervisor. He has increased my knowledge of snow, avalanches, and melt-freeze crusts to a level I could not have imagined. I am sincerely grateful for his motivation and assistance in making the completion of this project possible.

I would like to thank Dr. Sascha Bellaire for assistance in the development of this project. His ideas, feedback, and technical assistance were crucial to the establishment of the methods and the technical analysis for this project.

The constant discussion of ideas, methods, and literature amongst ASARC students is what makes this program special. I would like to thank all the ASARC students, staff, and alumni for their constant support and willingness to help me throughout this project. Scott Thumlert, Dave Tracz, Katherine Johnson, Mike Smith, Mike Conlan, Simon Horton, Alex Sinikas, Cam Ross, Thomas Exner, Shane Haliduk, Dr. Cora Shea, and Dr. Michael Schirmer – I am forever grateful.

I would like to thank everyone who made the collection of field data possible. This includes everyone mentioned above, our field technicians, Mike Wheater and Michael Shynkaryk, and all of the staff of our host organizations, Glacier National Park Avalanche Control Section and Mike Wiegele Helicopter Skiing.

For financial support of the ASARC program, I would like to thank the National Science and Research Council of Canada (NSERC), Helicat Canada, Canadian Avalanche Association, Canadian Avalanche Centre, Parks Canada, Mike Wiegele Helicopter Skiing, Canada West Ski Area Association, Association of Canadian Mountain Guides, Backcountry Lodges of British Columbia Association, Canadian Ski Guide Association, and Teck Coal.

Finally, I would like to thank my family - Ethel McCracken, Linda and Alan Chell, Art Buhler, and Kyle Buhler - for their financial and moral support during this project.

TABLE OF CONTENTS

LIST OF TABLES

LIST OF FIGURES

CHAPTER 1: INTRODUCTION

Snow avalanches can affect people and property living in mountainous areas. Avalanches cause disruptions to transportation networks, damage or destroy infrastructure, and cause human fatalities. In Canada, avalanches are estimated to cost ten million dollars per year in impacts and an additional ten million dollars per year on avalanche control (Jamieson and Stethem, 2002). Between 1978 and 2007, an average of 10.2 fatalities occurred per year in Canada (Campbell et al., 2007). The majority of avalanches affecting infrastructure and causing fatalities are slab avalanches. These slab avalanches typically release on critical avalanche layers within the snowpack. A common critical avalanche layer is a melt-freeze crust. In the Columbia Mountains of British Columbia, Canada, about 32% of slab avalanches occur at a melt-freeze crust interface or within a melt-freeze crust (Hagaeli and McClung, 2003).

Recent work with snowpack models has shown the need for field based research on the formation and evolution of melt-freeze crusts (Smith, 2009; Bellaire and Jamieson, 2013). Field-based data on the formation and evolution of melt-freeze crusts may be used to improve snowpack evolution models. Recently the Swiss SNOWPACK model (Bartelt and Lehning, 2002; Lehning et al., 2002 a,b) was adapted for the Columbia Mountains with the purpose of increasing the data available to avalanche forecasters in data-sparse areas. The initial work with this model was able to successfully model the existence of 65% to 77% of crusts depending on aspect (Bellaire and Jamieson, 2013). While these numbers are good for research, they would not be considered adequate for applied use by an avalanche forecaster. Therefore, further work is required to improve and validate crust formation and evolution for snowpack models in the Columbia Mountains.

1.1 Avalanche characteristics

A snow avalanche is defined as a mass of snow of at least several cubic meters moving down slope at visible speed (Jamieson, 2001). An avalanche path typically consists of three parts (Figure 1.1): the start zone, the track, and the run-out zone. This project primarily focuses on conditions in the start zone where slab avalanches typically form. There are several important

terrain characteristics of avalanche start zones that determine the snowpack properties and resulting avalanche frequency including the following (from McClung and Schaerer, 2006):

- Slope angle
- Orientation to wind
- Orientation to sun
- Forest cover
- Ground surface
- Slope dimensions
- Shape of slope
- Elevation
- Aspect

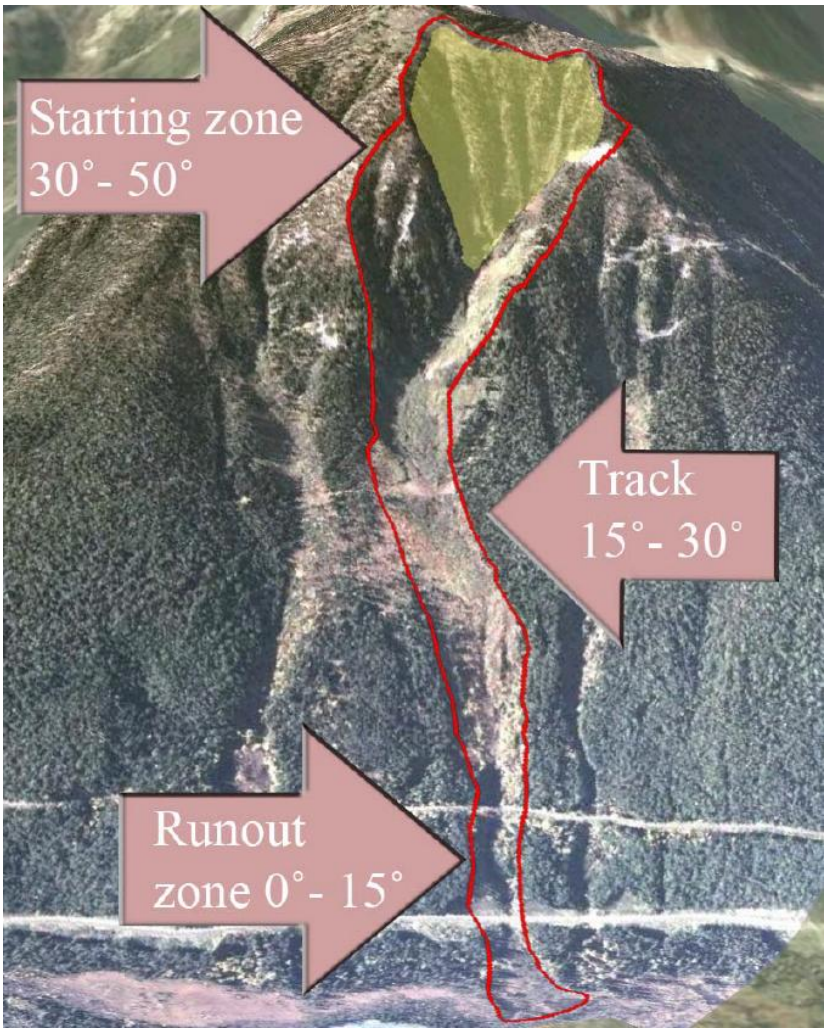

***Figure 1.1**: An example of an avalanche path showing the start zone, the track, the run-out zone, and the typical slope angles of each (from Delparte, 2008).*

The two primary types of avalanches are loose snow avalanches and slab avalanches (Figure 1.2). Loose snow avalanches occur when snow with low cohesion releases from a point and entrains snow as it moves downhill (McClung and Schaerer, 2006). Dry loose snow avalanches (also commonly referred to as *sluffing*) are typically small and start on steep slopes or cliffs. Wet loose snow avalanches can be much larger and can travel farther into the run out zone than the same mass of dry snow (McClung and Schaerer, 2006). Loose snow avalanches are generally easier to predict and account for far fewer impacts and fatalities when compared with slab avalanches. 95% of fatal avalanche accidents in Canada between 1984 and 1996 (n = 94) were due to slab avalanches (Jamieson and Geldsetzer, 1996). This project focuses on slab avalanches.

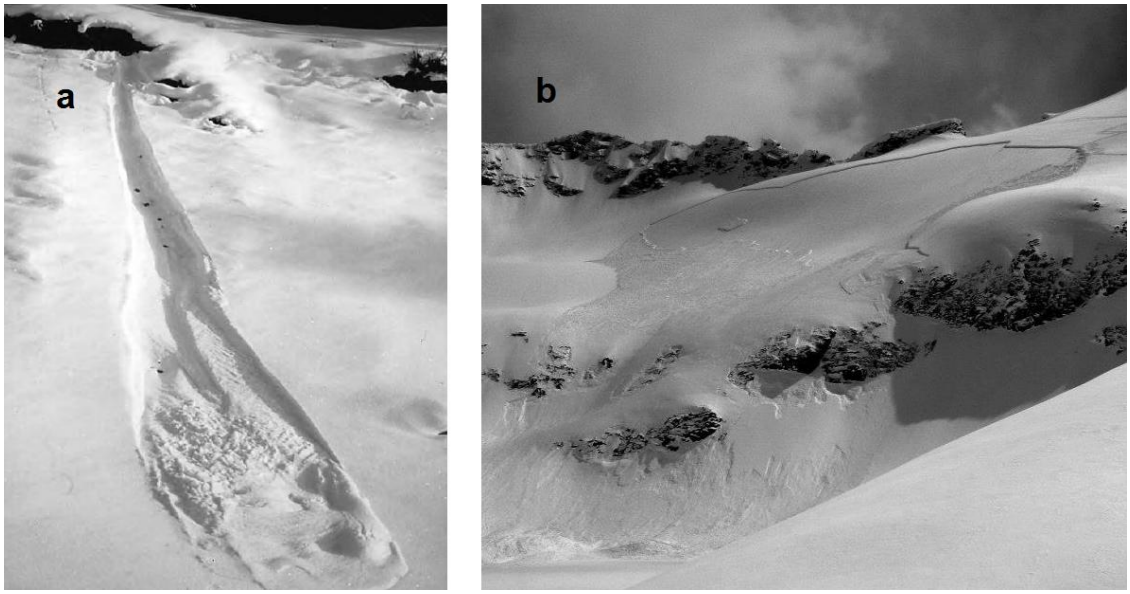

Figure 1.2*: Example of a loose snow avalanche (a) and a slab avalanche (b). Photos: B. Jamieson (a) and C.J. Wright (b).*

1.2 Slab avalanche release

Slab avalanches occur when a cohesive slab of snow overlying a weak layer releases (Figure 1.3). In order for a slab avalanche to release, a failure must initiate in the weak layer and the failure must propagate outward within this layer (Schweizer et al., 2003). The basic principal of initiation is that stress intensity on the weak layer exceeds its fracture toughness or the strain

rate exceeds a critical value. Fracture toughness is a measure of the layer's resistance to fracture propagation. This can occur by localized dynamic loading or by spontaneous natural release. Localized dynamic loading includes any point load applied to the slab that causes additional stress on the weak layer. This includes humans, explosives, cornice falls, large snowballs releasing from trees, etc. Spontaneous release typically occurs due to warming of the slab, slow loading by snowfall or wind, or, perhaps, by rapid cooling. These slow changes to the slab properties are believed to cause a ductile failure in the deficit zone of a weak layer (e.g. Schweizer et al., 2003). The deficit zone, sometimes called a super-weak zone, is a small area within a weak layer where the layer does not support the weight of the overlying slab in shear. If this ductile failure is large enough, it progresses to a brittle fracture in the same manner as localized dynamic loading.

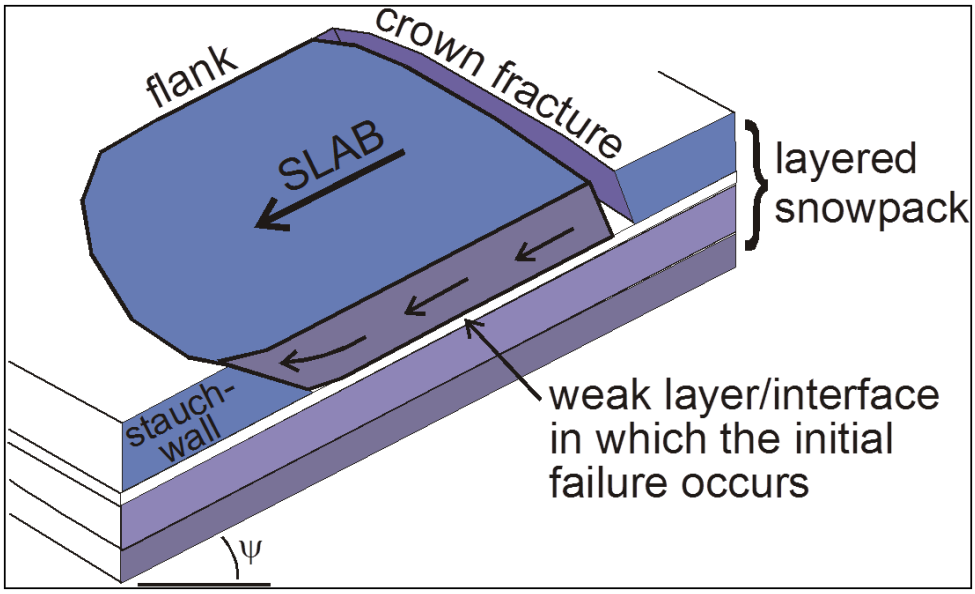

***Figure 1.3**: Diagram of slab avalanche release showing important terminology (Image: B. Jamieson)*

Failure initiation is the first step towards slab avalanche release, but alone does not cause slab avalanches. Small, localized initiations are constantly occurring as people travel over snow and apply additional stress. In order for slab avalanche release to occur, the initiated failure in the weak layer must propagate far enough for the slab to become unsupported. Provided this initiation and propagation occurs on a sufficiently steep slope, tensile failure at the crown and

shear failure along the slab edges will occur and the slab will release. Propagation of the failure occurs when the energy released by the failure exceeds the fracture toughness of the weak layer. As long as the energy being released by the fracture exceeds the fracture resistance, the failure will continue to propagate. The distribution of fracture toughness within a weak layer, along with the properties of the overlying slab and terrain characteristics, will determine the size of the avalanche that is able to release.

1.3 Persistent weak layers and critical avalanche layers

The initiation and propagation of fractures described above typically occurs on a thin layer of snow in the snowpack that is weaker in strength that the surrounding snow. The two primary types of weak layers are persistent and non-persistent weak layers. Non-persistent weak layers generally exist in the upper snowpack and generally have a short life, typically less than one week. These are often interfaces between two layers where a difference in grain size or density between the layers causes a weakness. Non-persistent weak layers often result in storm slab avalanches which are typically shallow and less challenging to forecast. As the properties of the adjacent layers change over time, the weak layer and adjacent layers become more similar and the strength of the interface bonding increases.

Persistent weak layers are layers made up of unique grain types that are more resistant to change and cause greater instability within the snowpack. These grain types include surface hoar, depth hoar, and facets. These grain types do not always cause instabilities, but generally the larger these grain types get, the more they become a problem for snowpack stability (Schweizer and Jamieson, 2007). Crusts are often grouped in with persistent weak layers because they are often associated with faceting and tend to persist for a long time in the snowpack. A more appropriate term is critical avalanche layer, since crusts can act as an avalanche bed surface (without observations of a persistent weak grain types) due to local stress concentrations at the crust (see Section 1.6.3). Critical avalanche layer is a broad term that includes persistent weak layers, melt-freeze crusts, and other problematic avalanche layers such as wind slabs.

1.4 Surface energy transfer

The formation of melt freeze crusts is dominated by the interaction between the atmosphere and the snow surface. Energy transfer dominates this interaction (Figure 1.4). Crusts form when the surface of the snowpack melts and then subsequently refreezes. Melting of the snow surface can be caused by solar radiation, rainfall, warm air, or a combination of the above.

A simplified model of surface energy transfer can be created using the conservation of energy. Net energy flux to the snow surface, Q_N, is defined as (Marshall, 2012):

$$Q_N = Q_S^{\downarrow} - Q_S^{\uparrow} + Q_L^{\downarrow} - Q_L^{\uparrow} + Q_G + Q_H + Q_E + Q_P - Q_R \qquad (1)$$

where $(Q_S^{\downarrow} - Q_S^{\uparrow})$ is the net short-wave radiation, $(Q_L^{\downarrow} - Q_L^{\uparrow})$ is the net long-wave radiation, Q_G is the sub-surface energy flux associated with radiative transfer and heat conduction in the snow, Q_H is the sensible heat flux, Q_E is the latent heat flux, Q_P is sensible heat from precipitation, and Q_R is the sensible heat from run-off. There are many variations on this equation based on the application.

1.4.1 Short-wave radiation

The sun releases energy in the form of short-wave radiation. Short-wave radiation energy exists between 0.2 and 2.5 μm on the energy wavelength spectrum (Marshall, 2012). This energy is a driving force for snow surface melting. The amount of energy released by the sun is relatively constant at 1366 W m^{-2}, but the amount of energy reaching the earth's surface varies substantially (Marshall, 2012). This is influenced by atmospheric conditions including cloud cover, duration of daylight, and solar elevation angle. The amount of available incoming shortwave radiation at any point in time is called the solar insolation and is a function of solar elevation angle and the duration of daylight (Stull, 2000).

The amount of short-wave radiation absorbed by the snowpack is a function of the incoming short-wave radiation and the albedo of the snow surface. The albedo is the coefficient of reflectance of a material measured as the ratio of reflected short-wave energy to incoming short-wave radiation (Ahrens, 2009). New snow has a relatively high albedo with values

ranging from 0.75 to 0.95 whereas old snow has values ranging from 0.35 to 0.70 (Stull, 2000). This means new snow requires more solar input energy to cause melting.

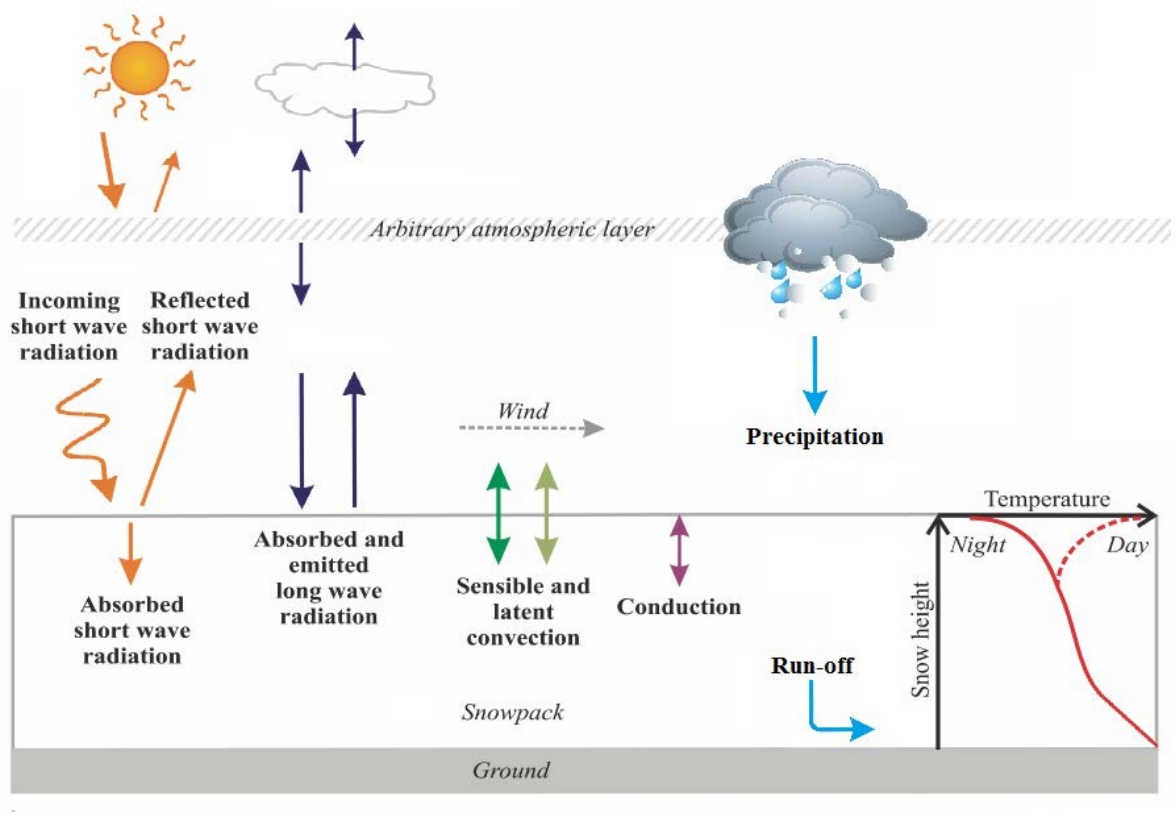

***Figure 1.4**: Surface energy transfer diagram showing dominate processes (modified from Bakermans, 2006).*

1.4.2 Long-wave radiation

All objects including clouds, trees, snow cover, and the earth's surface emit long-wave radiation energy which is also referred to as infrared radiation, thermal radiation, or terrestrial radiation. Long-wave radiation energy exists in the range of 3 to 100 µm in the wavelength spectrum (Marshall, 2012).

The net balance of incoming and outgoing long-wave radiation determines by the amount of long-wave radiation entering or leaving the snowpack. When the sky is clear, the net long-wave radiation is outgoing. This is the dominate process in cooling the snow surface, especially on clear nights. Cloud cover increases the incoming long-wave radiation, reducing the net

outgoing long-wave radiation, thus reducing cooling at the snow surface. Emissivity is the ratio of outgoing or reflected long-wave radiation to the incoming long-wave radiation (Marshall, 2012). New snow has a typical emissivity of 0.99 and old snow has a typical emissivity of 0.82 (Stull, 2000).

Outgoing long-wave radiation has a direct relationship with surface temperature based on the Stefan-Boltzmann equation:

$$Q_{LW\uparrow} = \sigma T^4 \qquad (2)$$

where $Q_{LW\uparrow}$ is the net outgoing long-wave radiation (W m^{-2}), σ is the Stefan-Boltzmann constant of 5.67 x 10^{-8} W m^{-2} K^4 and T is the temperature in Kelvins.

1.4.3 Convective and latent heat transfer

Convective heat transfer, or convection, at the snow surface can result in melting and the formation of temperature crusts. Convective heat transfer at the surface includes both sensible and latent heat transfer. Sensible heat is the heat energy associated with a change in temperature of a material and latent heat is the heat energy associated with the phase change of a material. Wind is the driving force behind convection at the snow surface. Sensible heat transfer results from differences between air temperature and the snow surface temperature.

Latent heat is the energy associated with phase change. This includes melting, freezing, condensation, sublimation, and vapour to solid deposition. The latent heat transfer associated with convective heat transfer at the snow surface includes melting, condensation, sublimation, and deposition. Other forms of latent heat transfer are important to crust formation and evolution for several reasons. Rainfall directly adds substantial latent heat to the snowpack. Melting of the snow surface by rain, solar radiation, or convective heat transfer means the snowpack is gaining latent heat energy and must release this energy in order to refreeze. This latent heat release during refreezing can cause strong localized temperature gradients and it the primary cause of dry-on-wet faceting. Near crust faceting is associated with the latent heat exchange of water vapour at crust boundaries.

1.4.4 Conduction

Conduction at the snow surface occurs by diffusion which is relatively minimal and is often omitted from surface energy balance for simplicity. Conduction plays a more active role within the snowpack (Section 1.6.1).

1.5 Crust formation in the Columbia Mountains

The previous section describes the main processes responsible for melting and refreezing of the snow surface. The study area for this project is the Columbia Mountains (see Section 3.1) and this section describes the general conditions for crust formation in this area.

Spatial variation across terrain plays an important role in crust formation. Table 1 shows the major terrain influences for each type of crust formation in the Columbia Mountains. Sun crusts are most likely to form in March and April but have the potential to form at any point during the winter (Jamieson, 2004a). The reliance of sun crust formation on aspect and slope incline means that early in the season, a sun crust may form on steep slopes only. Later in the spring, similar conditions may result in more widespread sun crust formation.

***Table 1.1**: Terrain effects and timing for wet layers in the Columbia Mountains (modified from Jamieson, 2004a)*

Cause	Major terrain effects			Most likely formation period
	Aspect	Elevation	Incline	
Rain	(windward)	Yes	Yes	Nov., March, April
Warm air (convection)		Yes		March, April
Sun	Yes		Yes	Feb, March, April
All	Yes	Yes	Yes	Less frequent in Dec., Jan.

Rain crust formation is most likely in the early winter and the spring, but rain is possible during all periods of the winter (Jamieson, 2004a). Rain crust formation is very dependent on elevation, but also on inclines because liquid precipitation penetrates less on steep slopes

compared to flat or gentle slopes (Wankiewicz, 1979). While rain crusts are generally expected to form across all aspects, wind can affect this formation. Windward slopes will receive more rainfall than leeward slopes. In some cases, if the wind is strong enough, rainfall may not affect steep leeward slopes.

Warm air (convection) is often considered a secondary influence on sun and rain crust formation, but also has the potential to result in temperature crust formation on its own. This is most likely to occur in March and April (Jamieson, 2004a). Elevation is the primary terrain effect for temperature crust formation.

1.6 Melt-freeze crusts in a seasonal snowpack

Melt-freeze crusts play several important roles in the seasonal snowpack. Facet grains often form around or within crusts resulting in persistent weak layers and avalanches. Crusts can also create stress concentrations within the snowpack and are common bed surfaces for avalanches even when facets are not present. When crusts are well bonded they can have the opposite effect, bridging stresses that would otherwise reach deeper into the snowpack.

1.6.1 Heat flow and vapour movement in the snowpack

Temperature gradients within the snowpack drive heat flow, vapour movement, and snow metamorphism. Because the ground is roughly 0 °C in a deep snowpack (> 1 m) and the snow surface temperature in the winter months is generally below 0 °C, heat typically flows up through the snowpack. Heat flows partly by vapour through the pore spaces, partly by grain-to-grain sublimation through the pore spaces, and partly by conduction through the ice structure (Colbeck, 1983). Water vapour in the snowpack is near saturation or super-saturated and the movement of this water vapour is responsible for snow metamorphism.

New snow first undergoes a reduction of surface-to-volume ratio. The branches or arms of precipitation particles (new snowflakes) detach or shrink. Due to differences in saturation vapour pressure, there is a net loss of mass from convex surfaces and net deposition at concave surfaces. Following this initial surface-to-volume reduction, snow metamorphism can be

divided into two broad categories based on the rate of change: equilibrium metamorphism (rounding) and kinetic growth (faceting). The common way to distinguish the two processes is using bulk temperature gradients. The rough threshold for kinetic growth is 10 °C m^{-1} when measured over 10 cm (McClung and Schaerer, 2006).

Equilibrium metamorphism involves preferential deposition of water vapour at concavities which results in the growth of blob-shaped spherical grains and the growth of bonds between grains. This is a slow process and is associated with the increasing strength and stability of the snowpack.

Kinetic growth is a much faster process and is driven by a strong vapour pressure gradient. Water vapour is deposited at the coolest part of the snow grain, which is usually the bottom, and does not preferentially deposit at the bonds between grains. The resulting grains become more angular with sharp corners and flat faces. This process typically results in weakening of the snow structure and therefore decreasing snowpack stability, but can also result in stable or increasing snowpack stability.

1.6.2 Faceting of melt-freeze crusts

There are three primary ways in which faceting can occur within or adjacent to crusts within the snowpack. They include near crust faceting, dry-on-wet faceting, and near-surface faceting.

Near-crust faceting is caused when dense, less permeable crust layers cause localized changes to the temperature and vapour gradients within the snowpack (Jamieson, 2006). The general theory is that locally strong temperature gradients form around the crust (Figure 1.5) which exceed the small scale threshold for faceting. These gradients cannot be measured using the conventional method of using a thermometer with 10 cm spacing. These locally strong temperature gradients result in kinetic growth around the crust. Impermeable crust layers additionally create a barrier to vapour flow within the snowpack. This results in vapour being deposited at the lower interface resulting in growth and sublimation causing erosion at the upper interface (Greene, 2007). Greene (2007) provides laboratory confirmation of this process.

Dry-on-wet faceting occurs when new dry snow falls onto an unfrozen wet layer of snow (Jamieson, 2004b). The wet layer is typically caused by rain, sleet, or wet snowfall, but could also result from melting by solar radiation or convective heat transfer. As the wet snow layer refreezes, latent heat is released creating a locally strong temperature gradient between the wet snow layer and the new dry snow layer above. This strong, localized temperature gradient drives kinetic growth at the interface and can result in the growth of faceted crystals (Jamieson, 2004b).

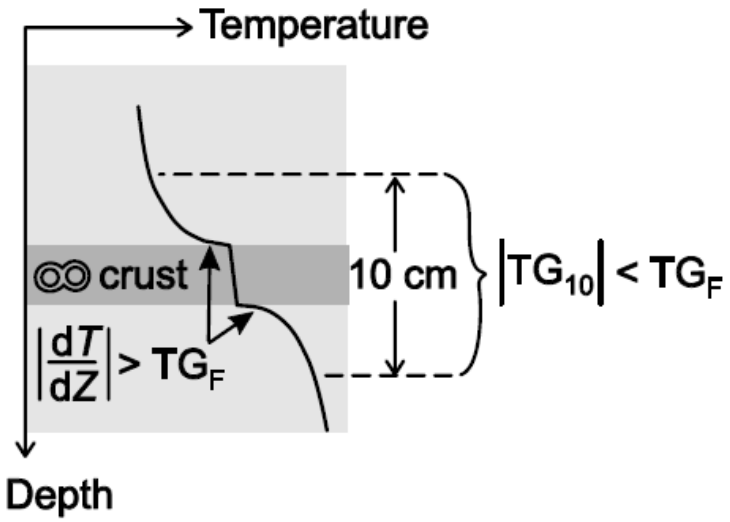

Figure 1.5*: Diagram showing the basic principle of near-crust faceting. Locally strong temperature gradients (dT/dZ) exist around the crust which exceed the threshold gradient for faceting (TG_F), but are not able to be measured using conventional methods (thermometer using 10 cm spacing) (from Jamieson, 2004a; after Colbeck, 1991)*

Near-surface faceting does not require a crust layer, but can result in faceting of a crust layer. Near-surface faceting occurs when strong cooling of the snow surface creates a large temperature gradient with the snow directly below. This typically occurs under clear skies when outgoing long-wave radiation dominates the surface energy balance. The energy balance in the upper snowpack is positive throughout the daytime, gaining heat energy due to solar or atmospheric warming. The energy balance quickly shifts towards outgoing at night and the snow surface can become 5 to 15 °C cooler than the air temperature. This strong temperature

gradient below the snow surface can result in kinetic growth of the snow. This process has the potential to cause faceting of a previously frozen crust or can exaggerate the dry-on-wet faceting process.

1.6.3 Stress concentration around melt-freeze crusts

In addition to the formation of facet crystals which can result in a persistent weak layer, crusts are also common bed surfaces for avalanches. Applied stresses in the snowpack are concentrated at these hard, dense layers which can lead to avalanche release (Schweizer, 1993). This can occur with most types of snow grains that may overlay the crust. For this reason, crusts may be referred to as critical avalanche layers rather than persistent weak layers. A well bonded crust can have the opposite effect, bridging applied stresses that would otherwise reach deeper layers within the snowpack (Camponovo and Schweizer, 1997; Habermann et al., 2008).

1.7 Avalanche forecasting

There are several principles and methods of avalanche forecasting that are discussed throughout this project. This includes snowpack observations, weather observations, and spatial variability. The importance of melt-freeze crusts to avalanche forecasting is also discussed.

1.7.1 Snow profiles

A snow profile is a record of the snowpack properties at a given location focusing on the layered structure of the snowpack. An example of a snow profile completed by University of Calgary observers is attached in Appendix C. The process starts by excavating a snow pit with three vertical walls, often to the ground (Figure 1.6). Because of destructive nature of digging snow profiles, subsequent data must be collected at different locations. This introduces an element of uncertainty associated with spatial variability and establishes the need for study plots. This is discussed further in Section 1.5.4 on spatial variability. Once the snow pit has been dug, a series of data are collected. These are well established methods and are described

in detail in the Canadian Avalanche Association (CAA) Observation Guidelines and Recording Standards for Weather, Snowpack, and Avalanches (OGRS) (CAA, 2007). The first step of the snow profile is to identify the layering of the snowpack. Several methods can be used to identify the layered structure of the snowpack including differences in density or layer hardness, visual differences, and differences in grain structure. Thin, weak layers are also important to identify with the snowpack.

For each layer in the snow profile, the following properties are typically measured:

- Depth of each of the layers from the snow surface or the ground, measured vertically in cm
- Grain type and size: grain type is defined by the *International Classification for Seasonal Snow on the Ground* (Fierz et al., 2009). Table 2 contains the grain types used in this project. Grain size can be defined as a single average value or as a range of values (Fierz et al., 2009). Often when reporting a range, the upper value of the range will be average maximum grain size;
- Hand hardness (HH): a simple test which approximates the snow strength in compression. Various objects of decreasing size are pushed into the snow using roughly 15 N force until the snow breaks (McClung and Schaerer, 2006). Table 3 contains the hand hardness scale;
- Density: typically measured using a sampling tube (typically 100 cm^3) and scale, or using the methods described in Section 3.3.3.2. Recorded in kg m^{-3}; and
- Moisture content: determined by squeezing a sample of snow and by looking at a sample under 10x magnification. Table 4 contains the moisture content classifications.
- A snow profile also includes snow temperature measurements. Snow temperatures are measured with a thermometer at 10 cm vertical spacing. Due to the wide spacing of the temperature measurements with respect to grain structure, the resulting temperature gradients are referred to as bulk temperature gradients in this project. This contrasts to small scale temperature gradients which can be measured using a thermal imager (Section 3.3.3.6). One of the primary uses of bulk temperature measurements is to look for temperature gradients which exceed the threshold for kinetic metamorphism, 10 °C m^{-1} (McClung and Schaerer, 2006).

***Figure 1.6**: Example of a snow profile (photo: B. Jamieson)*

***Table 1.2**: Grain types used in this project. Indentation indicates subclasses of grain types. (after Fierz et al., 2009)*

Grain Type	Code	Symbol
Precipitation particles	PP	+
Decomposing and fragmented precipitation particles	DF	/
Rounded grains	RG	●
Faceted crystals	FC	□
Rounding faceted particles	FCxr	⌂
Surface hoar	SH	V
Melt forms	MF	○
Clustered rounded grains	MFcl	⚇
Rounded polycrystals	MFpc	⚇
Melt-freeze crust	MFcr	⊙⊂

***Table 1.3**: Hand hardness scale (after CAA, 2007)*

Hand test	Term	Code
Fist in glove	Very low	F
Four fingers in glove	Low	4F
One finger in glove	Medium	1F
Blunt end of a pencil	High	P
Knife blade	Very High	K
Too hard to insert knife	Ice	I

***Table 1.4**: Moisture content classifications (after CAA, 2007)*

Classification	Definition	Water content by volume	Code
Dry	Usually the snow temperature is below 0 °C, but dry snow can occur at any temperature up to 0 °C. Disaggregated snow grains have little tendency to adhere to each other when pressed together, as in making a snowball.	0 %	D
Moist	T = 0 °C. Water is not visible even at 10x magnification. When lightly crushed, the snow has a distinct tendency to stick together.	< 3 %	M
Wet	T = 0 °C. Water can be recognized at 10x magnification by its meniscus between adjacent snow grains, but water cannot be pressed out by moderately squeezing the snow in the hands.	3 – 8 %	W
Very Wet	T = 0 °C. Water can be pressed out by moderately squeezing the snow in the hands, but there is an amount of air confined within the pores.	8 – 15 %	V
Slush	T = 0 °C. The snow is flooded with water and contains a relatively small amount of air.	> 15 %	S

1.7.1 Snowpack Tests

There are numerous snowpack tests which can be used by avalanche forecasting to assess snowpack stability. Two of these tests, the compression test and the propagation saw test, were used in this project.

The compression test is a test of failure initiation of weak layers in the snowpack. It is a good test for identifying potential weak layers in the snowpack. A column of snow measuring 30 cm wide x 30 cm wide x 120 cm high is isolated (CAA, 2007). A shovel is placed on the top of the column and is progressively loaded. This loading starts with ten light taps from the wrist, followed by ten moderate taps from the elbow, and finally ten hard taps from the shoulder. The number of taps resulting in a fracture is recorded along with the depth, failure plane grain type/size, and character of the fracture (CAA, 2007). The fracture character is a classification describing how the fracture fails once initiated and provides information about the potential for large-scale propagation of the fracture (van Herwijnen and Jamieson, 2007). Table 1.5 contains the fracture character classifications.

The propagation saw test is used to assess the propagation propensity of a specific weak layer and the overlying slab (Gauthier, 2007). Unlike the compression test, the propagation saw test does not test the likeihood of fracture initiation. It is, however, considered a better predictor of propagation propensity than observing fracture character in the compression test. A block of snow 30 cm wide by 100 cm long by the weak layer depth is isolated (Figure 1.7.a). If the weak layer is deeper than 100 cm, than the column length should equal the weak layer depth. The blunt edge of a snow saw (3 mm thick) is run along the weak layer until a fracture occurs (Figure 1.7.c). The resulting type of fracture arrest (Figure 1.7.b) is recorded along with the cut length and total length of the block.

***Table 1.5**: Fracture character classifications (after CAA, 2007)*

Fracture character	Definition	Code
Progressive compression	Fracture usually crosses the column with single loading step, followed by gradual compression of the layer with subsequent loading steps.	PC
Resistant planar	Fracture requires more than one loading step to cross the column and/or the block does not slide easily on the weak layer.	RP
Sudden planar	Fracture suddenly crosses column in one loading step and the block slides easily on the weak layer.	SP
Sudden collapse	Fracture crosses the column with a single loading step and is associated with noticeable vertical displacement.	SC
Non-planar break	Irregular fracture	B
No fracture	No fracture	NF

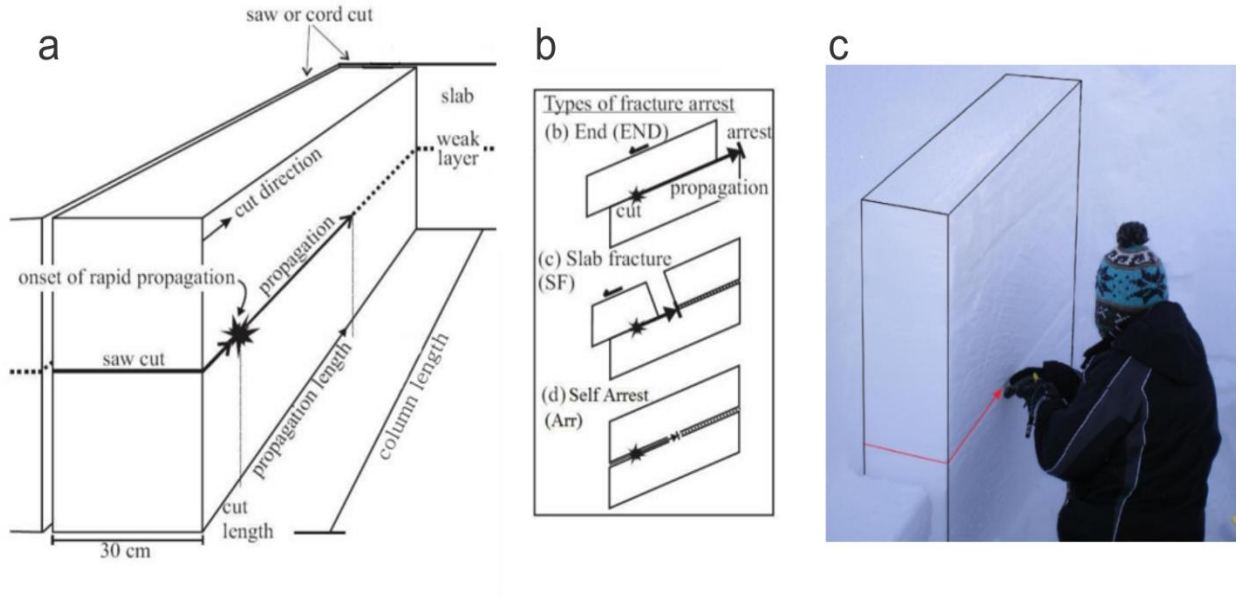

***Figure 1.7**: Diagram of the propagation saw test (a), propagation saw test fracture arrest types (b), and an example of cutting the propagation saw test (c) (after Gauthier, 2007; Ross, 2010).*

1.7.2 Weather observations

Avalanche forecasting involves collecting various manual and automatic weather data. Manual weather observations are made at regular intervals at a weather plot. Manual weather observations are also made during field work or travel through terrain. This includes observations prior to a snow profile observation and observations of changing or unexpected weather conditions in the field. These manual weather observations may include any or all of the following: sky cover, precipitation type and intensity, air temperature, relative humidity, snow temperatures, depth of snowfall, total snowpack depth, density of new snow, surface penetrability, grain form/size of surface snow, wind rate and intensity, and blowing snow (CAA, 2007). Sky cover is a classification based on the percentage of cloud cover as estimated by the observer. It is discussed throughout this project and the sky cover classifications are shown in Table 1.6.

The use of automated weather stations has become standard for avalanche forecasting operations. Larger operations will run their own weather station, whereas smaller operations rely on sources such as the network of weather stations used by provincial highway maintenance operations. These weather stations typically record air temperature, precipitation and snowfall amounts, relative humidity, wind speed and direction, and barometric pressure. Most of the weather stations operated for avalanche forecasting use remote telemetry to view data in real time and look at current trends in weather variables from an office environment. Other stations, such as those used for research, operate using a data-logger where data are received afterwards. Advanced weather stations may have incoming and outgoing short-wave radiation sensors, incoming long-wave radiation sensors, and snow surface temperature sensors.

***Table 1.6**: Sky cover classifications (from CAA, 2007)*

Sky Cover	Description
Clear	No Clouds
Few	Less than 25% of the sky is covered with clouds
Scattered	25 – 50% of the sky is covered with clouds
Broken	50-99% of the sky is covered with clouds
Overcast	Sky is completely covered with clouds
Obscured	Observer is prevented from seeing sky (fog, within clouds)

1.7.3 Spatial Variability

Spatial variability of the snowpack exists across all terrain scales and contributes one of the critical sources of uncertainty in avalanche forecasting. Crust formation is subjected this spatial variability across terrain as described in Section 1.5. These major terrain influences include aspect, elevation, and slope incline.

***Table 1.7**: Spatial scales and their characteristic lengths (from Campbell et al., 2004)*

Name	Description	Characteristic length
Grain scale	The size of individual snow grains or crystals	0.1 mm – 1 cm
Layer scale	Typical snow layer thickness	1 cm – 10 cm
Snowpack scale	Typical snowpack thickness	10 cm – 5 m
Study plot scale	The size of a typical study plot	5 m – 30 m
Slope scale	The size of typical avalanche slopes	5 m – 100 m
Basin scale	The size of typical mountain basins or bowls	100 m – 1 km
Regional scale	One or a few mountains	1 km – 10 km
Mountain range scale	Several mountains	10 km – 100+ km

The various spatial variability scales used in avalanche forecasting and snow research are shown in Table 1.7. Avalanche forecasters are generally interested crust formation at the larger scales, such as slope scale to regional scale, because these scales are representative of their operational areas. Data for this project is typically obtained at a study plot scale and is extrapolated to be representative of slope scales. Variability of melt-freeze crust properties can exist across all scales.

Avalanche forecasting often involves the generalization of conditions in order to fit an idealized model. The typical model used for public avalanche forecasting includes three elevation bands and the eight primary aspects (Figure 1.8).

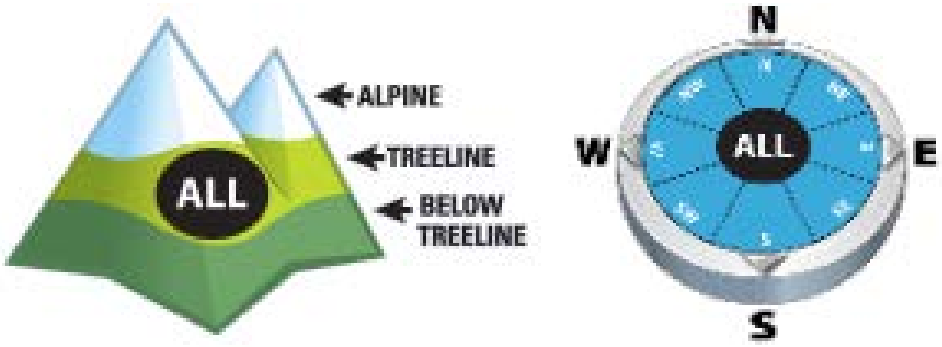

Figure 1.8*: Public avalanche forecasting spatial information icons (from Parks Canada avalanche bulletin, http://avalanche.pc.gc.ca/bulletin-eng.aspx)*

1.7.4 Avalanche forecasting model

The various weather, snowpack, and avalanche activity, along with weather forecast data, are used by avalanche forecasters to make operational decisions. There are several methods used by forecasters to mitigate avalanche risk. Closures and explosive control may be used by highways, industrial operations, and ski resorts. Backcountry ski guides use terrain selection to mitigate avalanche risk. Municipalities may use evacuations or avoidance to mitigate risk. Public forecasters use daily hazard advisories to inform the public of the avalanche risk.

The basic process of avalanche forecasting is shown in Figure 1.9. The various sources of data are used to determine the stability on various slopes, typically divided into three elevation or vegetation bands and eight aspects (Figure 1.8). The stability is combined with slab properties,

terrain factors, and the elements and exposure to determine the risk to various features, avalanche paths, or ski runs. Operational factors or objectives are coupled with the risk to make operational decisions. Data is summarized and shared with other operations. In Canada these data are submitted to the InfoEx, a database operated by the Canadian Avalanche Association, with the purpose of sharing and receiving data from neighbouring operations.

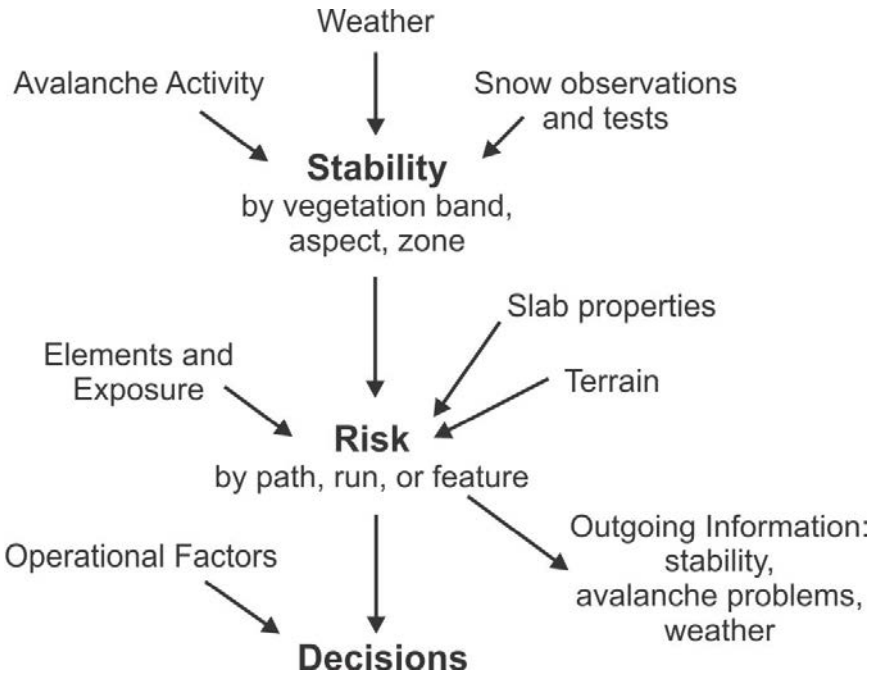

***Figure 1.9**: Avalanche forecasting flowchart (image (modified): B. Jamieson)*

1.8 Research Objectives

While melt-freeze crust formation and evolution are generally well understood in practice, there is a lack of field studies on these topics. Current snowpack models are capable of modeling general crust formation but are not adequate for modeling changes to crust properties at the microstructural level (Smith, 2009). Recent work using the Swiss SNOWPACK model (Bartelt and Lehning, 2002; Lehning et al., 2002 a,b) in the Columbia Mountains of western Canada was able to successfully model the existence of 65% to 77% of crusts depending on aspect (Bellaire and Jamieson, 2013). However, the properties of these crusts are not adequately modeled. Work with snowpack models highlight the need for field studies for

the properties of crusts and the evolution of critical avalanche layers, especially crusts and surface hoar.

The research objective was to improve our understanding of the formation and evolution of melt-freeze crusts by:

1. Evaluating specific meteorological conditions associated with the formation of different types of crusts and the properties of these crusts
2. Tracking changes to buried melt-freeze crust properties in the field
3. Applying new methods to tracking crust evolution

Historical snowpack and weather data were obtained from Parks Canada Avalanche Control Section for the first objective. Field data were collected over two winters in Glacier National Park and Blue River, BC, for the second objective. The author specified the field methods and made about half of the measurements, mostly at the Rogers Pass field station. The other measurements were made by fellow graduate students and seasonal research technicians. A thermal imager, thin-blade push gauge, and new crust indices were used to achieve the third objective.

CHAPTER 2: LITERATURE REVIEW

Observations and measurements of melt-freeze crusts have been made since the early periods of snow research. Primary applications of this work include both avalanche risk mitigation and hydrological purposes. The basic principles of crust formation have long been understood and to a certain extent the principles of crust evolution are also well understood. Colbeck (1991) summarizes the general understanding of melt-freeze crusts very well in the following statement: "While the mechanisms for the formation of all of these layers seem clear, direct observations of these processes are still needed throughout the history of their formation and degeneration."

Church (1914), Horton (1915), Seligman (1936), and Atwater (1954) made some of the earliest recorded observations of melt-freeze crusts. From this early research, several observations on the processes and importance of melt-freeze crusts were made. Church (1913) used a new snow sampling device to measure snow density in the Sierra Nevada Mountains and recorded increased densities of layers that had undergone a melt-freeze process. Horton (1915) lists several observations of conditions that exist during the melt-freeze process. The basic conditions for rain crusts and for crusts resulting from surface melting were defined. Some basic properties of crusts were also described including increases in grain size, pore space, and density resulting from the melt-freeze process. Seligman (1936) was the first to recognize the importance of crusts to avalanche formation. He described crust formation types with respect to avalanche formation as sun, rain, thaw, and wind crusts. Other surface crust classifications were made including breakable and unbreakable crusts, spring crust, film crust, marble crust, perforated crust, and ploughshares or foam crust. Seligman (1936) also described two crust burial conditions related to avalanche formation. The first condition is when new snow falls onto a crust at low temperatures, the snow will bond poorly and avalanches occurring on this crust are likely. The second condition is when new dry snow is preceded by rain or wet snow, the new snow layer will bond to the crust and avalanches will be unlikely. This second condition has since been recognized as dry-on-wet faceting and is a common condition for avalanche formation (Jamieson 2004a, Jamieson 2006). Figure 2.1 shows Seligman's (1936)

diagrams of crusts within the snowpack and their relationship to avalanche formation. Atwater (1954) listed ten factors that contribute to avalanche hazard which included two related to crusts. This included cohesion of new snow to melt-freeze crusts on the surface and the role wind and warm air can play in the formation of warming crusts.

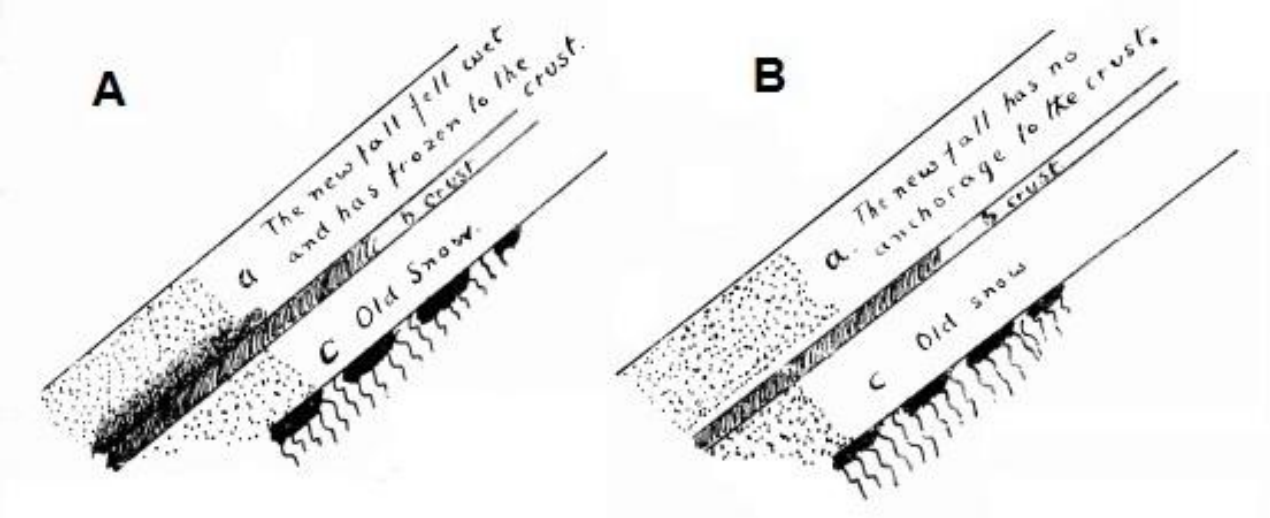

Figure 2.1*: One of the earliest diagrams of melt-freeze crusts which shows well bonded snow on a crust layer (A) and poorly bonded snow on a crust layer (B) from Seligman (1936).*

The study area for this project was the Columbia Mountains in British Columbia, Canada, and we therefore focused on crust formation conditions for this area. Jamieson (2004a) and Jamieson (2006) are good resources that summarize these general formation conditions in the Columbia Mountains including general weather conditions, frequency of crust formation throughout the winter season, and crust properties related to formation. Haegeli and McClung (2003) describe the conditions for avalanche formation in a transitional snow climate which is represented by the Columbia Mountains. This includes the frequency of melt-freeze crust formation as a critical avalanche layer and the resulting frequency of avalanche sizes related to these critical avalanche layers.

There are several computer snow-cover models capable of modeling the formation of melt-freeze crusts. The two widely used in an avalanche context are the Swiss SNOWPACK model

(Bartelt and Lehning, 2002; Lehning et al., 2002a,b) and the French Safran-Crocus-Mepra (SCM) model chain (Durand et al., 1999). These are complex numerical snowpack evolution models driven by weather station data and/or meteorological forecasting model data. Recent work by Bellaire and Jamieson (2013) has adapted the SNOWPACK model to be driven by the GEM-15 weather model in the Columbia Mountains. The formation of melt-freeze crusts was successfully modeled with accuracy between 65% and 77% depending on the aspect.

Early work on the evolution of melt-freeze crusts focused on theory and modeling of metamorphism related to temperature gradients and other properties which cause faceting around melt-freeze crusts. Moore (1982) observed the temperature gradient weakening of snow around or within melt-freeze crusts in the upper snowpack. Adams and Brown (1983) discuss how a dense crust layers caused a local vapour density gradient which in turn caused local faceted crystal growth. Colbeck (1991) used variations in the Rayleigh number to describe how layers of low permeability formed barriers to vapour, heat, and air flow which in turn promoted kinetic metamorphism at the boundaries of crusts. Jamieson (2006) summarizes the various processes which can result in faceting of a crust including near-surface faceting, dry snow faceting near crusts, and dry-on-wet faceting, as well as discussing various terrain and weather conditions which influence these processes. Jamieson (2004b) describes the specific conditions for the formation of dry-on-wet (DW) faceting. DW faceting occurs when cold, dry snow falls on a wet snow surface, and as the wet snow refreezes, the latent heat released from the wet layer creates a locally strong temperature resulting in faceting above the soon-to-be crust layer.

Research on near-crust faceting involving cold-lab and field based research includes Fukuzawa and Akitaya (1993), Jamieson and Johnston (1997), Jamieson et al. (2001), Jamieson and van Herwijnen (2002), Jamieson and Langevin (2004), Greene (2007), and Smith and Jamieson (2008). Fukuzawa and Akitaya (1993) provide a case study of faceting of a crust at their study site in Japan. Various properties of this layer including temperatures and microscopic photographs were tracked over time. They were able to recreate this faceting process in a cold lab by subjecting a crust layer to strong temperature gradients (100 to 300 K m^{-1}). Jamieson and

Johnson (1997) wrote a case study focusing on a faceted crust layer which formed across Western Canada in November 1996, which resulted in persistent destructive avalanches in the North Columbia Mountains throughout the winter season. The formation process was described using historic weather data, and the resulting crust properties and stability tests were tracked over time at a study plot near Blue River, BC. They described how the weak facets above a hard, thick crust layer were ideal to form a deep, persistent weak layer and avalanche problem. This was contrast to other regions of western Canada where the same crust/facet layer had generally stabilized by mid-January. Jamieson et al. (2001) also focused on the November 1996 near-crust facet layer but contrasted it to a crust layer that formed in November 1997 and did not result in a deep, persistent avalanche problem. Jamieson and van Herwijnen (2002) used a thin wet layer of snow between two dry layers to create dry-on-wet faceting in a cold-lab environment. Temperatures and resulting temperature gradients were tracked using an array of thermistors and microscopic photography was used to observe changes to the grain structure over time. This method of manual dry-on-wet faceting has been used in subsequent cold-lab work as a relatively simple method of creating artificial weak layers. Jamieson and Langevin (2004) tracked changes to two dry-on-wet faceted crust layers which formed in March 2003 and January 2004 at a study site on Mt. Fidelity in Glacier National Park, British Columbia. These two case studies include evolution data on shear strength, grain structure, and temperature gradients measured in the field. Smith et al. (2008) measured the properties of several melt-freeze crusts over time in the Columbia Mountains including shear strength, stability test results, and bulk temperature gradients across crusts.

In his thesis, Greene (2007) investigated the effect of a crust layer within the snowpack on the thermal properties of snowpack at a microstructure level. In a cold lab environment, a thin (~3-4 mm) ice lens was created in a homogeneous snow sample. This was compared to a sample of the same snow with no ice lens. The samples were subject to a temperature gradient of at least 60 K/m which is significantly higher than the threshold temperature gradient for kinetic growth, or faceting. This threshold is usually defined at around 10 ˚C m when measured over 10 cm (McClung and Schaerer, 2006). Both samples underwent general faceting with the crust samples yielding interesting local results. At the bottom of the thin crust, water vapour was

deposited and the ice structure experienced growth. At the top of the crust layer, sublimation caused erosion of the structure resulting in a smooth, poorly bonded surface. While the number and strength of bonds above the crust were decreasing, the size of the remaining particles was increasing. The faceting process occurred within approximately 2 to 3 particles of the crust. This was laboratory confirmation of dry near-crust faceting commonly observed in the field. Both the crust and the snow sample were subject to a strong temperature gradient, and while bulk temperature measurements showed a steady state temperature gradient throughout the sample, localized temperature gradient variations were expected but could not observed using thermocouples. As generally observed in field sampling (Jamieson, 2006), bulk temperature measurements are not adequate to measure the small-scale local temperature gradient across a thin crust.

Field based research on melt-freeze crust evolution has been quite limited and has typically focused on properties such as grain structure, bulk temperature gradients, shear strength, and stability tests/indices. Some new methods for tracking crust evolution have recently been developed by the ASARC group at the University of Calgary including near-infrared photography, measurement of thermal properties, and use of thermal imaging. Smith and Jamieson (2009), Smith and Jamieson (2010), and Smith (in press) used a near-infrared camera to measure changes to specific surface area over time. Specific surface area is the ratio of surface area to volume. Smith showed that over time the specific surface area of crusts generally decreases. Smith (in press) used a thermal conductivity probe to measure the thermal conductivity of crusts and the adjacent layers over time. The thermal conductivity of crusts generally increases over time and has a complex relationship with density, grain structure, and temperature. The field work by Smith at the University of Calgary, Applied Snow and Avalanche Research group (ASARC) precedes my research.

Another important area of research recently undertaken by ASARC involves the use of a thermal imager to measure snow temperatures. Smith (in press) was the first to use a thermal imager to investigate temperature gradients around melt-freeze crusts in a cold lab environment. Shea and Jamieson (2011) established the fundamental methods for field based

snow surface thermal imaging. Shea et al. (2012) established the methods for the use of a thermal imager for measuring snow layer temperatures in a snow pit. In this work Shea also tracked temperature gradients around a crust layer over time. Schirmer and Jamieson (2013) identify the limitations of using a thermal imager to measure snow pit temperatures. They specifically identify problems with using a thermal imager to measure temperature gradients around crusts. Concavities and convexities that inherently occur around hard crust layers during cutting of the pit wall affect point temperatures and hence temperature gradients, especially when convection due to wind is present. Convexities tend to change temperature faster after the pit wall is exposed than planar areas and concavities tend to change temperature slower than planar areas. This occurs on a macroscopic scale when attempting to cut a planar pit wall containing a hard crust layer, and on a microscopic scale due to difference in grain structure between dry snow and melt-freeze crusts. The work at ASARC by Shea precedes my research and the work done by Schirmer follows my research.

CHAPTER 3: METHODS

This chapter describes the methods used for the two primary topics of this project. Crust formation uses historical snowpack and weather data to create a seven-year dataset of crust events in Glacier National Park. Crust evolution involves the collection of field data over two winters and the interpretation of these data. Field safety and sources of error are also discussed in this chapter.

3.1 Field study areas

The primary study area for this project was the Columbia Mountains of Western Canada. The Columbia Mountains are located in the south-east corner of British Columbia and compromise the Monashee, Selkirk, Purcell, and Cariboo ranges. Within Canada, the Columbia Mountains are bordered by the Rocky Mountains to the east and the interior plateau to the west. These mountains occupy roughly 97,000 km^2. Figure 3.1 shows a map of the Columbia Mountains including the locations of the study areas.

The Columbia Mountains are classified as a transitional snow climate (Haegeli and McClung, 2003). Approximately 32% of natural avalanches in the Columbia Mountains are associated with melt-freeze crust layers (Haegeli and McClung, 2003). This primarily consists of crust/facet interfaces, crust/surface hoar interfaces, and pure crust interfaces. A pure crust interface is where the crust was the primary weakness and no other persistent weak grains were observed (Haegeli and McClung, 2003). This may also include crust interfaces where an additional grain type has been omitted from the data collection process. Crust formation in the Columbia Mountains is possible during all winter months but is most likely during November, March, and April (Jamieson, 2004a).

3.1.1 Glacier National Park study area

Glacier National Park is a mountain park located in the Selkirk Mountains sub-range of the Columbia Mountains. The Trans-Canada highway runs through the park and is exposed to numerous large avalanche paths. The top of the highway corridor is named Rogers Pass and is

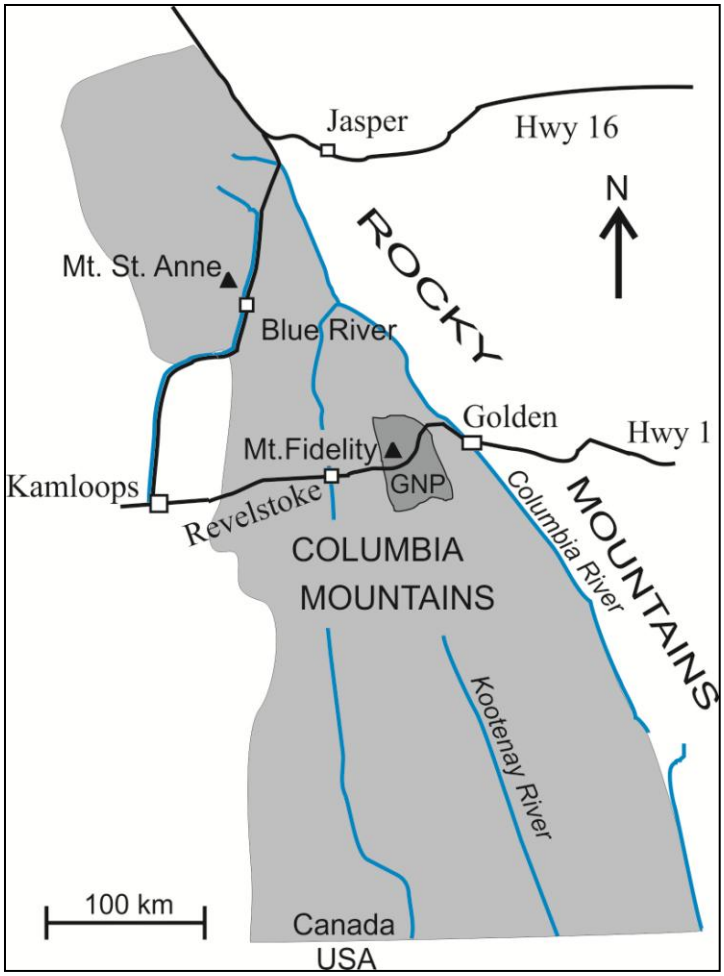

Figure 3.1*: Map of the Columbia Mountains including the Mt. St. Anne, Mt. Fidelity, and Glacier National Park (GNP) study areas*

a national historic site. Since the construction of the highway in the 1960s, the Avalanche Control Section (ACS) of Parks Canada has run an avalanche forecasting and control program in the park. An important part of this program is the regular collection of snow cover and weather data. Snow profiles are completed on a regular basis at a variety of locations, which are representative of the start zones of numerous avalanche paths affecting the highway. Weather data are collected at numerous automatic weather stations throughout the park. The ACS also maintains and collects regular snow observations at two manual snow and weather stations. One is at highway elevation (1315 m) and the other is located at the Mt. Fidelity research area (1905 m). A map of weather stations and study areas in and around Glacier National Park is shown in Figure 3.2.

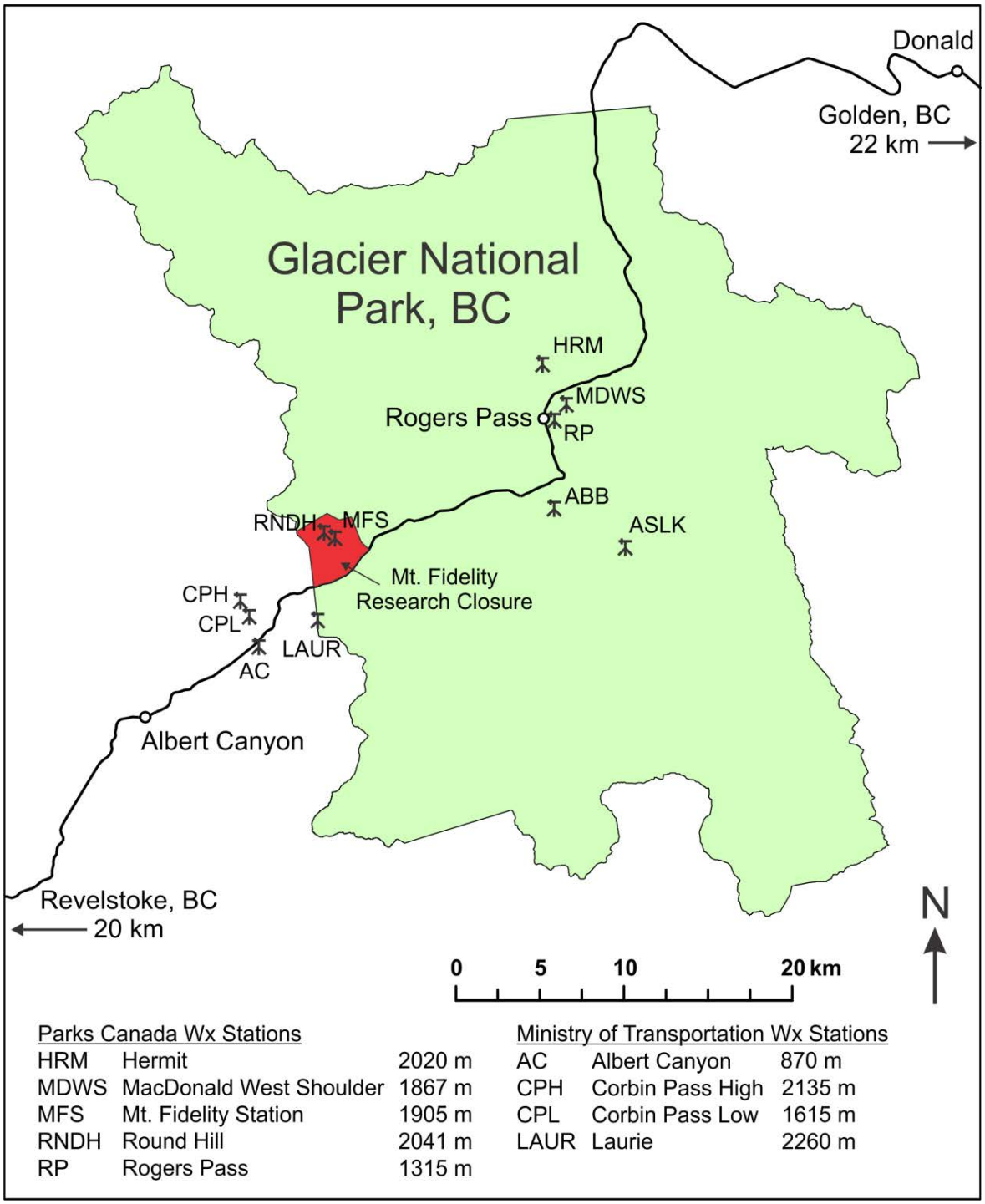

***Figure 3.2**: Map of weather stations and study plots in and around Glacier National Park. Weather stations outside of the park (AC, CPL, CPH, and LAUR) are operated by BC Ministry of Transportation. Base data obtained from Government of Canada GeoGratis (http://www.geogratis.gc.ca)*

3.1.2 Mt. Fidelity study area

Mt. Fidelity is located on the southwest side of Glacier National Park. In this area, typical weather systems first arrive from the southwest. This results in more snowfall which is considered representative of the deep snowpack in the Columbia Mountains. In contrast, the east side of the park receives less overall snowfall and more variability in snowfall amounts making it similar to the Purcell Mountains. Mt. Fidelity is a permanently closed research area and is the location of the ACS research area and weather station (Figure 3.2). The research building and study plot are located adjacent to the weather station (MFS). The University of Calgary also maintains a weather station on Mt. Fidelity. The research station and weather plot are at 1905 m elevation. The Roundhill weather station (RNDH) is located further up the ridge at 2041 m elevation. It is less sheltered by terrain and vegetation than MFS and is therefore used to measure open wind and direction.

Regular study sites were maintained on north and south aspect slopes as well as a flat site adjacent to the Mt. Fidelity weather station. These study sites were all between 1850 m and 1950 m elevation which is considered treeline elevation in the area. The main research station was accessed by snow-cat or by snowmobile and the regular study sites were accessed by ski touring from the station. Study sites were marked with bamboo stakes to ensure they were undisturbed. Specific details regarding site selection are discussed in Section 3.3.1.

3.1.3 Mt. St. Anne study area

Blue River, BC, is located in the North Thompson Valley in the Columbia Mountains, situated between the Cariboo and Monashee sub-ranges. Blue River is home to Mike Wiegele Heli-Skiing, which provides logistical support to the ASARC research in the area. Part of this support was the use of snowmobiles and the occasional use of helicopters to access study areas.

Mt. St. Anne was used as a regular study area because it has a road to treeline elevation that allowed access during most conditions by snowmobile. It was also home to a weather station at 1900 m elevation. As with Mt. Fidelity, regular study plots were maintained on north and south aspects as well as a flat site.

3.2 Crust formation methods

Historic field observations and historic weather data were used to create a large dataset of melt-freeze crust formation events. These data were obtained from Parks Canada and span November 2005 to April 2012. This period was selected because short-wave and long-wave radiometers were installed on Mt. Fidelity in the fall of 2005. The study area for this dataset is Glacier National Park. Another small dataset used for this project included manual sky cover observations collected by ACS at Mt. Fidelity during the same period.

3.2.1 Historic snow profile data

The Parks Canada ACS collects detailed snow profile data throughout each winter season. These data are primarily used by avalanche forecasters to assess snowpack and avalanche conditions to make avalanche control decisions for the highway corridor. Field teams are dispatched throughout the park to collect snow profile data on a regular basis. As described in Section 1.7.1, these profiles are created by digging a pit in the snow and identifying snowpack layering. For each layer the hand hardness, density, grain size, and grain type are recorded. The teams also measure snow temperatures at 10 cm intervals and perform various snowpack tests to assess stability. Appendix B contains an example of typical snow profile obtained by the ACS.

For the study period of November 2005 to April 2012, there were 560 snow profiles, or an average of 80 profiles per season. From these profiles, all crust layers were extracted into a dataset. The two primary criteria for a crust to be included in the dataset were the following:

1. the layer identification date could be determined; and

2. the crust appeared in at least three profiles to ensure it was not an isolated event

The ACS identifies each sun crust by the date of burial by new snow and each rain crust by the date of the rain event. Once given date identification, these crust layers are generally labeled within a snow profile in the layer notes section. This is typical for crusts which are thicker and/or harder, and therefore tend to persist longer in the snowpack. Crusts which may be

active or recently active with respect to avalanches are typically labeled with an identification date. The lesser crust events may not be given a date identification and therefore are not included in this dataset. These crusts include thin and/or weak crusts which may not be associated with avalanche formation, crusts not found in regular study sites, or non-persistent crusts in the snowpack. This identification system is at the discretion of the ACS forecasters and the field teams. There are two other cases in which crusts were excluded from the dataset. The first was crust events formed by both sun and rain. These events are typically isolated to spring. The second case was crust complexes. These are cases when multiple crusts form just above one another within the snowpack. Over time these unique layers evolve into one complex layer. These layers are also most common in spring. An example of a crust complex is shown in Figure 3.3. Both of these types of crusts were excluded from the dataset because they cannot be confidently associated with their formative weather.

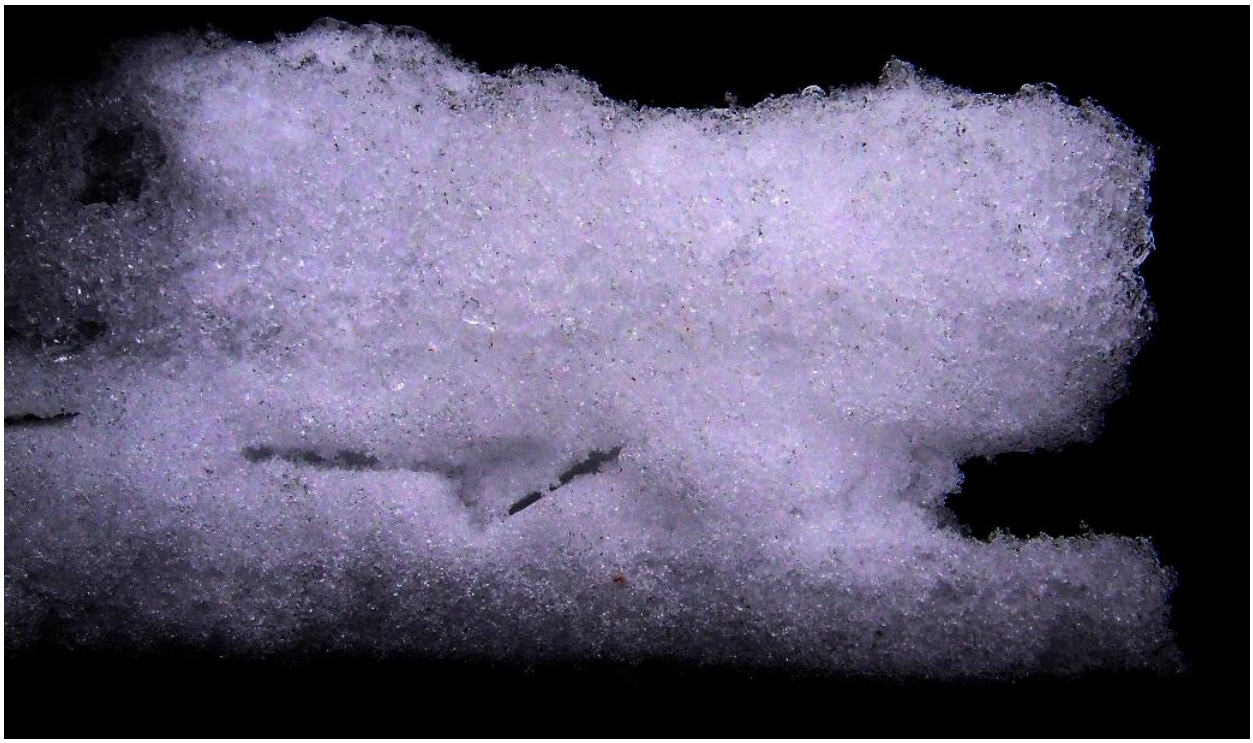

Figure 3.3*: An example of a crust complex shortly after burial. A thin layer of un-melted snow sits between two crust layers. Over time as this thin middle layer undergoes settlement and densification, all the layers will resemble a single layer. Note: cut marks in middle layer are made by a hack saw blade while investigating the hardness of the layer.*

The ACS is consistent with their use of snow grain type for melt-freeze crust observations in snow profiles. The grain type used for all melt-freeze crusts is melt-freeze poly-crystals (MFpc) (Fierz et al., 2009). This grain type is not used for any other type of layers by the ACS. This consistency makes the interpretation of these layers straightforward. Because several of these melt-freeze layers do not include date identification, some interpretation was required. If another layer in the profile had date identification and had a spatial relationship with a melt-freeze crust, this other layer was used to identify the melt-freeze crust. For example, in a well labelled snow profile the 15 January surface hoar layer was 30 cm below the 20 January sun crust. Therefore, the 15 January surface hoar layer could be used to identify the 20 January sun crust in profiles where the crust was not labeled with date identification. This method required some subjectivity and crusts were only included if they could be identified with a high level of certainty. All other crust layers which could not be identified were not included in the dataset.

The date and the crust type define each crust. For each crust a number of terrain details were recorded from the snow profiles. The terrain data included the maximum and minimum elevation, maximum and minimum slope angle, and aspects in which the crust was observed. The number of profiles in which the crust appears was also included.

3.2.2 Weather data

Parks Canada operates several automated weather stations within Glacier National Park including Mt. Fidelity (MFS), Round Hill (RNDH), MacDonald West Shoulder (MDWS), Hermit (HRM), and Rogers Pass (RP) (Figure 3.2). For this project, Mt. Fidelity was used as the primary station for weather data due to its proximity to the study sites. The other stations were used for verification, additional data, and to check for temperature inversions. The University of Calgary also operates a weather station on Mt. Fidelity adjacent to the research area. This station has several unique sensors including radiometers and an infrared snow surface thermometer.

Weather data recorded at Mt. Fidelity during the study period included the following: wind speed, wind direction, relative humidity, liquid precipitation (snow water equivalent), snowfall,

air temperature, incoming short wave radiation, and incoming long wave radiation. Snow surface temperature data were also recorded for the 2012 winter. These weather variables are summarized in Table 3.1.

For each crust event in the snowpack dataset, the preceding weather data were extracted from the weather dataset. These data were plotted for each crust event to help visualize the formation conditions. Each crust was assigned a formation period with a specific start and end timestamp. The criteria for selecting the formation period were based on the crust type. For sun crusts, the start of the period was the first hour following the last substantial precipitation recorded by the precipitation gauge. The end of the period was the last hour prior to burial of the crust by new snow. This was also based on substantial precipitation recorded by the precipitation gauge. Substantial precipitation is considered multiple hours of precipitation accumulating to at least a few millimeters snow water equivalent. This criterion is referred to as the *precip-to-precip rule* and assumes that everything that happens during this period influences the surface energy balance for sun crust formation. In reality, the solar inputs required to form a sun crust would occur during shorter periods while the sun is most intense but this can occur multiple times over several days. Narrowing down the formation period further would be difficult and would require too much subjectivity. An example of sun crust formation is shown in Figure 3.4.

Rain crusts were identified as the period where the precipitation gauge showed an increase while the snow height sensor remained constant or decreased. An example of a rain crust formation period is shown in Figure 3.5. Due to the possibility of wet snow and potential sensor error, small increases on the snow sensor are acceptable as long as they are not continuous. In cases involving uncertainty at the start or end of the formation period, air temperature is useful for verification. It is assumed that for a rain event the air temperature will be above or near 0°C. Rain crusts that occur at air temperatures well below the freezing level are classified as freezing rain crusts. These are more difficult to interpret using this method because they are often short events involving minimal amounts of precipitation. An example of a freezing rain crust event is analyzed as a case study in Section 4.1.10.1. Several

other freezing rain crusts that appear in the snow profiles were discarded because of the inability to identify the formation period from the data available.

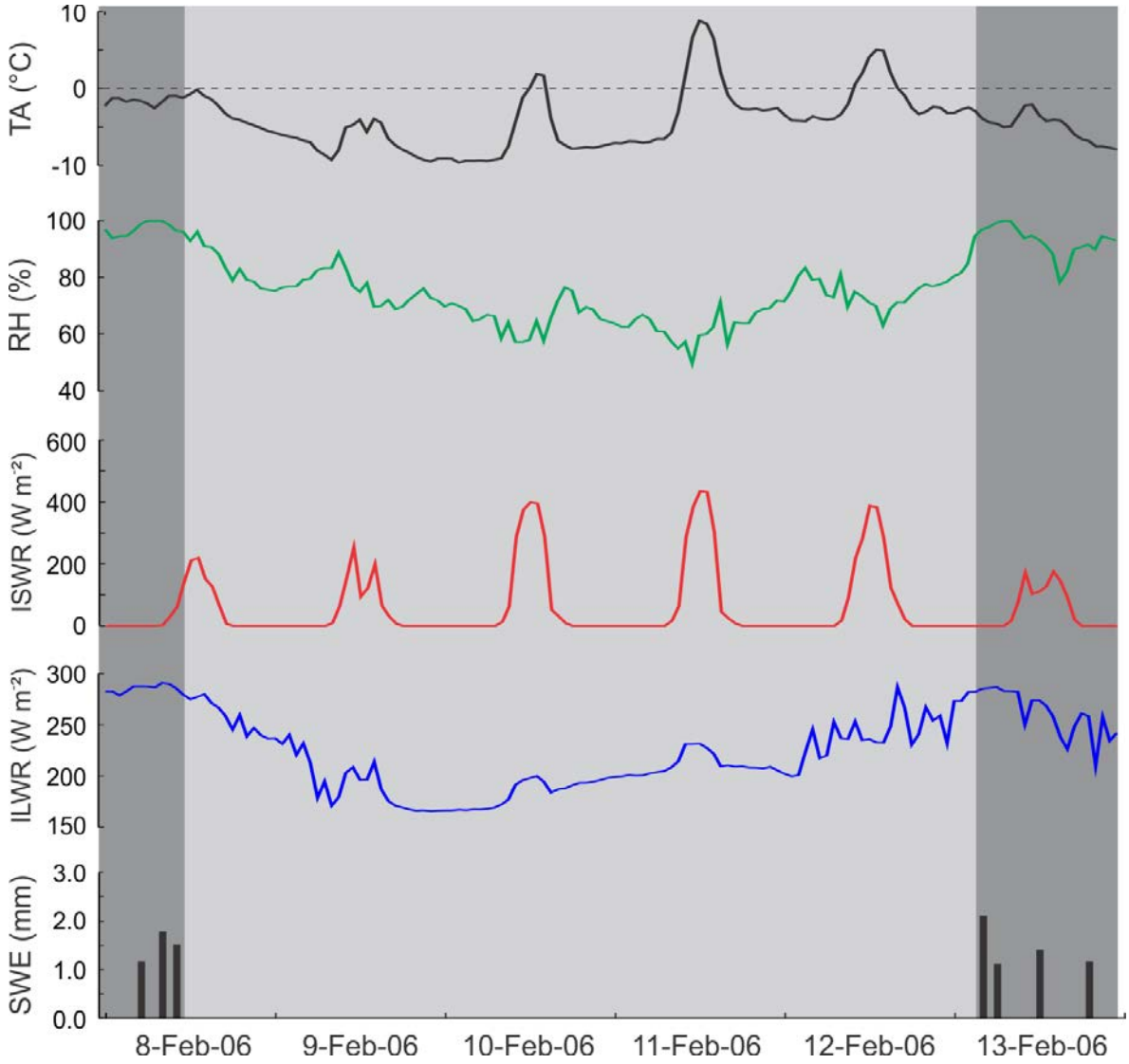

***Figure 3.4**: Example of a sun crust formation period (13-Feb-06 sun crust) and the data collected during this period. Sun crust formation periods (light grey) were defined from the last substantial accumulation of hourly snow water equivalent (SWE) precipitation until the crust was buried by new snow precipitation. Meteorological data recorded during this period included air temperature (TA), relative humidity (RH), incoming short-wave radiation (ISWR), and incoming long-wave radiation (ILWR). Specific variables extracted from these data are defined in Table 3.1.*

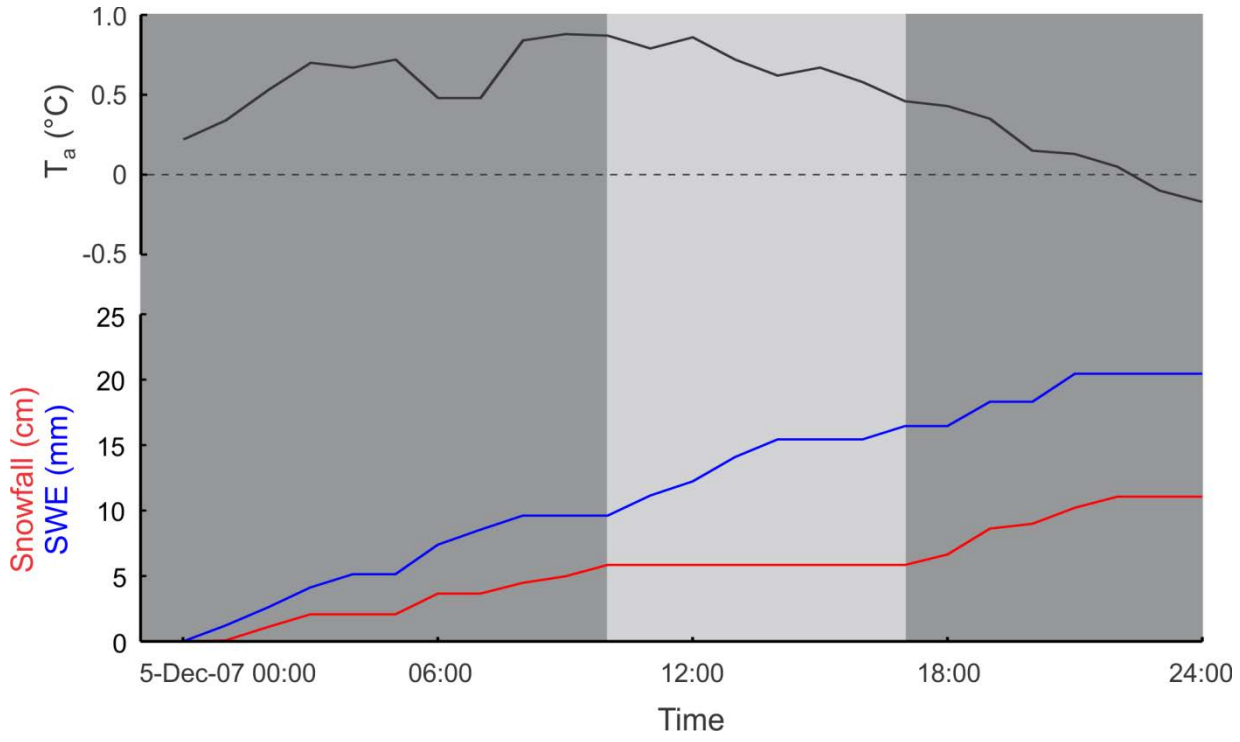

***Figure 3.5**: Example of a rain crust formation period (5-Dec-07 rain crust). Rain crust formation periods (light grey) are defined as the period in which liquid precipitation (snow water equivalent, SWE) increases while new snowfall remains constant or decreases. Decreases in the snow height sensor are not shown in the figure.*

Once each crust event was assigned a formation period, a number of meteorological data were extracted for each event. A list of data extracted for each event is summarized in Table 3.1. The air temperature, relative humidity, and incoming long-wave radiation variables are straightforward to calculate because they are measured continually. Precipitation and snow are also straightforward variables because they are discrete events. Shortwave radiation is more complicated because of the diurnal effects. Three primary variables of incoming shortwave radiation were selected for analysis. The maximum peak daily incoming short-wave radiation during the formation period was recorded. The formation periods often span several days so each day has a unique peak value. The maximum peak value for the example in Figure 3.4 occurred on 11 February 2006. The second variable was the maximum daily cumulative incoming long-wave radiation energy. Rather than a point observation of incoming radiation, this variable is an estimate of total incoming short-wave energy available on a given day, and

assumes that point measurement of incoming radiation is representative of the period equal to the sampling frequency. In Figure 3.4, the maximum daily cumulative incoming long-wave radiation energy occurs on 11 February 2006 and is equal to 7.2 MJ m^{-2} day^{-1}. In cases where the formation period starts or ends during the middle of the day, the radiation for the entire day is considered. Finally, the cumulative incoming short-wave radiation energy for the entire formation period was also calculated. The example in Figure 3.4 has a total cumulative incoming shortwave energy equal to 27.8 MJ m^{-2}.

Table 3.1: *Meteorological data and variables recorded for each crust formation event*

Meteorological Data	Abbreviation	Variables	SI Units
Air temperature	TA	Maximum, minimum, average, standard deviation	°C
Relative humidity	RH	Maximum, minimum, average, standard deviation	%
Incoming long wave radiation	ILWR	Maximum, minimum, average, standard deviation, total	W m^{-2}, J m^{-2}
Incoming short-wave radiation	ISWR	Maximum peak daily radiation, maximum cumulative daily radiation energy, total SW energy	W m^{-2}, J m^{-2} day^{-1}, J m^{-2}
Precipitation, snow water equivalent	SWE	Σ hourly	mm
Height of new snow (HN)	HN	Σ hourly	cm

Radiosonde data from the Kelowna airport (YLW) were used to investigate the existence of inverted air temperature in the atmosphere. Radiosonde data was obtained from the University of Wyoming Department of Atmospheric Science where it is publicly available (http://weather.uwyo.edu/upperair/sounding.html). This data are collected every 12 hours by a weather balloon and typically records data vertical data points every 150 to 250 m.

3.2.3 Formation data analysis methods

The primary use of this dataset was to summarize conditions during crust formation. Each of the meteorological variables obtained from the time series for each unique event was plotted

for sun and rain crusts separately. Properties that are not time dependant are plotted as box and whisker plots whereas time-dependant properties are plotted as scatter plots.

3.2.3.1 Methods for analyzing crust properties from historic profiles

Two physical properties, thickness and hand hardness, were measured consistently in the historic ACS snow profiles. The dataset of historic snow profiles consists of profiles observed at various aspects and elevations in order to access the representative conditions of the various avalanche start zones affecting the highway. This creates variability of the crust properties amongst the various snow profiles. Several criteria were used to reduce this variability. Profiles were selected from elevations between 1700 and 2100 meters which is typical of tree-line elevation. The sun crust dataset was limited to southeast through southwest profiles. Crust property data were limited to the first 30 days after burial to reduce the possible effects of evolution. The resulting layer property data were averaged for each crust event.

For each crust event, the average thickness and average hand hardness were calculated based on the above criteria. The relationship between these properties and the meteorological variables during formation were then investigated.

3.2.3.2 Methods for analyzing historic sky cover and incoming long-wave radiation

Each time the ACS staff visited the Mt. Fidelity research station – roughly 3 times per week - they took a set of manual weather and snowpack observations. One of the observations recorded was sky cover. Sky cover classifications are shown in Table 5.

These data were coupled with incoming long wave radiation data to quantify the incoming long-wave radiation for each sky cover classification. Sky cover data are discrete observations while incoming long-wave radiation was recorded continually, typically with a 0.5 hour sampling frequency. For each sky cover observation, the incoming long-wave radiation was recorded for three hours before and after the observation. From these data, the average and standard deviation of incoming long-wave radiation were calculated for each class of sky cover.

3.3 Crust evolution methods

The study of crust evolution after burial by snowfall is based on data collected in the field by the author and fellow graduate students. These data were collected over the two winters of 2010-11 and 2011-12 in both Rogers Pass and Blue River, British Columbia. The objective of this research was to track changes to a crust layer over time by making observations at regular intervals.

3.3.1 Site selection and setup

One of the most important parts of an evolution project is site selection. Because of the destructive nature of digging and sampling the snowpack on each observation day, a large area is required and it is important to ensure that the crust is uniform across this area. This way, as each observation is made, it can be assumed that changes to the properties of the crust layer are temporal and not spatial. In reality, all snow layers are subject to some spatial variation. Proper site selection allows the minimization of this spatial variation across a slope and increases confidence in subsequent observations.

General site selection for this project involves choosing several sites of different aspects, specifically south, north, and flat sites. More important to the site selection are the properties of each site. The first important site property is to have a planar slope. This means selecting a slope with a constant slope angle and constant aspect. It is important to minimize undulations across and up the slope. Crust properties can vary substantially due to subtle changes to these slope properties. The second important site property is exposure to sun. This is most important for sun crusts. The aim is to ensure the site is not partially shaded by trees. Visiting the site several times during a sunny day is an effective way to map the shade across a slope. The third important site property is exposure to wind. For all sites we wanted to avoid exposure to all strong wind effects as indicated by snow drift accumulations or wind scoured surfaces. The effect of wind substantially increases the spatial variability of layer properties on a slope. For rain crusts, light wind can affect the properties during formation. Sheltered areas may receive less precipitation and windward areas may receive more precipitation. If there is

wind during the formation of a rain crust, it is important to understand how the wind has affected the site. This is achieved by selecting study sites well away from trees, especially if the trees are oriented across the predominate direction for the region. This restriction can make it difficult to find ideal study sites below treeline. Fourthly, it is important to ensure that there is enough space to dig numerous snow profile pits within the selected slope. In the case of crusts formed early in the season, 20 or more pits may be required. A space of roughly 100 m^2 for each study site was targeted. Figure 3.6 shows an example of a typical layout for a study site and the progression of snow profiles within the site. The last important characteristic is the ground roughness and ground cover of the study site. Rocks, shrubs, small trees, and other protruding objects affect the metamorphism of the surrounding snow. Faceting is common around rocks which tend to store more heat through the summer and then create strong temperature gradients through the early winter. Substantial variation in snowpack properties is expected up to 20 cm above the height of the ground roughness in the Columbia Mountains. A smooth ground cover is desired for study sites. This can be achieved by improving the site in the summer or probing the site in the early winter to find an area with desirable ground cover.

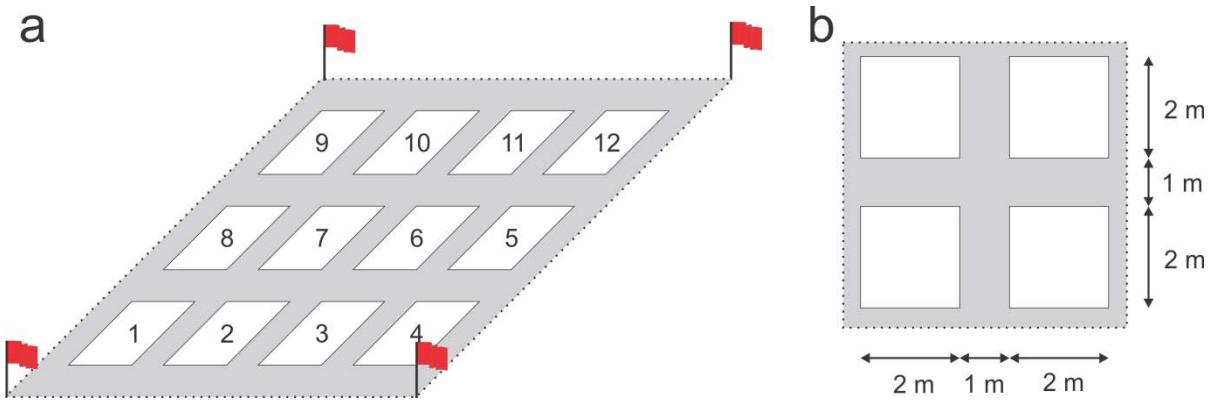

***Figure 3.6**: Hypothetical study plot layout on a slope showing the progression of snow profiles (a). A typical snow profile is roughly 2 m by 2 m upon completion and at least 1 m of undisturbed snow is required between profiles (b).*

Once the site was selected it was important to establish a system to mark the site and ensure the efficient use of space. If the site is near a ski run or near an area used by the public, it may be necessary to mark or rope the boundaries of the site, and signage may be appropriate. The

sequence of pits should be dug in a grid system, especially when multiple observers may be using the site. For internal marking, two stakes or pieces of bamboo are optimal. Because snow is excavated to the downhill side of the snow pit, the first pit should be dug in lower corner of the site and the first marking stake placed on the outer edge. Subsequent profiles should proceed across the slope with the second marking stake moving across the slope to mark the progress. When the first row is complete, the two marking stakes will clearly mark the upper line of the completed profiles, even with the older pits obscured by snowfall as is common in heavy snowfall areas. The rows tend to drift slightly diagonal uphill across the row if the observers are not vigilant or the older pits are not marked well. The row marking makes placement of the subsequent rows easy and the number of profiles on a slope can be maximized. Communication amongst observers is also important to ensure that the regular study site use is consistent and efficient.

3.3.2 Equipment

Several pieces of equipment were required in the field. Some of this equipment is standard snow study tools that would be carried by an avalanche technician in the field based on CAA Observation Guidelines and Recording Standards for Weather, Snowpack, and Avalanches (OGRS) (CAA, 2007). Other equipment used specifically for research includes shear frame equipment, thin-blade resistance equipment, and a thermal camera.

3.3.2.1 Standard snow study equipment

The standard equipment recommended by OGRS (CAA, 2007) for snow profiles includes the following: probe, shovel, thermometer, ruler, loupe (magnifier), crystal screen, density kit, field book, pencil, gloves, compass, altimeter, inclinometer, snow saw, paint brush, camera, and GPS. A digital scale was required because a non-standard method was used for measuring crust density. A project specific field book is used and an example of a field book page is attached as Appendix A.

3.3.2.2 Shear frame test equipment

Specialized equipment is required to do shear frame tests as described in Sommerfeld (1984) and Jamieson and Johnston (2001). This includes a metal cutting plate, a shear frame, a cutting tool, and a pull force gauge as shown in Figure 3.7. We used an aluminum cutting plate with dimensions of roughly 40 cm by 50 cm and a 250 cm² shear frame. The cutting tool is a small paint scraper and is used to cut around the edge of the shear frame. We used three Imada brand manual push-pull force gauges with capacities 9.8 N, 98 N, and 294 N. More recent work by the ASARC group has shown that a digital push-pull gauge is more practical because multiple manual gauges can be replaced by one digital gauge which has a wider functional range of force values.

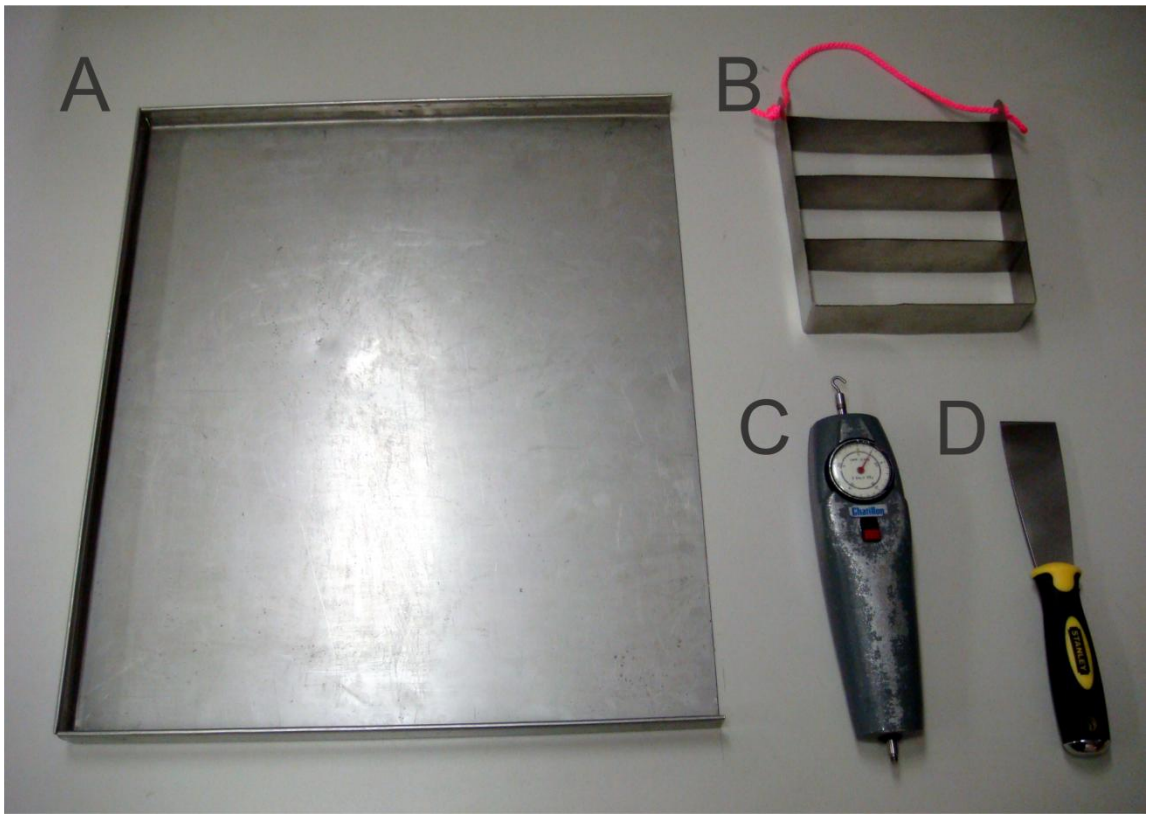

Figure 3.7*: Specialized tools used for performing shear frame test: Aluminum cutting plate (A), 250 cm^3 shear frame (B), push-pull force gauge with a hook (C), and a small putty knife for cutting around the shear frame (D).*

3.3.2.3 Thin-blade resistance test equipment

The equipment required for this test was a push force gauge with a thin-blade attachment (Borstad and McClung, 2011). The same Imada brand manual push-pull gauges used for the shear frame tests were also used for this test. The thin-blade is a custom attachment which is built from a 4" (~10 cm) paint scraper. The handle was removed from the paint scraper and the blade was attached to a metal rod that attaches to the push-pull gauge. Two u-bolts were used to attach the blade to the rod. Figure 3.8 shows the basic set-up.

Figure 3.8*: Basic equipment set-up for thin-blade resistance measurements is a force gauge with a custom blade attachment made from a 4" (~10 cm) paint scrapper*

3.3.2.4 Thermal camera equipment

A FLIR B300 thermal camera was used during the 2011-12 winter. Figure 3.9 shows the FLIR B300 thermal camera. The camera has a 320×240 pixel resolution. This is the same camera used by Shea and Jamieson (2011), Shea et al. (2012), and Schirmer and Jamieson (in preparation). The cutting plate that was used for the shear frame test or a flat blade shovel was used to create a flat pit wall. A crystal screen was used to make spatial reference marks in the thermal photo.

***Figure 3.9**: FLIR B300 thermal camera used for thermal imaging of melt-freeze crusts.*

3.3.3 Crust tracking procedures

Crust tracking involved taking a specific set of observations at fixed study sites on a semi-regular schedule. For the 2011-12 field season, the observations included location data, weather observations, basic snowpack layering around the crust, compression tests, density measurements, shear frame tests, thin-blade resistance tests, crust indices observations, and thermal photos. The typical sampling schedule was once per week but varied depending on weather conditions and safe access to the study sites. More frequent sampling often occurred in the first week following formation.

3.3.3.1 Standard field observations

The standard observations are those which are defined in the Canadian Avalanche Association Observation Guidelines and Recording Standards for Weather, Snowpack, and Avalanches (OGRS) (CAA 2007). The observation procedures are clearly defined in this document and, therefore, are not defined here.

The first set of standard field observations included the observation header, the site details, and basic field weather observations. The observation header includes the date and time, the identity of the observers, the crust identification date, and the crust type. The site details includes the location name, the UTM coordinates, elevation band (alpine, treeline, or below

treeline), elevation (m), aspect, and slope angle. The field weather observations include air temperature, precipitation type and rate, wind speed and direction, and sky cover.

While a standard snow profile was not observed for this project, some of these standard observations were made for the crust layer and the layers above and below the crust. For each of these three layers the grain form, grain size, and hand hardness were recorded. The depth to the top of the crust was measured. The thickness of the crust was measured three times to obtain an average thickness. This was done by extracting a sample of the crust from the snowpack and gently removing any attached snow in order to ensure the layer boundaries of the crust are planer. An example is shown in Figure 3.10. The thickness was measured slope normal in order to increase the accuracy. The thickness can be converted to the typical vertical measurement using the slope angle measurement.

Figure 3.10*: Example of an isolated block of crust for thickness measurement. The excess snow is removed (as on the right) until the natural boundaries are isolated. If the natural crust boundary is undulated like the lower boundary of this example, the typical or median value was recorded.*

If the crust was in the upper 1.2 m of the snowpack, two compression tests were done (CAA, 2007, p. 36). The recorded results included the number of taps, the fracture character, and the location of the failure relative to the crust (above, below, or within the crust). Tests in which no fracture occurred above, within, or below the crust were also recorded.

3.3.3.2 Density measurement methods

To measure the density of a melt-freeze crust, a non-standard method was utilized. Standard density measurements use a metal tube with a diameter of approximately 4 cm and a volume of 100 cm^3 to sample the snow. There are two limitations to this standard method including the thickness of the layer and the hardness of the layer. Inserting the density sampling tube into a hard layer such as a crust tends to break the layer and it is difficult to sample the desired undisturbed volume. Crust layers are typically thinner than the sampling tube and therefore cannot be sampled using this method.

The method used to measure the density of a crust was to isolate a piece of a crust in a rectangular block shape. The length, width, and thickness of the sample were measured to calculate the volume and the mass of the block was measured. The sample was taken where the thickness is representative of the layer across the exposed pit wall and the median measurement of thickness was recorded. The density was then calculated from the mass and volume of the sample. This is a unique method for measuring crust density because most other types of snow do not have the cohesion required to isolate a block without substantial damage. This method does not work for all crusts including thin crusts and poorly bonded crusts that break during isolation. An example of a density measure is shown in Figure 3.11.

It is important to ensure that the block has right angles and parallel sides in order to ensure the dimension measurements are accurate. During the 2010-11 season a single sample was taken at each observation. It was difficult to interpret the results because the error could not be quantified. For the 2011-12 season three density measurements were taken for each observation to reduce uncertainty.

Figure 3.11*: An example of a crust density measurement. A block of crust is isolated using a small saw and the three dimensions are measured and recorded. The mass of the block is measured using a small digital scale and the density can then be calculated. Three measurements were made for each observation to reduce uncertainty.*

3.3.3.3 Thin-blade resistance methods

The use of thin-blade resistance is a method developed by Borstad and McClung (2011). Previously, the push gauge has been used with a round disk to measure resistance. The thin-blade is an improvement over the round disks because it reduces the effect of snow compaction. The measure of resistance is used as a way to quantify the hardness of a layer. Quantitatively measuring resistance is an improvement over the traditional hand hardness observation which tends to be somewhat subjective, especially for harder layers.

Borstad and McClung (2011) performed their work with the thin-blade resistance parallel to the layering of the snowpack in the same way that hand hardness is measured. Because of the thin

nature of crusts and the vertical variability that is common in crusts, the thin-blade resistance for this project was measured slope normal to the crust layer. Using the blade in this fashion effectively measures the resistance of the hardest part of the crust, assuming the crust is relatively uniform horizontally. The thin-blade resistance of the layer below was checked to ensure that it was lower than the resistance of the crust and would not influence the results.

The basic method for these measurements was to remove the snow above a crust for an area of roughly 0.5 m^2. Typically, 14 measurements were taken for each observation. The first measurement was generally not recorded as it was used to determine the required push rate and push gauge capacity. Each measurement had a spacing of at least the width of the blade (~100 mm). In the cases where the crust tended to break the spacing was increased to ensure the sample was not compromised prior to testing.

3.3.3.4 Shear frame methods

Shear frame methods have been well established (Sommerfeld, 1984; Jamieson and Johnston, 2001) and therefore only a brief overview is included here. Shear frame measurements were made by placing the shear frame 2-3 millimeters above a crust and pulling it with a force gauge. By dividing the force measurement by the area of the frame, the strength of a weak layer was calculated. Twelve measurements were obtained for each crust observation using a 250 cm^2 shear frame. No correction for grain size was applied to the resulting data. An example of shear frame tests in the field is shown in Figure 3.12.

3.3.3.5 Crust indices

For the winter of 2010-11, the primary way to describe a crust during the tracking process was to make detailed descriptive notes. These notes were useful for individual observations but did not suffice for time series observations. There was not enough consistency between observations and different observers used different structure in their notes. Based on the common notes taken during the 2010-11 season, the crust indices were introduced to create a common description of a crust in order to effectively track changes.

Figure 3.12*: An example of shear frame tests during winter field work. Two tests have been completed and the author is preparing the third test.*

The crust indices comprise an ordinal classification system based on two parts, bonding to adjacent layers and the internal lamination of the crust. It also includes six questions used to describe additional, non-typical crust properties. These questions are also useful for verification of the observations. The numerical indices were established on a scale of 1 to 5. Table 3.2 shows the descriptions of the index for bonding to adjacent layers. Two numbers were recorded for each observation, one for the upper boundary and one for the lower boundary. The interface bonding classifications vary from *little to no bonding* to *very well bonded*, and the associated descriptions can be done with the equipment carried by the typical practitioner. Table 3.3 shows the descriptions of the index for the internal lamination of the crust. The classifications are similar to the interface bonding and the descriptions are based on how the

crust breaks apart. Table 3.4 shows the additional questions that describe the properties of the crust and are used for verification. These are yes/no type questions and descriptive notes are strongly encouraged for non-typical responses.

***Table 3.2**: Crust Bonding Index scale and descriptions. Recommended changes to the descriptions are included in Section 5.2.6.*

Class	Description
1	Little to no bonding between layers; clean separation with minimal shear force input
2	Poorly bonded; separates easily; fractures suddenly with light pressure; light brushing may be required to isolate crust layer
3	Moderate bonding; requires hard brushing or very light scraping to isolate crust layer
4	Well bonded; requires light to moderate scraping to isolate crust layer
5	Very well bonded; difficult to separate layers; requires hard scraping or saw to isolate crust layer

***Table 3.3**: Crust Lamination Index scale and descriptions. Recommended changes to the descriptions are included in Section 5.2.6.*

Class	Description
1	Little to no bonding; Very difficult or not possible to handle without breaking / crumbling.
2	Bonds between individual ice grains are discernible, but not strong or extensive; Difficult but possible to isolate block; Sample crumbles easily.
3	Bonding between individual ice grains is moderate; Bonds are discernible and hold the sample together with light handling; Sample crumbles slightly with light handling.
4	Well bonded; Sample has strong bonding between individual ice grains; Sample maintains shape with handling and cutting; Sample has a tendency to break rather than crumble when handled roughly.
5	Sample is almost completely bonded; Bonds and grains are difficult to discern as the sample is nearly uniform; Pure ice would be 5+ as it would be entirely bonded. Sample does not crumble, but rather breaks if loaded to failure.

***Table 3.4**: Crust indices questions and possible answers used to describe additional properties of crusts*

Questions	Answers
Uniform vertically?	Yes/No (If no, describe)
Uniform horizontally?	Yes/No (If no, describe)
Well defined upper boundary, planar?	Yes/No (If no, describe)
Well defined lower boundary, planar?	Yes/No (If no, describe)
Near crust faceting?	Yes/No (If yes, describe)
Ice lens?	Yes/No (If yes, options: continuous or intermittent, top, middle, or bottom, planar or non-planar)

3.3.3.6 Thermal camera methods

During each field observation at Mt. Fidelity, a thermal photo was taken for each crust. The general methods follow Shea et al. (2012) which are briefly described here. The thermal photography was typically done at the end of the site visit after the pit wall was exposed. Because the thermal properties of the pit wall begin to change immediately after being exposed to the air, the pit wall was further excavated about 30 cm in the area being photographed immediately prior to taking the thermal photos. The camera was oriented normal to the planar pit wall. Achieving a planar pit wall can be difficult with brittle crusts as they tend to break in an undulated fashion, and can increase the variability of the temperature gradients around a crust as observed by the thermal camera. As soon as the pit wall was exposed, two marks were made in the pit wall using a crystal screen or another thin, warm tool. One mark was made above the crust and one below. The spacing of the marks was recorded, but a standard distance of 10 cm was typically used for thin crusts. These warmer marks provided the spatial reference necessary for analysis. An example is shown in Figure 3.13. The thermal photos were typically taken within one minute of exposing the pit wall. The camera was typically 30-40 cm from the pit wall. The operator was fully clothed and wearing gloves to minimize the effect of operator heating. The operator also had their face behind the camera for the same reason. Ideally several photos were taken during each observation because several may be discarded

during analysis. This often required cutting back the pit wall multiple times. All photos were taken between 1000 and 1200 h to reduce diurnal effects.

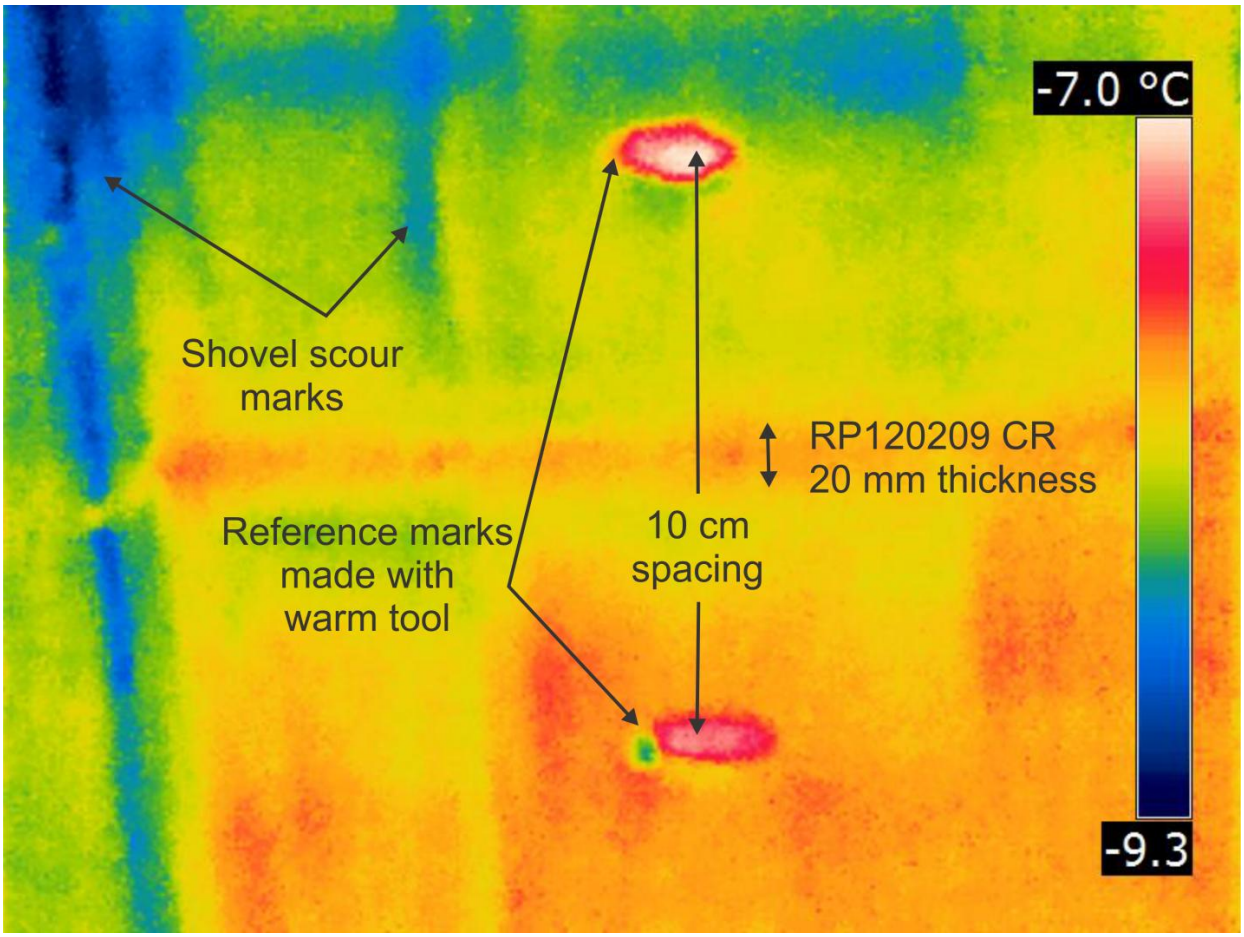

***Figure 3.13**: Example of a thermal photo of the 9 February 2012 sun crust (RP120209) taken 6 March 2012. Spatial reference marks were made on the pit wall using a warm tool and were typically 10 cm apart. Vertical shovel scour marks were avoided when placing vertical transects during the photo analysis.*

3.3.3.7 Thermal image analysis

There are numerous possible methods for the analysis of thermal images. A thermal image is a raster of temperature data with each pixel having a unique value. Each pixel has a spatial extent of roughly 0.25 mm^2 when the camera is 30 to 40 cm from the pit wall. Shea et al. (2012) calculated the gradient for each pixel that exists between the pixel and the eight adjacent

pixels. An early method attempted for this analysis was to take a row average of temperature values and create a vertical temperature profile based on these averages. The problem with using row averages is that they assume the crust is aligned horizontally and that the crust boundary is uniform across the crust. In reality, very few photos showed perfectly horizontally aligned crusts. Also, the isolation of the hard crust layers often resulted in undulations along the crust boundary, projecting both out of and into the pit wall. Using row averages would have reduced the magnitude of the temperature gradients at the boundaries of the crust.

3.3.3.7.1 Taking transects from thermal images

The method used to determine the temperature gradients around a crust without reducing the strength of these gradients by using row averages was to use single pixel vertical transects. An example is shown in Figure 3.14.a. A vertical transect was placed through the crust where the gradient appeared representative and unaffected by physical damage associated with pit wall excavation. The example in Figure 3.13 shows shovel scour marks that were avoided when placing the vertical transects. Because of the numerous sources of uncertainty with thermal photography, spatial variation of the layer, and the subjectivity of this method, five unique transects were used. When possible, these transects were taken from two unique thermal photos. The data from each transect was plotted as a vertical temperature profile as shown in Figure 3.14.b. The upper and lower deflection points were determined based on where the influence of the crust on the temperature profile ceases.

3.3.3.7.2 Calculating variables

Three variables were calculated from each temperature profile. The average upper temperature gradient ($|\nabla T_{Upper}|$) was calculated from the upper boundary of the crust to the upper deflection point (see Figure 3.14). The same thing was done below the crust for the average lower temperature gradient ($|\nabla T_{Lower}|$). The temperature difference (TD) between the crust and the surrounding snow was the horizontal difference between the crust maximum or minimum temperature and the line connecting the two deflection points. Each of these

variables was recorded for each of the five transects. This resulted in a range of values of each variable for each observation. The results were then plotted as box plots on a time series.

The typical spatial extent of the measurements of the upper and lower temperature gradients was 5-10 mm. The spatial extent of the average temperature difference (TD) was dependent on the thickness of the crust but was typically 50-150 % larger than the thickness.

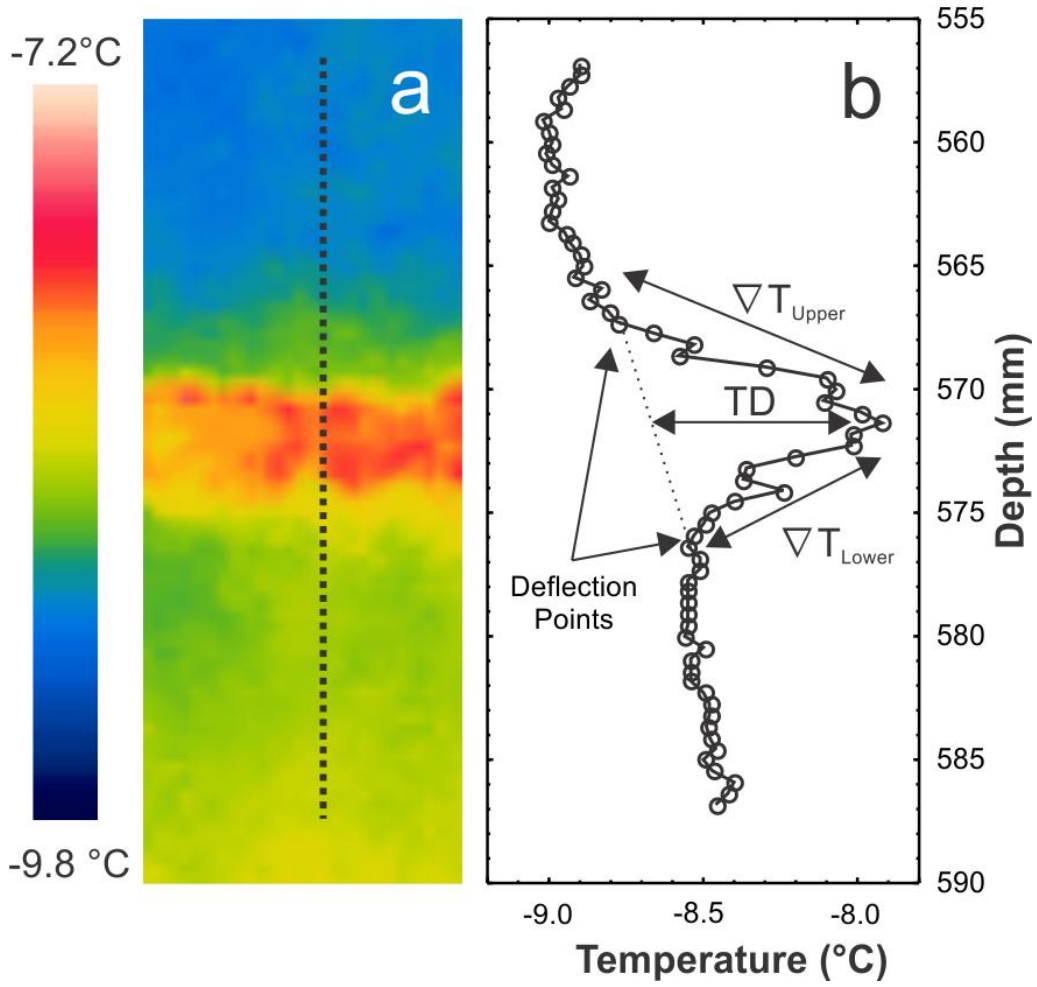

***Figure 3.14**: A thermal image from 11 January 2012 of the 3 January 2012 freezing rain crust (a). The pixels along the transect line produce the temperature profile (b). The average upper temperature gradient ($|\nabla T_{Upper}|$) and average lower temperature gradient ($|\nabla T_{Lower}|$) were calculated from the upper and lower deflection points and the temperature at the upper and lower boundary of the crust, respectively. The temperature difference (TD) was measured from the maximum temperature and the line connecting the upper and lower deflection points.*

3.3.3.7.3 Creating the dataset

A dataset was created that consists of crust burial depth, temperature gradients ($|\nabla T_{Upper}|$ and $|\nabla T_{Lower}|$), average crust temperature, average snow temperature, and measured air temperature. The average crust temperature and the average snow temperature were obtained from the thermal photos. The average snow temperature was calculated as the average of all the pixels from all five transects from each observation. Also included in the dataset are the differences between the air temperature and the snow temperature (T_{sn-a}), and the difference between the air temperature and the crust temperature (T_{cr-a}).

3.4 Safety

Safety is critical to a field-based avalanche research program. Regular travel in mountain terrain is required and workers are exposed to many mountain hazards including avalanches. Winter field work is governed by a safe work plan and workers complete annual safety training. Annual training was provided by professional mountain guides and included safe winter travel methods and avalanche rescue techniques. A “refresher” day of training was expected midway through each winter field season. Other annual training includes the safe use of snowmobiles and winter highway driving procedures. All workers had a valid advanced first aid certification.

Each morning prior to field work, researchers completed a daily hazard assessment. This hazard assessment involved collecting and analyzing data from the host and neighbouring operations including snowpack, weather, and avalanche observation data. Based on these data the researchers created a synopsis of the current conditions and a forecast for the day. A discussion of the conditions and hazards follows and the research objectives and terrain options were selected. Following the internal ASARC hazard meeting, researchers attended a morning safety meeting at the host operation. At these meeting, daily objectives were discussed and permission was obtained prior to going into the field. Regular radio check-ins were maintained with the host operation.

Standard safety equipment for travel in avalanche terrain included an avalanche transceiver, shovel, probe, radio, and first aid kit. Avalanche balloon packs were also mandatory when

travelling in complex terrain. Many of the regular study sites were located in simple or challenging terrain and balloon packs were not required but encouraged. Helmets were required when operating or riding as a passenger on a snowmobile. Adequate winter clothing and necessary gear for specific conditions were assessed each morning prior to departure. Avalanche transceiver checks were completed by all team members prior to travel in avalanche terrain.

3.5 Sources of uncertainty

Recognizing the sources of uncertainty is important because they help define the limits of the dataset. By understanding the sources of uncertainty we can attempt to minimize it. Each of the two parts of this project, formation and evolution, has their own unique sets of uncertainty which are described below.

There are sources of uncertainty that are common to both datasets and to snow science in general. This includes the subjective qualitative observations that are standard practice for snow profiles and field weather observations. Examples include hand hardness, grain type and size, snowpack tests, sky cover, wind speed and direction, and precipitation type and rate. This uncertainty in minimized through mentorship and ongoing training. The CAA Observation Guidelines and Recording Standards for Weather, Snowpack, and Avalanches (OGRS) (CAA, 2007) is used as the standard for these field observations.

3.5.1 Crust evolution uncertainty

Snow research inherently includes uncertainty associated with snow cover variability over terrain. This variability exists at all scales (Schweizer et al., 2008) but the evolution section of this project is primarily concerned with the variability at a slope scale. A slope scale is defined as the size of a typical avalanche slope with a length range of 5 – 100 m (Schweizer and Kronholm, 2007). The primary method used to reduce variability of melt-freeze crusts at regular study sites is the proper selection of the study sites as discussed in Section 3.3.1. A second method to reduce variability of the crust evolution dataset is to check the crust observation data and ensure the crust thickness is comparable to previous observations.

Thickness should not change substantially over time and therefore is a good observation for verification. If the thickness in one observation varies substantially from the typical observations it is not included in the crust evolution dataset.

There is uncertainty associated with having multiple researchers taking crust evolution observations. This includes subjective observations such as snow properties and the crust indices but also includes the methods used to measure quantitative data. This would include the speed at which the shear frame is pulled and the loading rate of the push gauge test. We aim to reduce this bias between observers by thorough pre-season training and ongoing field training. Mentorship is important to ensure new observers are using the proper methods to increase consistency of observations.

3.5.2 Crust formation uncertainty

The data used for crust formation came from the Glacier National Park ACS. Both the snowpack and manual weather observations were collected by avalanche technicians. Using externally collected data introduced a level of uncertainty into the analysis; however, ACS staff hold high standards for data collection and use standard and consistent snowpack and weather observation methods. New staff members are mentored for several years before they are able to collect data on their own. Variation amongst observers exists but it is assumed to be minimized by these practices.

Weather stations are generally reliable but there are inherent errors. The sensitivity of precipitation and snowfall gauges was the largest source of error for this part of the project. New snowfall was measured using a downward facing ultrasonic gauge and a snow board that was cleared on a semi-regular basis, typically a few times per week during periods of snowfall. Error may exist within the new snowfall measurements as the ultrasonic wave may be reflected from below the surface of low density snow. The reported accuracy for this sensor is ±1.0 cm (Campbell Scientific, 2013). Although the board is generally sheltered, new snowfall on the board can be subject to wind during snowfall which can create variation in snow depth. The precipitation gauge is a cylinder which contains anti-freeze to melt snow and the resulting

measurement is snow water equivalent (SWE) measured in millimeters. Strong wind can also result in precipitation not entering the precipitation gauge. Over time the precipitation gauge can have problems with ice forming if the anti-freeze is not maintained at the proper concentration. These variables are important because they were used to determine the formation periods of rain crusts. In cases of uncertainty, other nearby weather stations may be used for verification. Other sensors may have small associated errors but the results are less sensitive to the variability from there sensors. Data with obvious instrument errors were excluded from the data. For example, long-wave radiation data were excluded for the 2011-12 winter season dues to errors with the data logger programming related to the long-wave radiometer.

3.5.3 Errors in temperature and temperature gradient measurements

The tool with the most potential for error is the thermal camera. Proper training and understanding the fundamentals of thermal photography can reduce some of this uncertainty. Possible errors include the ability of the operator to create a smooth pit wall, air temperature, difference in air temperature and temperature of the crust and surrounding snow, orientation of grains along the pit wall, orientation of the camera relative to the pit wall, heat exposure from the operator, exposure time after excavating the pit wall, influence of warm or cold wind on the pit wall, and the ability to interpret the spatial reference in each photo. The current methods and potential errors are defined in Shea and Jamieson (2011), Shea et al. (2012), and Schirmer and Jamieson (in press). It was assumed that substantial error existed in the absolute temperatures produced by the camera. The absolute temperature of the pit wall changes immediately after exposure to the air but it is assumed that this change occurred evenly across the pit wall, although Schirmer and Jamieson (in press) question this assumption. This means that the accuracy of the temperature gradients should be higher than that of the absolute temperatures.

However, Schirmer and Jamieson (in press) identified errors associated with convexities and concavities when thermal images were taken of recently exposed pit walls. In less than 30 seconds after the pit wall was exposed when the air temperature and the average pit wall

temperature differed by as little as a few degrees, convexities changed temperature faster than planar areas, and concavities changed temperature more slowly. This can be seen in the score marks in Figure 3.13. With a high resolution thermal camera, this may also apply to pore spaces concavities. Because small concavities and convexities may occur where the hardness changes at layer boundaries when attempting to cut a planar pit wall, the magnitude of the temperature gradients at crust boundaries may be increased when the air and pit wall temperature are different by as little as a few degrees. This effect of air temperature on non-planar areas of the pit wall is called the non-planar air temperature effect (NP_Ta). This effect was discovered after the field work for this project was completed.

CHAPTER 4: DATA AND RESULTS

4.1 Crust formation data and results

This section presents data on weather and snowpack conditions during the formation of melt-freeze crusts. Three datasets were used, all based on historic snow profiles and weather data from Glacier National Park. The first investigated the meteorological conditions during formation. Each of the meteorological variables is presented separately for rain and sun crusts. The second used manual sky cover observations coupled with incoming long-wave radiation to determine the sky cover conditions during formation. The third dataset coupled meteorological variables and crust properties from historic snow profiles to determine how the formation conditions affected the resulting properties. A second smaller dataset of crust properties measured during winter fieldwork on Mt. Fidelity was also used for this purpose.

This section is divided into three primary topics. Sections 4.1.1 through 4.1.8 focuses on meteorological and aspect data, Section 4.1.9 focuses on crust properties resulting from formation, and Section 4.1.10 presents two cases studies on other formation events.

4.1.1 Crust formation dataset

The primary data used for the crust formation analysis was obtained from Parks Canada ACS in Glacier National Park. The data include snow profiles collected between November 2005 and April 2012 and weather data collected by automatic weather stations. The data analysis methods are described in Section 3.2.3. A total of 8 rain crusts and 31 sun crusts were included in the analysis of crust formation meteorological conditions. An additional 8 crusts were identified from the profiles but were excluded from the dataset because of difficulty in accurately determining formation periods or lack of weather data. An additional 13 crusts were identified that did not meet the criteria of appearing in at least three snow profiles. These are considered isolated events for the purpose of this project. For the dataset of crust properties and formation conditions, 8 rain crusts and 20 sun crusts were used.

4.1.2 Crust formation by aspect

Based on the occurrence of crusts in the historic ACS snow profiles, crust formation was plotted by aspect. Crusts were grouped by the major aspects flat, south, and north. South-east and south-west were grouped into south, and north-east and north-west were grouped into north. East and west aspects were excluded from this dataset. The flat aspect is unique because the study site on Mt. Fidelity was the only flat site used by the ACS. While this inherently limited the frequency of crust occurrences on flat aspects, full profiles were completed at least once per month. This contrasts to other sites where test profiles were common and occasionally only had data from the upper part of the snowpack. The resulting data for crust formation by aspect are shown in Figure 4.1.

Note that this dataset was reliant on the sites where the ACS chose to dig snow profiles. Certain aspects may have been sampled at a higher frequency if those aspects posed a higher avalanche hazard to the operation of the highway. Because melt-freeze crusts often create avalanche problems, it is assumed that once a crust formed on specific aspects, sufficient data would be collected from those aspects to reliably capture representative data for most melt-freeze crusts.

Sun crusts in this dataset always appeared on south aspects. Data from the Mt. Fidelity flat site is interesting because it is a regular ACS study site and it can be assumed that layer properties are close to uniform across the site. At the flat site, sun crusts were infrequent between early January and early March. There were some unique crust events that occurred at specific north aspect locations. These events were associated with warming in two possible ways. The first was typical atmospheric warming and the second was temperature inversions which are discussed as case studies. This warming was enough to create crusts on north aspects where it is assumed that the sun has not shone directly on the snow surface. These warming crusts did not appear at all north aspect locations and appeared to require special conditions. These warming crusts on north aspects were typically softer and thinner than the equivalent sun crust on south aspects formed during the same event.

Sun Crust Date	S	Flat	N
26-Nov-05			
20-Dec-05			
25-Dec-08			
29-Dec-09			
1-Jan-07			
9-Jan-10			
19-Jan-11			
27-Jan-09			
4-Feb-07			
8-Feb-12			
10-Feb-10			
13-Feb-06			
20-Feb-06			
22-Feb-09			
22-Feb-11			
24-Feb-10			
27-Feb-08			
1-Mar-09			
5-Mar-06			
6-Mar-09			
8-Mar-10		*	
9-Mar-11			
16-Mar-09		*	
17-Mar-10		*	
18-Mar-12			
23-Mar-08			
25-Mar-11		*	
26-Mar-12			

Rain Crust Date	S	Flat	N
31-Oct-09			
7-Nov-06			
1-Dec-08			
5-Dec-07			
18-Dec-09			
26-Dec-05			
3-Jan-12			
5-Jan-12			
13-Jan-06			
13-Jan-08			
4-Mar-09			
12-Mar-07			
20-Mar-09		*	

Figure 4.1*: Crust formation by aspect for sun crusts and rain crusts. Darker shading indicates that the crust appeared in two or more snow profiles. Lighter shading indicates that the crust appeared in one location only. These may be isolated events. Flat aspect profiles were taken at one location (Mt. Fidelity) on a monthly basis. An asterisk means the crust only appeared in the last flat profile of the season but was well developed (at least P- hardness or greater than 2 cm thickness) and would likely be present in a subsequent profile.*

The majority of crusts in the rain crust dataset appeared on all aspects. There were three exceptions. The first was the 12 March 2007 crust, which did not appear on any north aspect profiles because no profiles were observed on north aspects after the formation date. The second and third were the two 2009 March crusts, where there were profiles on north aspects after the formation dates. It is unclear whether the reason these crusts did not appear on north aspects was related to spatial variation during formation or site selection of the profiles.

4.1.3 Crust formation periods

The methods used to determine formation periods for rain and sun crusts are described in Section 3.2.2. The distributions of lengths of the resulting formation periods are shown in Figure 4.2. The range of lengths for rain crusts was much lower than for of sun crusts. By defining the sun crust formation period as the period between two precipitation events we ensured that all the conditions which may have influenced the formation were included. The downside of this method is that it included periods which did not affect crust formation such as periods of cloud cover and night conditions. In contrast, the rain crust formation criteria only included periods of rain precipitation. As a result, the range of values for sun crust formation periods were from 0.5 to 11.6 days compared with the much shorter rain crust formation periods, which ranged from 0.3 to 0.9 days, with an outlier of 2.7 days. This outlier was a warm period in early November, 2006, in which the air temperature was above 0 °C for three daytime periods and approximately 70 mm of precipitation fell.

4.1.4 Air temperature data

Air temperature data for rain and sun crust formation are shown in Figure 4.3. The range of values for maximum, average, and minimum temperatures during formation are shown for each crust type. The range of temperatures for rain crusts was lower than sun crusts. Of the eight rain crusts in the dataset, seven had a maximum temperature greater than 0 °C and the remaining crust had a maximum temperature of -0.4 °C. This contrasts with sun crusts which commonly formed at temperatures below freezing. The range of minimum temperatures for rain crusts was between -0.2 and -3.5 °C. This means it was possible for rain events to occur at local air temperatures below the freezing point, possibly due to a temperature inversion. The

contrast between maximum and minimum ranges of temperatures for sun crusts was substantial. This was likely a result of the long formation periods of sun crusts and the large diurnal temperature fluctuations that typically occur under clear skies. Figure 4.4 shows the ranges of standard deviations for rain and sun crusts. Rain crusts had a range between 0.2 and 2.0 °C compared with sun crusts which had a higher range of 1.5 to 6.8 °C.

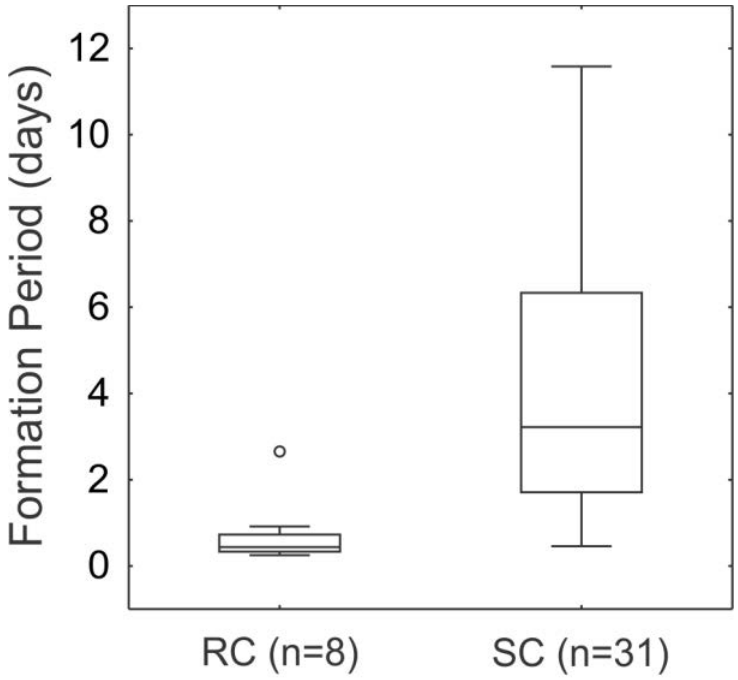

Figure 4.2*: Range of values for length of formation periods of rain crusts (RC) and sun crusts (SC). Rain crust formation periods are defined based on periods of accumulating liquid precipitation while the height of snow remains constant or decreases. Sun crust formation periods are defined as the period between two precipitation events. The box plots are defined with the centerline representing the median value, the box spanning the inter-quartile range, the whiskers spanning 1.5 times the inter-quartile range, and outliers are circles and greater than 1.5 times the inter-quartile range.*

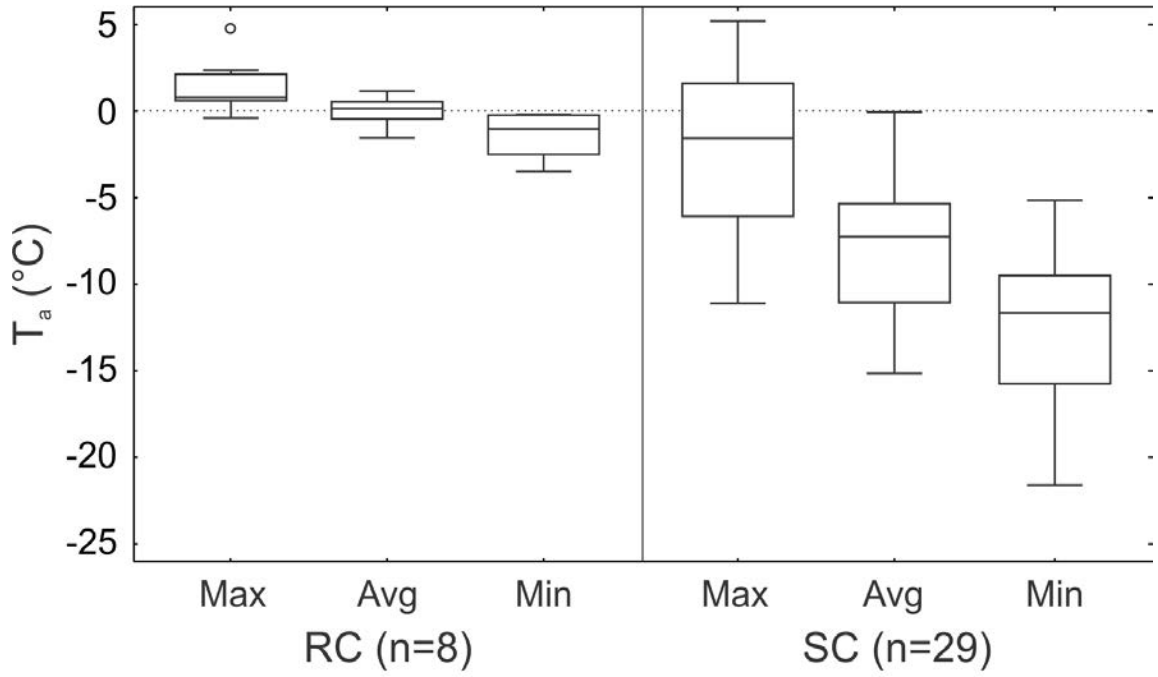

***Figure 4.3**: Range of values of maximum, minimum, and average air temperatures (T_a) during rain (RC) and sun crust (SC) formation periods. Box plots as per Figure 4.2.*

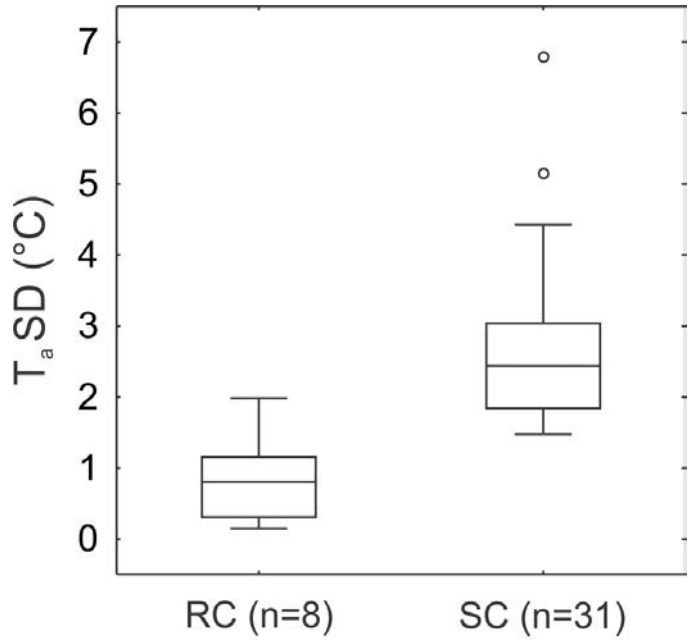

***Figure 4.4**: Air temperature standard deviation (T_a SD) values during rain (RC) and sun crust (SC) formation periods. Box plots as per Figure 4.2.*

4.1.5 Short-wave radiation data

The average daily insolation of short-wave radiation varies with the time of year due to the solar declination angle. Figure 4.5 shows the peak incoming short-wave radiation during rain and sun crust formation. Figure 4.6 shows the maximum cumulative daily incoming energy from short-wave radiation during rain and sun crust formation. The shape of the polynomial fit of these data roughly correlates to the insolation of short-wave radiation which follows a sinusoidal curve over one year. The fit of maximum daily cumulative incoming short-wave radiation energy for sun crusts had an R^2 value of 0.93. The fit of the peak incoming short-wave radiation had an R^2 value of 0.87. The minima of the quadratic fit for maximum cumulative daily incoming short-wave energy of sun crusts fell on December 21 which is the winter solstice, or the shortest day of the year. The minima of the quadratic fit for peak incoming short-wave radiation fell earlier on December 10. The fits for rain crusts had roughly the same shape as the sun crusts. The fit of maximum cumulative daily incoming short-wave radiation energy for rain crusts had an R^2 value of 0.80. The fit of the peak incoming short-wave radiation had an R^2 value of 0.35. This lower R^2 value was due to the way the formation period was defined. Because many rain crusts form over short periods, the peak incoming short-wave radiation may occur in the morning or evening rather than the middle of the day where it is expected to be the greatest. Maximum cumulative daily incoming short-wave radiation was therefore better at representing average conditions on days where rain crusts formed because the data can be compared to each other with more certainty.

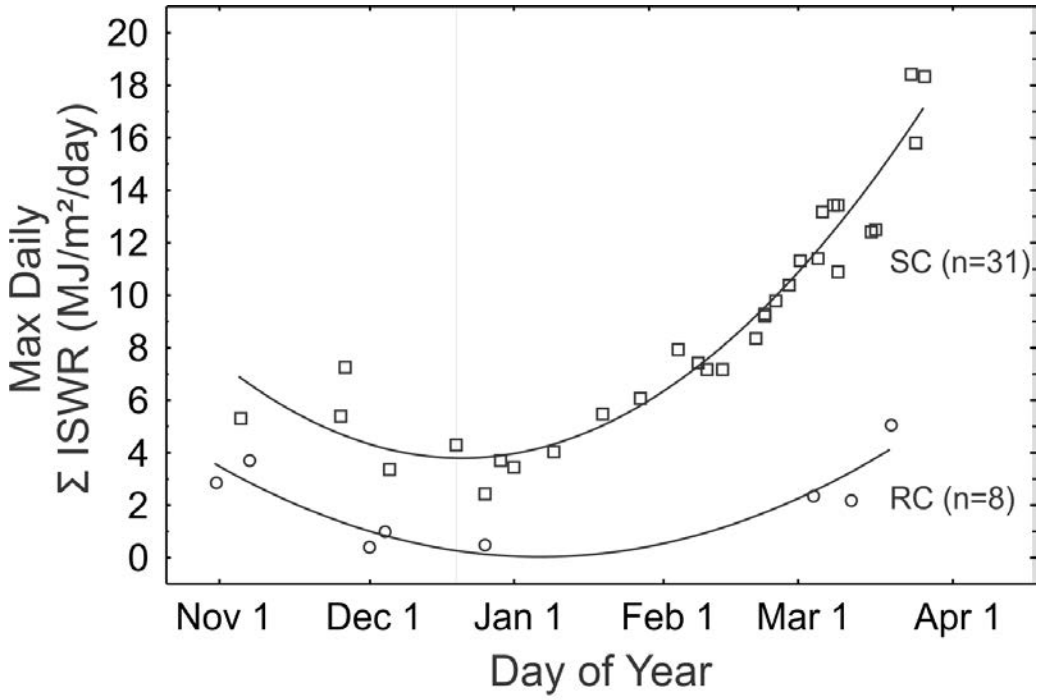

***Figure 4.5**: Maximum one day sum of incoming short-wave radiation (ISWR) during rain (RC) and sun crust (SC) formation periods.*

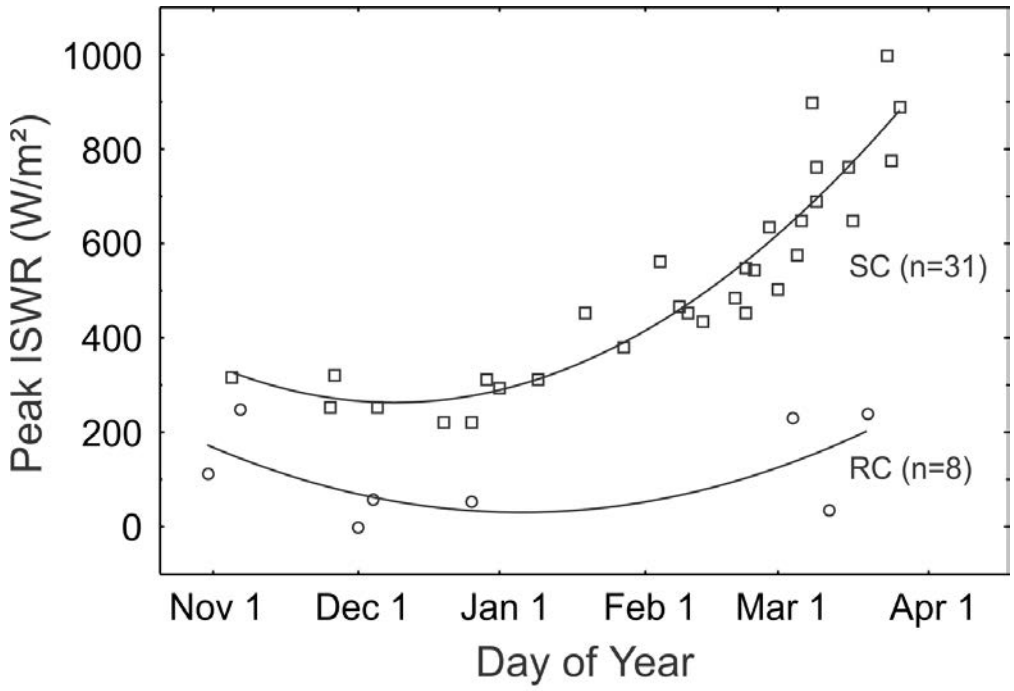

***Figure 4.6**: Peak incoming short-wave radiation (ISWR) during rain (RC) and sun crust (SC) formation periods.*

4.1.6 Sky cover data

Figure 4.7 shows the range of values of average incoming long-wave radiation for each of the classifications of sky cover. Figure 4.8 shows the standard deviation during the same period for each classification of sky cover. For each classification of sky cover there was a range of overlapping values. There is error associated with taking a point observation of sky cover rather than continual observations. Looking at the median values in Figure 4.7 we see an increasing trend. The median values of standard deviation shown in Figure 4.8 show a normal distribution which is expected because there should be less variability in cloud cover during clear, overcast, and obscured conditions.

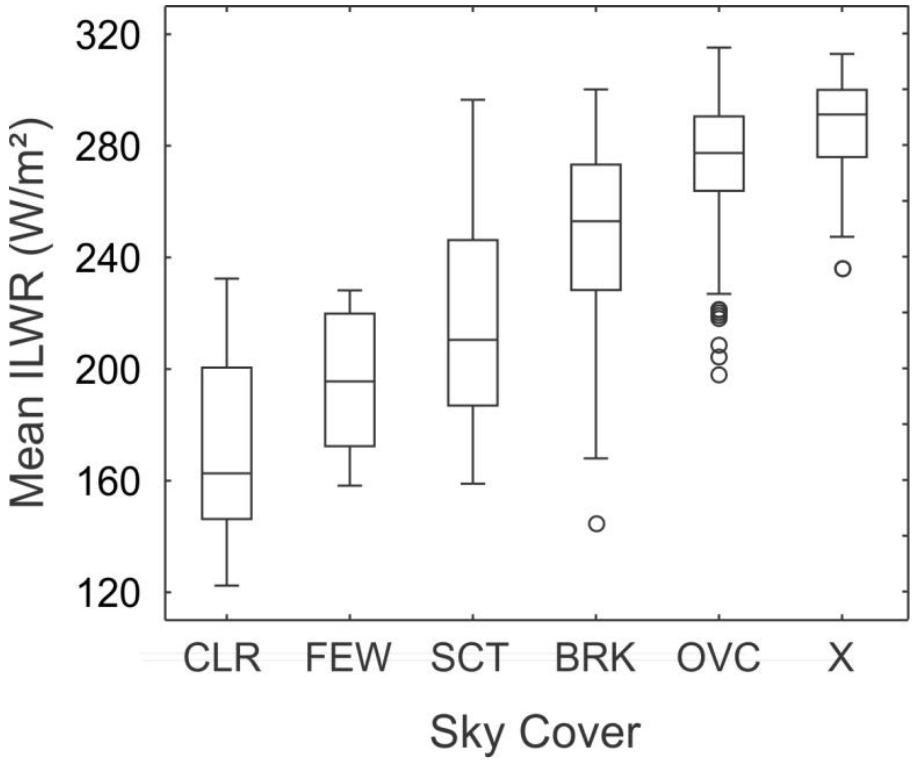

***Figure 4.7**: Relationship between sky cover and mean incoming long-wave radiation (ILWR). For each observation of sky cover, long-wave radiation data are collected for three hours before and after the observation. Long-wave radiation data has a 30 minute sampling frequency. Sky cover classifications as per Table 1.6. Box plots as per Figure 4.2.*

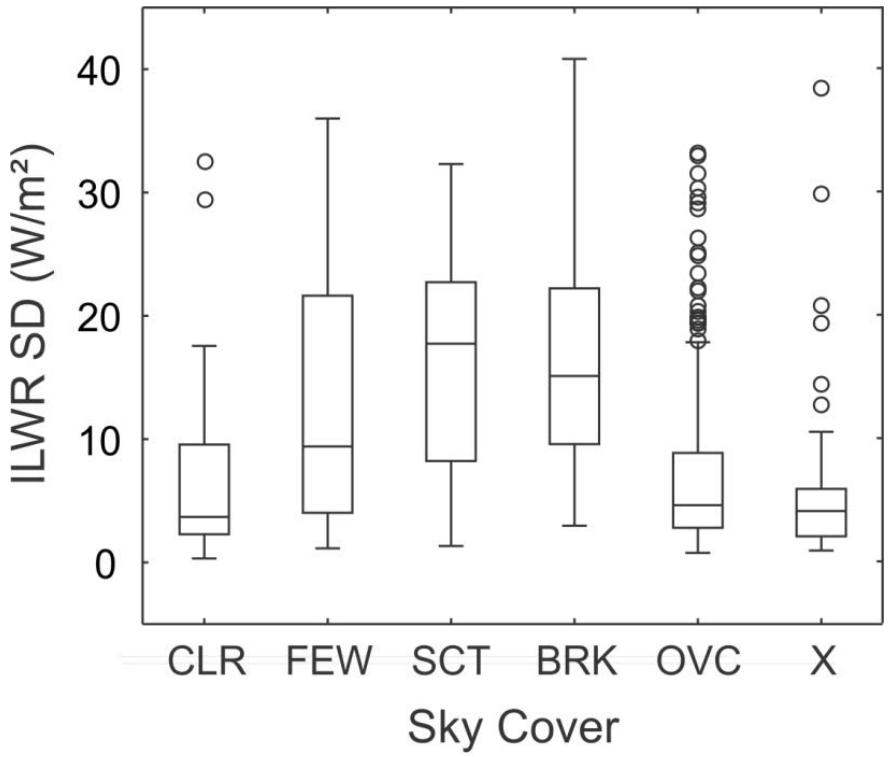

***Figure 4.8**: Relationship between sky cover and incoming long-wave radiation (ILWR) standard deviation (SD). For each observation of sky cover, long-wave radiation data are collected for three hours before and after the observation. Incoming long-wave radiation data has a 30 minute sampling frequency. Sky cover classifications as per Table 1.6. Box plots as per Figure 4.2.*

4.1.7 Incoming long-wave radiation

The range of values of maximum, minimum, and average incoming long-wave radiation during rain and sun crust formation are shown in Figure 4.9. The median sky cover values from Figure 4.7 are labeled on the y-axis for reference. The maximum and average values for rain crust formation all fell above the median value for overcast sky cover of 278 W/m². With the exception of the one rain crust that formed over 2.7 days, the remaining rain crusts formed during periods with minimum incoming long-wave radiation values that fell above the median value for broken sky cover. Rain crust formation was therefore typical during overcast cloud cover conditions with periods of broken cloud cover. Figure 4.10 shows the standard deviation of incoming long-wave radiation during rain and sun crust formation. For sun crusts there was

a much higher range of standard deviations and also a larger spread of values separating the maximum and minimum incoming long-wave radiation. This was likely caused by the long formation periods. The minimum incoming long-wave radiation values likely represent the actual conditions for sun crust formation because this was when there was the least cloud cover. Figure 4.11 shows the minimum incoming long-wave radiation during sun crust formation by day of the year. In November, late February, and March sun crusts formed under few and scattered cloud cover conditions. From December to mid-February sun crust typically formed during clear periods. This is likely related to the local solar zenith and azimuth angles. The shape of fit on Figure 4.11 is similar to the fit on Figure 4.5 and 4.6 but the minimum is shifted more towards mid-January.

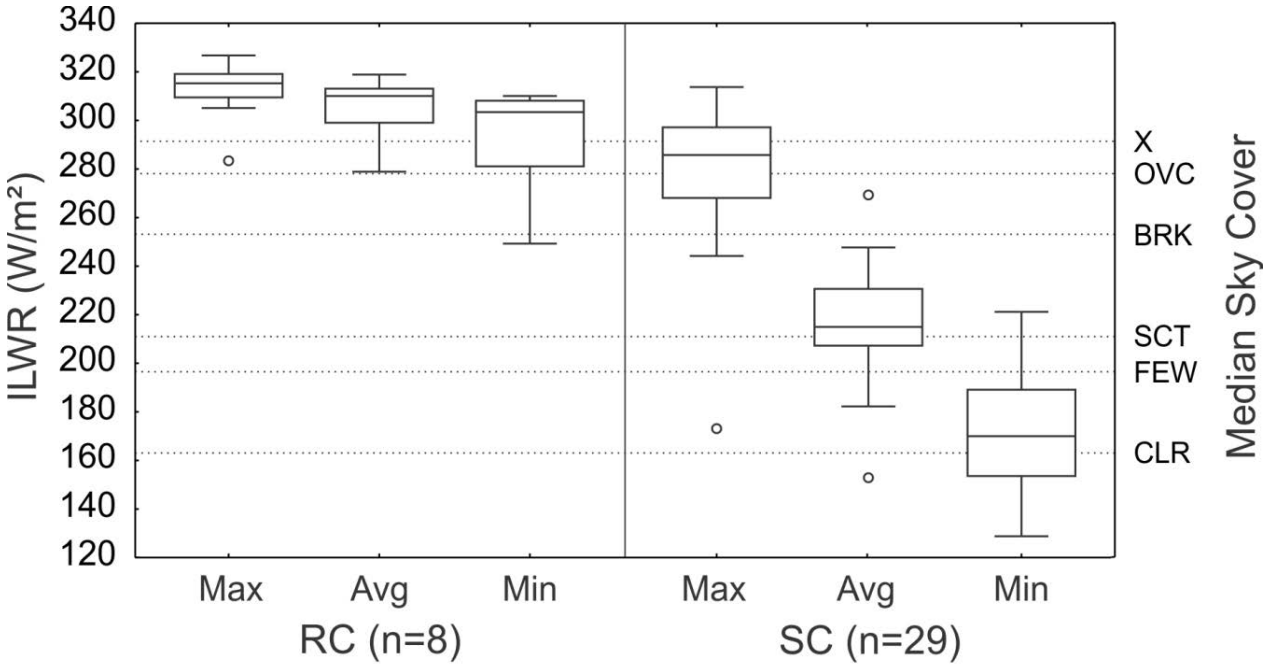

Figure 4.9*: Range of values of maximum, minimum, and average incoming long-wave radiation (ILWR) during rain crust (RC) and sun crust (SC) formation periods. Median sky cover values which were calculated in Section 4.1.6 are shown for reference on the right axis. Box plots as per Figure 4.2.*

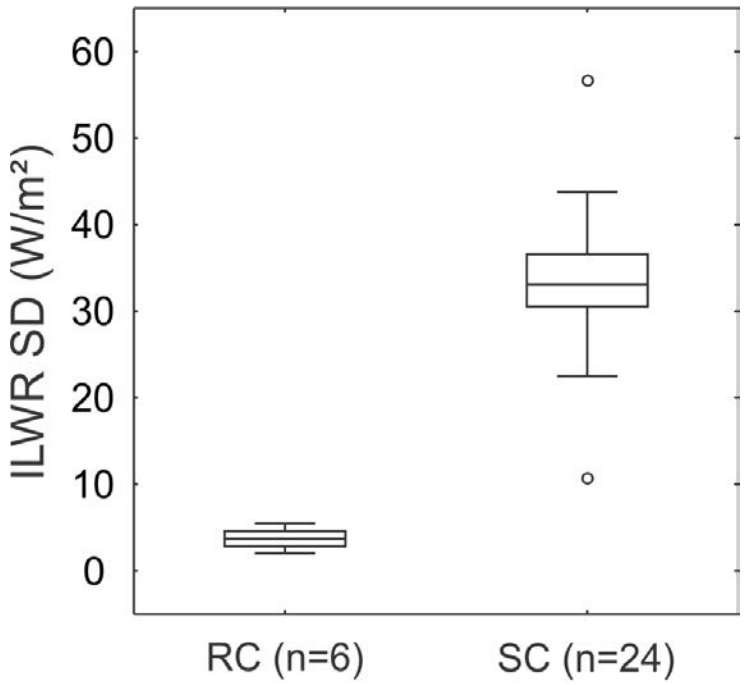

***Figure 4.10**: Range of values of incoming long-wave radiation (ILWR) standard deviation (SD) during rain (RC) and sun crust (SC) formation. Box plots as per Figure 4.2.*

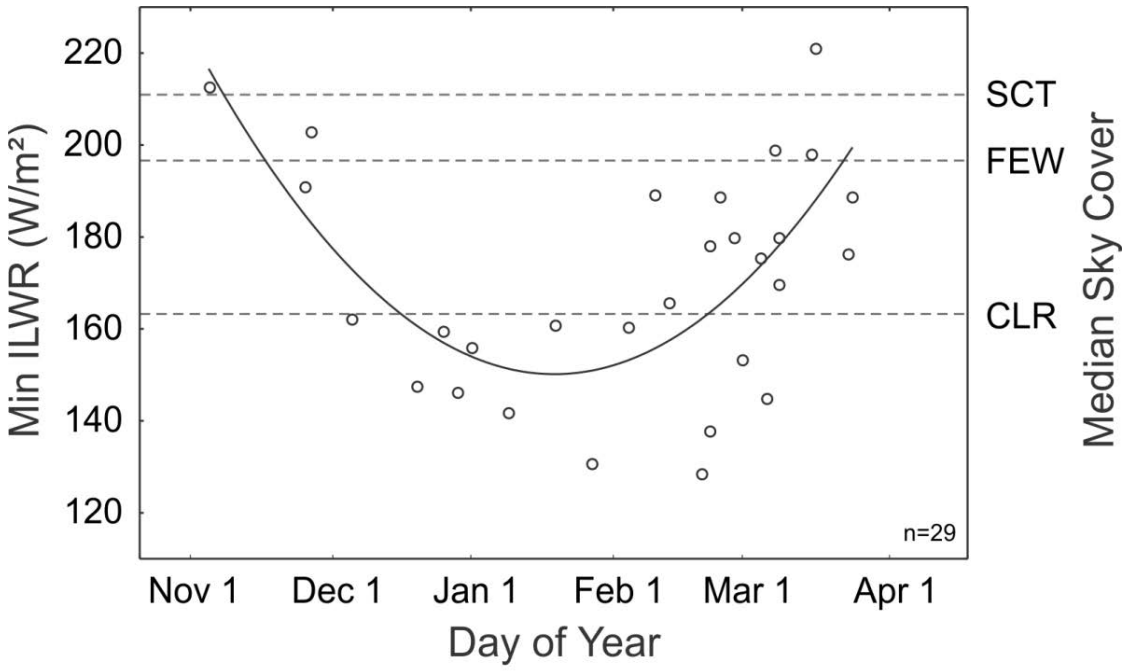

***Figure 4.11**: Minimum incoming long-wave radiation (ILWR) during sun crust formation by day of the year. Median sky cover values which were calculated in Section 4.1.6 are shown for reference on the right axis and includes clear (CLR), few (FEW), and scattered (SCT).*

4.1.8 Relative humidity

The ranges of values of maximum, minimum, and average relative humidity during rain and sun crust formation are shown in Figure 4.12. Rain crusts formed when average relative humidity was typically much closer to 100% than for sun crusts, although there are periods during sun crust formation where the RH did increase to 100%. The difference between maximum and minimum relative humidity was much greater for sun crusts. Figure 4.13 shows the distribution of relative humidity values during all precipitation events from 2006 to 2012. The relative humidity was above 90% during 95% of all precipitation events. This distribution was tested for precipitation events above and below 0°C separately and there was no substantial difference. Using the opposite approach, precipitation only occurred 30% of the time when the relative humidity was above 90%. Even when relative humidity was at 100%, measureable precipitation only occurred 57% of the time.

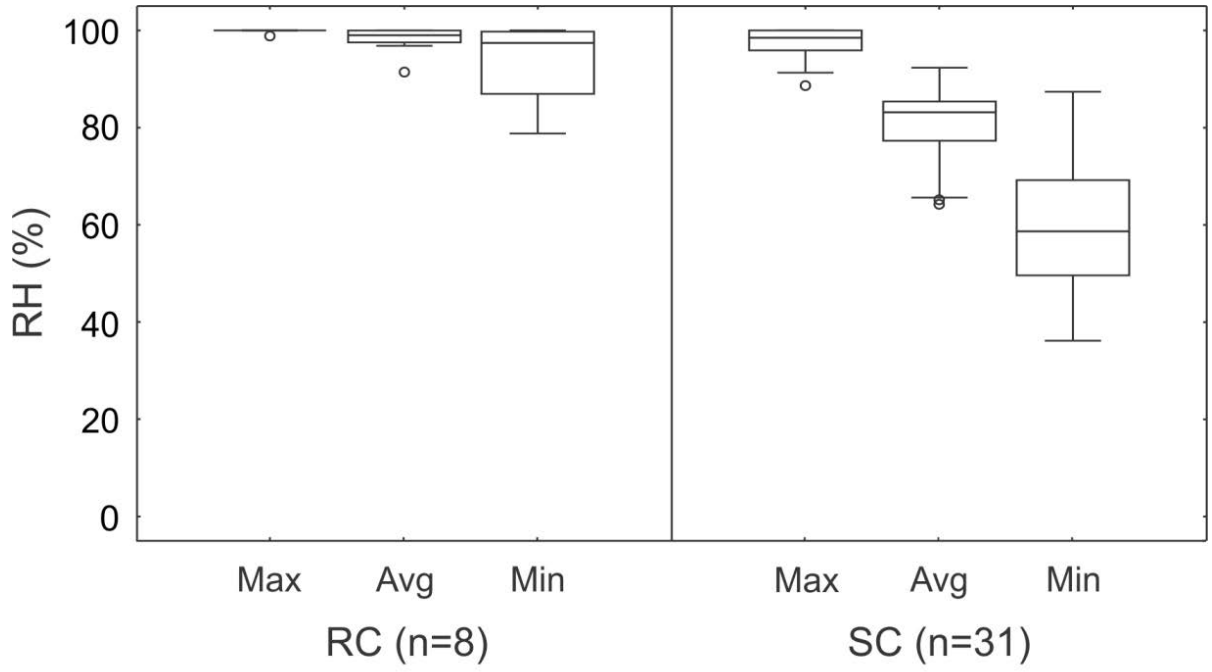

***Figure 4.12**: Distribution of values of maximum, minimum, and average relative humidity (RH) during rain (RC) and sun crust (SC) formation. Box plots as per Figure 4.2.*

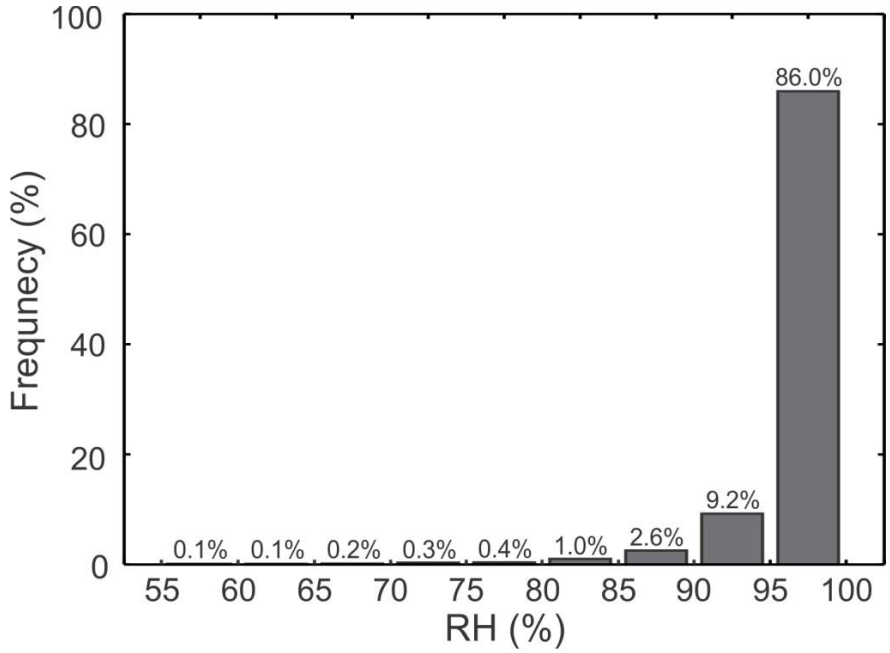

***Figure 4.13**: Distribution of relative humidity (RH) values (n=5615) during all periods of precipitation at Mt. Fidelity weather station from November 2006 to April 2012.*

4.1.9 Melt-freeze crust properties

Crust thickness and hand hardness are the two physical properties consistently recorded by the ACS in the historic snow profiles. These properties were coupled with the meteorological variables measured during crust formation to create a dataset of expected crust properties based on formation conditions. There was higher uncertainty associated with the crust property dataset than with other analysis for this project because the ACS snow profile sampling occurs at various locations, aspects, elevations, and slope angles. The methods used to filter the data to reduce this uncertainty are described in Section 3.2.3.1. From the filtered data, the average thickness and average hand hardness were calculated for each crust event. The resulting dataset consists of eight rain crusts and 20 sun crusts.

A second dataset was created using the sun crusts observed during winter field work by the author and colleagues during the winter of 2010-11 and 2011-12. This dataset improves upon the use of historic profiles because the crust properties were measured at the same south study site, which is roughly 500 m from the weather station. Unfortunately this dataset only includes five crusts and the hand hardness of these five crusts only varies between P and P+. Because of

the lack of hand hardness data, only thickness was considered from this dataset. There were not enough rain crusts observed at our treeline study site on Mt. Fidelity to create a dataset for rain crusts over the period of field work.

The Spearman correlation matrix for historic sun crusts is shown in Table 4.1. This dataset consists of 20 sun crusts. A smaller dataset (n = 5) was created for sun crusts observed at the south study site on Mt. Fidelity during field work between January 2011 and April 2012. The Spearman correlation matrix for this dataset is shown in Table 4.2. This dataset does not include incoming long-wave radiation variables because these data are lacking for three of the five crusts. For Tables 4.1 and 4.2, the number in each box is the Spearman R value and the red highlighted numbers have a p-value of less than 0.05.

***Table 4.1**: Spearman correlation matrix for sun crust formation properties (bold) and meteorological conditions based on historic snow profiles in Glacier National Park from November 2006 to April 2012 (n = 20). Day of the season begins on October 1. Spearman R values are shown and red highlighting indicates a p-value of less than 0.05.*

	Day of Season	**Mean Thickness**	**Mean HH**	Peak ISWR	Max Daily ISWR	Total ISWR	Max Ta	Formation Length	Total ILWR	Mean ILWR
Mean ILWR	0.28	0.27	-0.03	0.30	0.26	0.03	0.48	-0.31	-0.16	1.00
Total ILWR	-0.52	0.27	0.59	-0.49	-0.49	0.47	0.37	0.98	1.00	
Formation Length	-0.48	0.14	0.63	-0.45	-0.47	0.53	0.25	1.00		
Max Ta	0.03	0.17	0.33	0.02	0.06	0.29	1.00			
Total ISWR	0.34	0.11	0.67	0.41	0.35	1.00				
Max Daily ISWR	0.96	0.14	0.04	0.97	1.00					
Peak ISWR	0.95	0.05	0.05	1.00						
Mean HH	-0.05	0.25	1.00							
Mean Thickness	0.13	1.00								
Day of Season	1.00									

***Table 4.2**: Spearman correlation matrix for sun crust formation properties (bold) and meteorological conditions based on field data collected on Mt. Fidelity South Run between January 2011 and April 2012 (n = 5). Day of the season begins on October 1. Spearman R values are shown and red highlighting indicates a p-value of less than 0.05.*

	Day of Season	**Mean Thickness**	**Mean HH**	Peak ISWR	Max Daily ISWR	Total ISWR	Max Ta	Formation Length
Formation Length	-0.10	0.46	0.00	0.00	0.80	0.00	0.60	1.00
Max Ta	0.30	0.97	-0.58	0.10	0.90	0.10	1.00	
Total ISWR	0.90	0.21	-0.58	1.00	0.30	1.00		
Max Daily ISWR	0.40	0.87	-0.58	0.30	1.00			
Peak ISWR	0.90	0.21	-0.58	1.00				
Mean HH	-0.87	-0.74	1.00					
Mean Thickness	0.46	1.00						
Day of Season	1.00							

Based on the two different sun crust datasets, three meteorological variables were selected for analysis as well as the length of the formation period. This included total cumulative incoming short-wave radiation energy, total cumulative incoming long-wave radiation energy, and maximum air temperature. Figure 4.14 shows the relationships between the selected variables and physical properties for historic sun crusts. Figure 4.15 shows the same relationships for the field data. The historic dataset had stronger correlations between the meteorological variables and hand hardness whereas the field data had strong correlations between the meteorological variables and crust thickness.

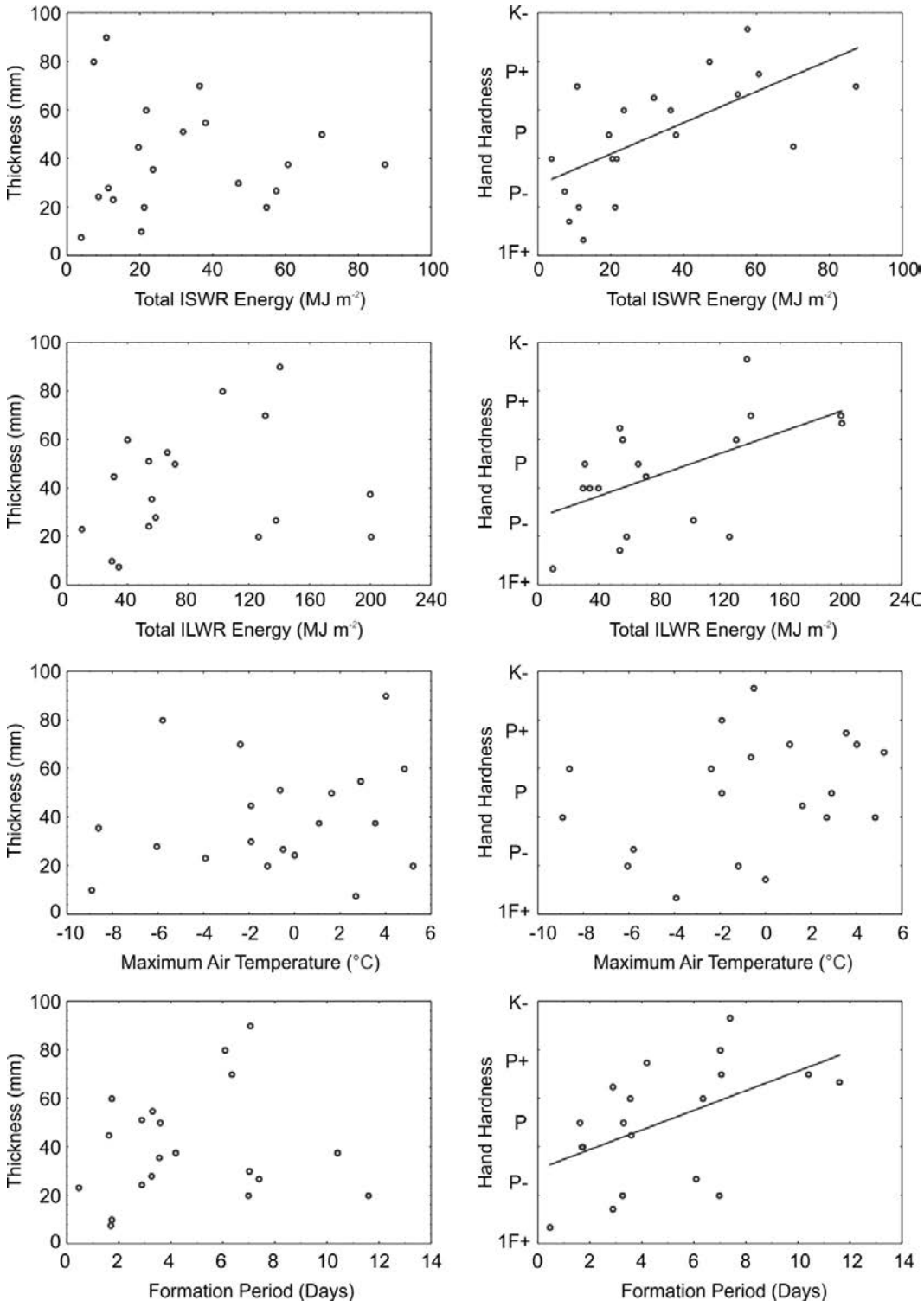

***Figure 4.14**: Relationships between selected meteorological variables and sun crust properties for the historic ACS sun crust dataset. Linear fit lines are shown for relationships with p-values less than 0.05.*

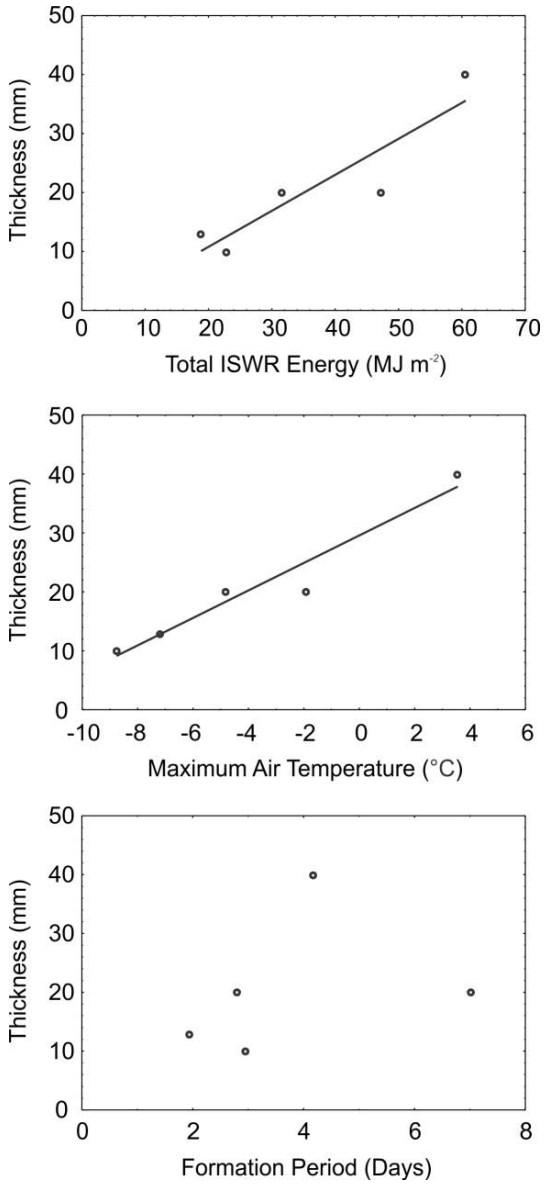

Figure 4.15*: Relationships between selected meteorological variables and sun crust thickness for the field data collected at the south study site on Mt. Fidelity between January 2011 and April 2012. Linear fit lines are shown for relationships with p-values less than 0.05.*

The average rain crust thickness and hand hardness were coupled with several meteorological variables during the formation period and the resulting Spearman correlation matrix is shown in Table 4.3. The number in each box is the Spearman R value and the red highlighted numbers have a p-value of less than 0.05.

***Table 4.3**: Spearman correlation matrix for rain crust formation properties (bold) and meteorological conditions based on historic snow profiles in Glacier National Park from November 2005 to April 2012 (n = 8). Day of the season begins on October 1. Spearman R values are shown and red highlighting indicates a p-value of less than 0.05.*

	Day of season	Max Ta	Mean ILWR	Total ILWR	Max Daily ISWR	Total ISWR	Peak ISWR	Formation Length	**Mean HH**	**Mean Thickness**	SWE
SWE	-0.33	0.83	0.45	0.64	-0.14	-0.05	-0.10	0.64	0.40	0.90	1.00
Mean Thickness	-0.10	0.74	0.26	0.69	0.19	0.24	0.19	0.69	0.50	1.00	
Mean HH	0.02	0.36	0.33	0.57	0.45	0.21	0.12	0.57	1.00		
Formation Length	0.00	0.62	0.05	1.00	0.12	0.12	0.07	1.00			
Peak ISWR	-0.02	0.02	-0.74	0.07	0.88	0.98	1.00				
Total ISWR	-0.14	0.05	-0.64	0.12	0.90	1.00					
Max Daily ISWR	0.12	0.02	-0.55	0.12	1.00						
Total ILWR	0.00	0.62	0.05	1.00							
Mean ILWR	-0.17	0.12	1.00								
Max Ta	-0.31	1.00									
Day of season	1.00										

The relationship between crust thickness and the two statistically significant variables – precipitation and maximum temperature - is shown in Figure 4.16 with straight fit lines for reference. The relationship between hand hardness and the two variables is also shown. There was a positive relationship between thickness and precipitation, which appears to be linear. There is one outlier, a rain event lasting 2.7 days in early November of 2006. This outlier was excluded from the linear fit line. There is also a positive linear relationship between thickness and maximum air temperature. Both precipitation and maximum air temperature appear to increase with hand hardness but the correlation is not significant.

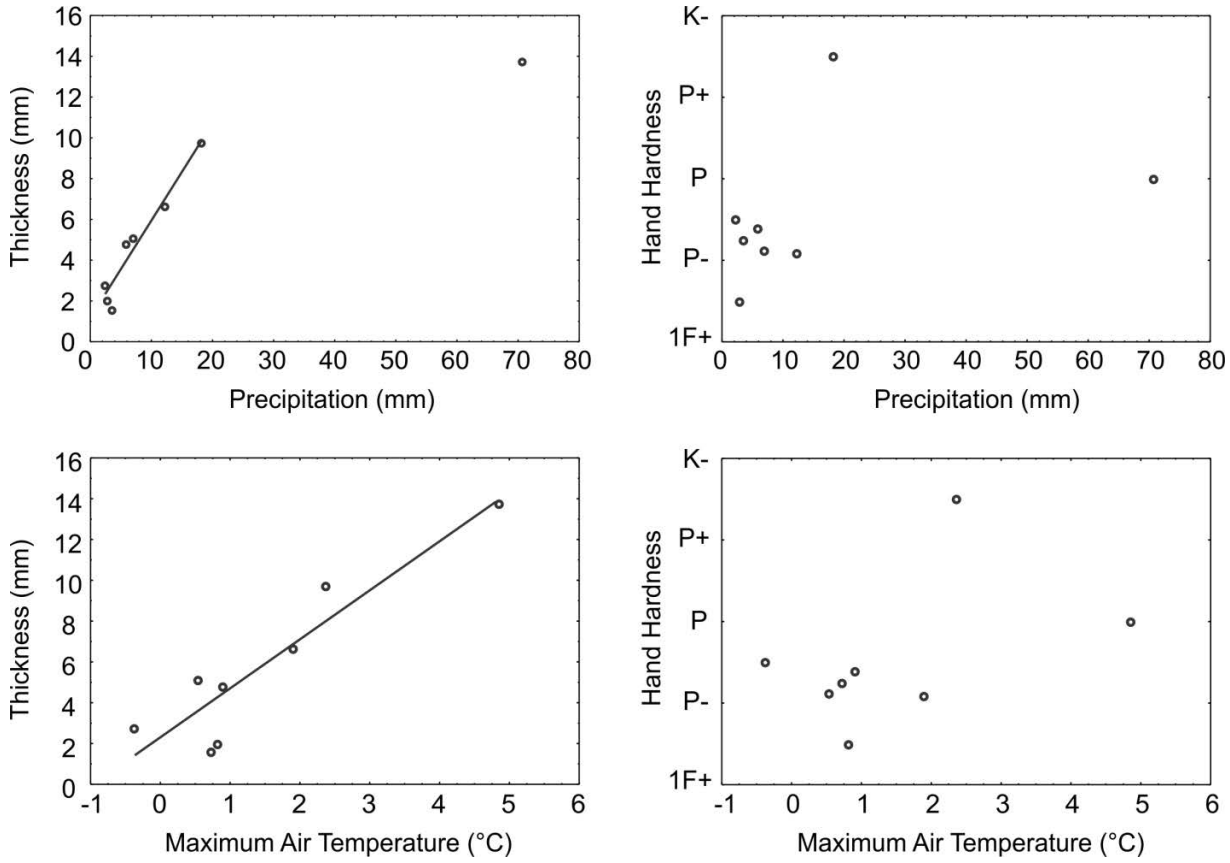

***Figure 4.16**: Relationship between selected meteorological variables and rain crust properties. Rain crust thickness is positively correlated to precipitation and maximum air temperature during formation.*

4.1.10 Crust formation case studies

Two crust events were selected for further investigation as case studies because they highlight other important formation processes. The case studies include the 3 January 2012 freezing rain crust and the 26 March 2012 sun-temperature crust complex.

4.1.10.1 Rogers Pass 3 Jan 2012 freezing rain crust

Between the afternoon of 2 January 2012 and the morning of 3 January 2012, a thin freezing rain crust formed at treeline on Mt. Fidelity in Glacier National Park. Figure 4.17 shows air temperature data at selected weather stations and precipitation data from Mt. Fidelity during the crust formation period. The crust thickness varied between 3 and 4 millimeters at the south, north, and flat study sites. The specific formation period cannot be determined from the

weather station data at Mt. Fidelity using the precipitation gauge and snowfall sensor, likely due to the minimal amount of precipitation required to form this thin crust. During most of the day on 2 January there was a temperature inversion recorded by the various weather stations. The Roundhill weather station (2052 m), which is also located on Mt Fidelity, was roughly 2 °C warmer than the lower Mt. Fidelity weather station (1905 m). The Rogers Pass weather station (1315 m) is up to 10 °C colder than Roundhill. The inversion begins to break down at 16:00 on 2 January and by 11:00 on 3 January the temperatures had returned to normal conditions with colder temperatures at higher elevations. The first precipitation was recorded at 19:00 on 2 January and light precipitation was recorded through the night with accumulations of 5.1 mm by the morning of 3 January. The crust observation taken at 10:30 on 3 January at the south study site has the crust buried beneath 1 cm of new snow. This likely means the crust formed near the end of the precipitation period but there is too much uncertainty to determine the exact time of formation. In Figure 4.17, the period of temperature inversion is highlighted in dark grey (including light grey period) and the potential formation period is highlighted in light grey. The uncertainty in interpreting freezing rain crusts from this weather data stems from the relatively small amounts of precipitation required for freezing rain crust formation. Several other expected freezing rain crusts, which were excluded from the dataset due to inability to interpret the formation period, also showed the presence of temperature inversions. Therefore, temperature inversions appear to be a useful indicator of the potential for freezing rain formation.

4.1.10.2 Rogers Pass 26 March 2012 sun-temperature crust

Between 22 March and 26 March a crust complex formed on all aspects, likely caused partly by solar radiation and partly by warm air (convective heat flux). This was also the only crust that formed at the flat study site while the snow surface temperature gauge and reflected short-wave radiation sensor were operational. For these reasons it makes an interesting case study. Figure 4.18 shows the weather data during the formation period and the snow profile data for the south, flat, and north sites.

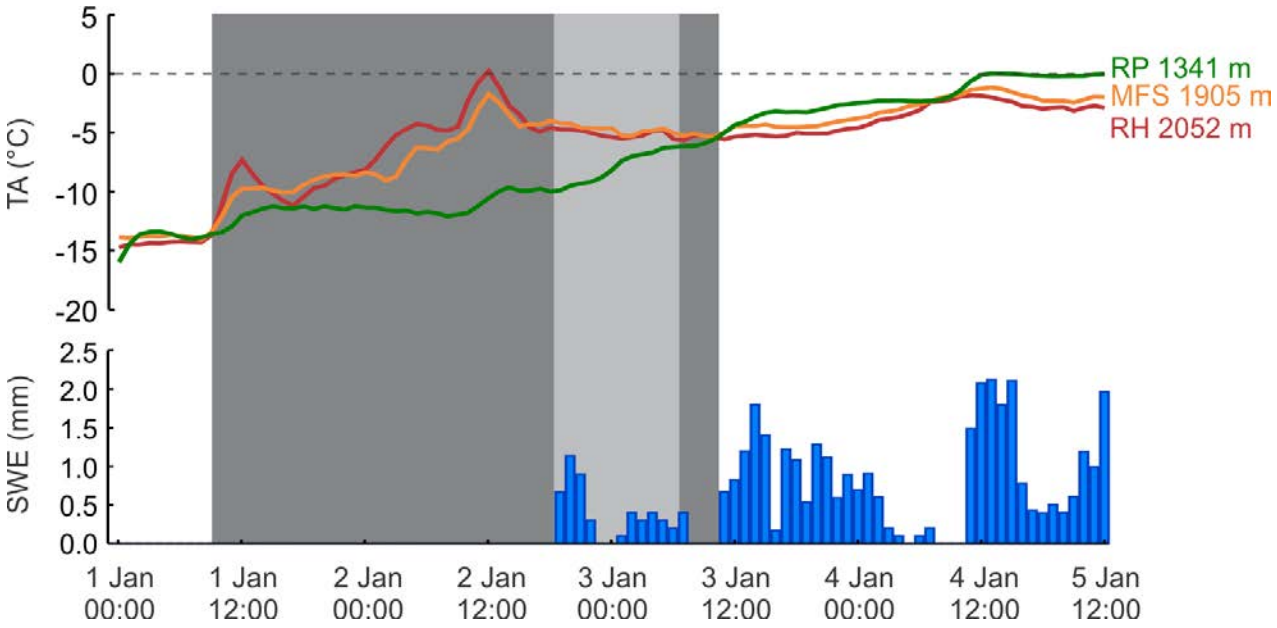

***Figure 4.17**: 3 January 2012 freezing rain formation data. Air temperature (TA) is shown for three weather stations in Glacier National Park. The temperature inversion is highlighted with dark grey and the possible formation period is highlighted in light grey. Precipitation (SWE) is recorded at the Mt. Fidelity weather station and is displayed hourly.*

From the weather data the two components of formation were identified. The peak incoming short-wave radiation occurred on 23 March and the air temperature exceeded 0 °C on both 25 March and 26 March. While the snow surface temperature did not quite reach 0 °C on these days, it was within 1 °C. The effect of the strong incoming short-wave radiation on 23 March was that the snow surface temperature exceeded the air temperature. On each of the formation days, the peak surface temperature corresponded to the peak incoming short-wave radiation. On each day there was also a lag in the peak air temperature relative to the peak surface temperature and peak incoming short-wave radiation. On 25 and 26 March there was likely some intermittent cloud cover which caused lower values of incoming short-wave radiation. The incoming long-wave radiometer was not functioning during this period so the cloud cover at the study site could not be determined for the peak periods of incoming short-wave radiation. However, manual sky cover observations from Rogers Pass (1315 m) showed scattered sky cover at 09:35 on 25 March and thin, broken cloud cover at 10:30 on 26 March. The increased cloud cover and increasing air temperatures were likely related to an

approaching warm front replacing a high pressure system. This is a common weather system for the region and generally results in precipitation.

Reflected short-wave radiation data were recorded during this formation period. The albedo of the snowpack surface is the ratio of the reflected short-wave radiation to the incoming short-wave radiation. Table 4.4 shows the albedo during the formation period. Mid-day albedo was calculated as the average albedo between 11:00 and 13:00, the period with the highest incoming short-wave radiation. Total daily albedo was calculated as the average of the entire day.

***Table 4.4**: Albedo values during the formation of the 26 March 2012 sun crust. Mid-day albedo is the average between 1100 and 1300 hours. Total daily albedo is the average of the entire day.*

	Mar 21	Mar 22	Mar 23	Mar 24	Mar 25	Mar 26	Mar 27
Mid-day albedo (%)	94.7	93.3	88.2	86.1	86.7	85.9	-
Total daily albedo (%)	92.7	93.4	88.0	83.3	83.8	84.9	-
Conditions	Snowfall		Formation Period				Snowfall

The resulting crusts can be seen in the profiles in Figure 4.18. At the north site the crust was 1 cm thick with a hand hardness of 1F. This crust was attributed entirely to warming. The north crust was thinner and less hard than the other two sites. Both the flat and south sites had a crust complex, or a crust made up of several unique layers. At the south and flat sites, the crust was comprised of a crust sandwich with a harder layer at the top and bottom of the crust and a softer layer between. This structure may be related to the two unique contributions of solar radiation and convective heat transfer, and is discussed further in Section 5.1.8.

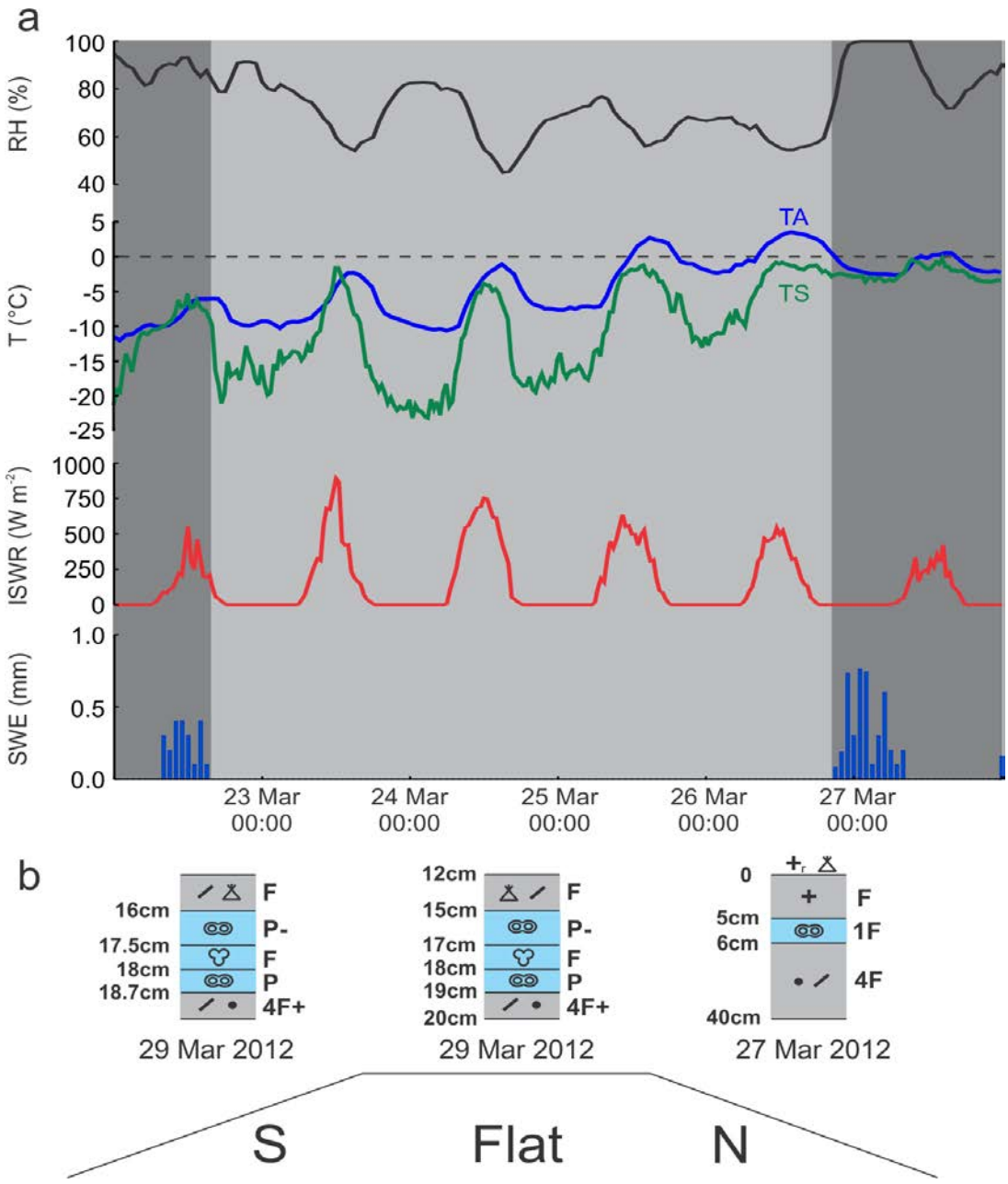

***Figure 4.18**: Meteorological conditions during the formation of the 26 March 2012 sun crust (a). The formation period is highlighted in light grey. Meteorological variables include relative humidity (RH), air temperature (T_a), incoming short-wave radiation (ISWR), and snow-water equivalent precipitation (SWE). The resulting snow profiles by aspect (b) have the crusts highlighted in light blue. The left axis of these profiles in the depth from the surface, the center is the snow grain type, and the right axis is the hand hardness. Snow grain type symbols are defined in Table 1.2.*

4.2 Crust evolution data and results

The crust evolution dataset is based on two seasons of observations at Mt. Fidelity in Glacier National Park, British Columbia, and Mt. St. Anne near Blue River, British Columbia. The data collected included physical measurements, crust indices observations, and thermal photos.

4.2.1 Crust evolution data summary

Crust evolution data were collected in the field as described in Section 3.3. Table 4.5 shows a summary of the data collected during the 2011-12 winter field season. Some additional density time series data from 2010-11 were also used in the analysis and is discussed further in Section 4.2.3.1. Time series data for each crust are presented separately in Figures 4.19 through 4.24. The data are presented in this format because it is easy to visualize how each variable evolves relate to each other for each unique crust event. Each set of physical properties (density, shear strength, and resistance) are also plotted separately in Figures 2.25 through 4.30. This way the evolution of each property can easily be visualized and several crusts can be compared.

Table 4.5*: Data collected during the 2011-12 winter season. For density, shear strength, thin-blade resistance, and crust indices, the value in the table indicates the number of unique days on which the property was observed (# obs.).*

Crust ID	Study Location	Crust Type	Elevation Band	Duration (Days)	Density (# obs.)	Shear Strength (# obs.)	Resistance (# obs.)	Crust Indices (# obs.)
3 Jan	Mt. Fidelity	Freezing Rain	Treeline	76	-	8	10	12
9 Feb	Mt. Fidelity	Sun	Treeline	56	10	9	6	10
12 Feb	Mt. St. Anne	Sun	Treeline	45	6	5	4	6
28 Feb	Mt. Fidelity	Sun	Treeline	36	6	4	3	6
5 Mar	Mt. St. Anne	Rain	Below Treeline	15	3	-	3	3
26 Mar	Mt. Fidelity	Sun	Treeline	9	4	-	3	4

4.2.2 Crust evolution case studies

The data for each of the six crusts tracked during the 2011-12 season are presented here. The various properties are presented as stacked time series. This allows the various properties to be easily compared for each crust event. Density data for these time series only includes measurements prior to the influence of free-water. Data for crust density before and after the presence of free-water are shown in Figure 4.26. The time series data are also grouped separately by each physical property and presented in Section 4.2.3 through 4.2.6. Linear fit lines obtained through least square linear regression are used throughout this analysis to display general trends.

4.2.2.1 Rogers Pass 3 January 2012 (RP120103) freezing rain crust

The specific formation conditions for this crust are described in Section 4.1.10.1. This crust was tracked at the flat site until 19 March 2012, for a total period of 76 days. Figure 4.19 shows the data collected during this period. Steady increases in thin-blade resistance and shear strength at the upper interface were recorded. Steady increases in the upper bonding index were likely related to the increases in shear strength at the upper interface.

This crust underwent near-crust faceting which began between 16 January 2012 and 19 January 2012 when air temperatures reached a low of -26 °C. On 16 January 2012 the crust was 77 cm below the snow surface. The faceting occurred at the lower interface of the crust. The grain evolution above, below, and within this crust is shown in Table 4.6. This changed the properties of the lower 2 mm of the 4 mm thick crust. As a result, two separate crust lamination values were recorded for each 2 mm thick layer as shown in Figure 4.19. By the end of February the two parts of the layer had merged back into a single layer. During the period of faceting, the lower bonding index reached a low of 1. As the air temperatures returned to seasonal values, progressive rounding of the faceted layer was observed. Over time the lower bonding index and the internal lamination of the lower part of the crust increased.

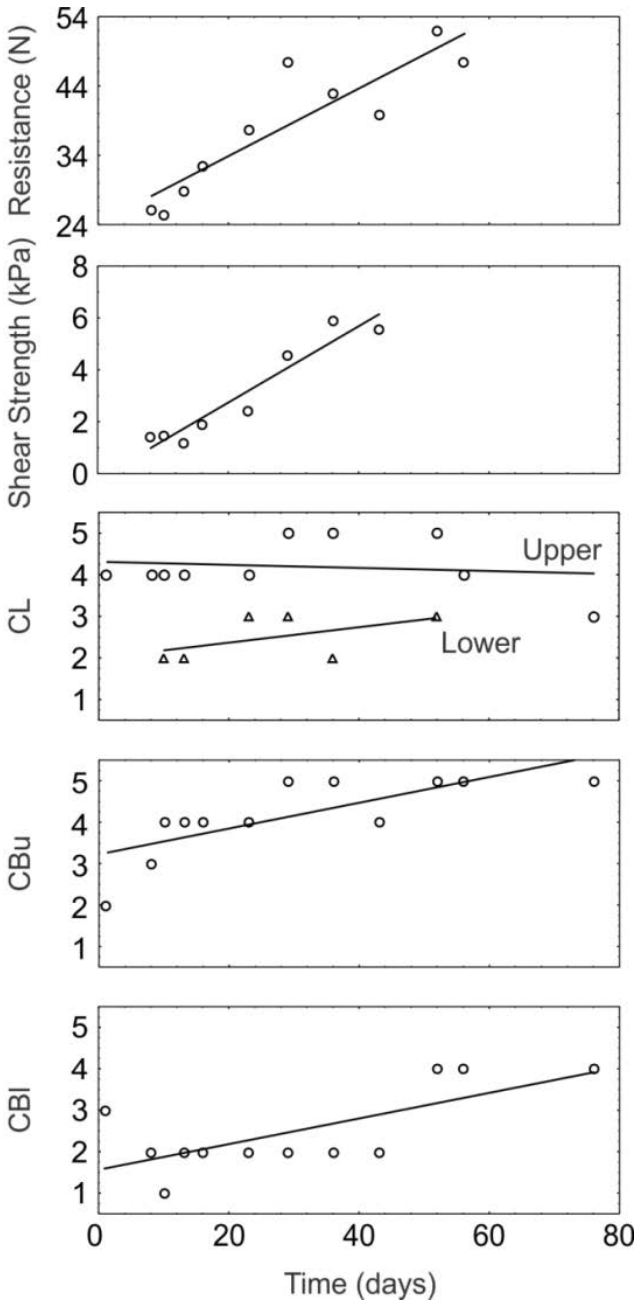

Figure 4.19*: Time series data for the 3 January 2012 freezing rain crust at the flat study site on Mt. Fidelity in Glacier National Park, BC. In sequence, the plots are the thin-blade resistance test, the shear frame test, crust internal lamination index (CL), crust bonding index upper (CBu), and crust bonding index lower (CBl). The crust internal lamination index (CL) has two parts, upper and lower, following the crust faceting that occurred in mid-January. Each of the upper and lower parts represents 2 mm of the 4 mm thick crust. By the end of February the two parts had merged.*

4.2.2.2 Rogers Pass 9 February 2012 (RP120209) sun crust

During early February, 2012, there was a long period of clear weather associated with a high pressure system. This clear weather formed two important persistent weak layers. A sun crust formed on south aspect slopes and a thick layer of surface hoar formed on all aspects. At our South study site the basic formation was a 20 mm thick crust with surface hoar crystals up to 9 mm overlying it. In areas with less exposure to sun, the surface hoar averaged between 20 and 30 mm. The crust formed over seven days with a peak incoming radiation value of 470 W m^{-2} occurring on 7 February. No crust formed at the flat and north study sites.

The crust was tracked until 4 April for a total period of 56 days. Ten observations were made during this period and the data are presented in Figure 4.20. The general trends show increasing density, thin-blade resistance, and shear strength over time. The internal lamination shows a slight decreasing trend but it remained between 3 and 4 for the entire period. The lower bonding index started high and increased slightly over time. There was no instability associated with the lower interface. The upper interface was interesting because of the surface hoar that overlaid the crust. The upper bonding index remained at 2 or below for the entire observation period. During this period there were multiple avalanche cycles on this layer. Even after the layer was deep in the snowpack, slab avalanches were still occurring on this layer in the Glacier National Park area. These deep persistent avalanches were difficult to trigger but the propagation potential of the layer remained adequate for slab avalanche release. The upper bonding index remaining at 2 may have represented the continued potential for this layer to release avalanches. Propagation saw tests (PST) (CAA, 2007) were completed on the same crust/surface hoar layer at an adjacent south facing study site on Mt. Fidelity by Horton et al. (2012). The results showed little change to the propagation potential of the surface hoar layer over the same observation period. While the shear strength of this layer did increase, the rate of increase was relatively low and does not appear to have changed the propagation potential of the layer. The shear strength of the layer and the rate of change are discussed further in Section 4.2.4.

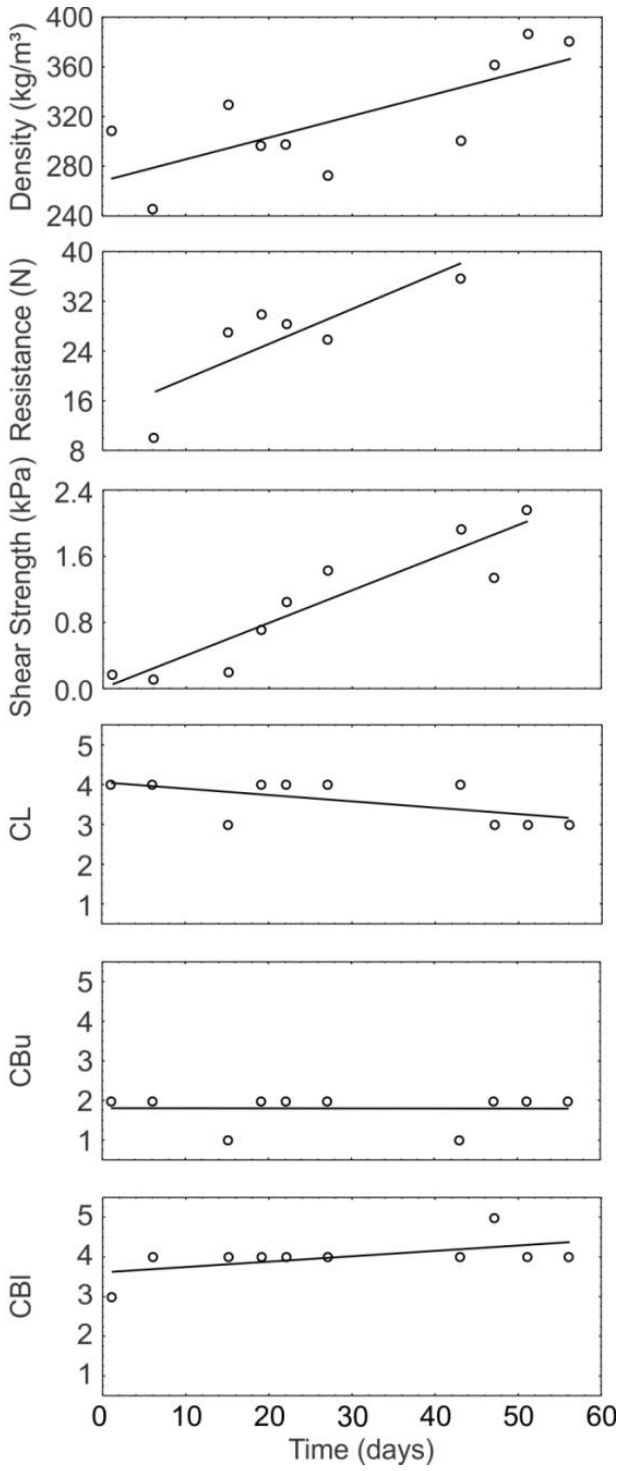

Figure 4.20*: Time series data for the 9 February 2012 sun crust at the south study site on Mt. Fidelity in Glacier National Park. In sequence, the plots are density, the thin-blade resistance test, the shear frame test, crust internal lamination index (CL), crust bonding index upper (CBu), and crust bonding index lower (CBl).*

4.2.2.3 Blue River 12 February 2012 (BR120212) sun crust

Five days of clear weather in mid-February 2012 formed a sun crust on Mt. St. Anne. This crust only formed at our south study site. The sun crust was typically 24 mm thick with small surface hoar above, typically 1-2 mm grain size. The formation was similar to the RP120209 sun crust but the clear period both started and ended several days later.

Data were collected until 28 March for a period of 45 days. However, due to data quality problems resulting from inconsistent site selection, the data prior to 27 February were discarded. A total of six observations were included in the dataset and these data are shown in Figure 4.21. The evolution trends were similar to the RP120209 sun crust. Shear strength of the surface hoar overlying the crust increased at a similar rate. Density appears to have increased over time but there is higher variability between observations than with other crusts in the dataset which causes more uncertainty in this data. Resistance was almost unchanging but again there was more variability between observations which increased the uncertainty associated with these data. Crust lamination and the upper bonding index remained unchanged through the observation period. The upper bonding index remained at 2 which was similar to the RP120209 crust. Persistent avalanches on this surface hoar layer were also active in the Blue River area during the period of observation. The lower bonding index showed a steady increase over time.

4.2.2.4 Rogers Pass 28 February 2012 (RP120228) sun crust

A sun crust formed at the south study site on Mt. Fidelity during a period of clear weather at the end of February, 2012. The formation period was 3 days long and the peak incoming short-wave radiation was 731 W m^{-2} on 28 February. The resulting crust was 10 mm thick and had a mix of new precipitation particles and small (1-2 mm) needle shaped surface hoar overlying it. Free water influenced the properties of the crust between 26 March and 30 March. The presence of free water at or around crusts is defined and discussed further in Section 4.2.3.1.

Data were collected until 4 April for a period of 36 days. A total of six observations were made on this crust and the data are presented in Figure 4.22. Some of the observed variables had less than six points and this increases the uncertainty of the trends. Density changed very little

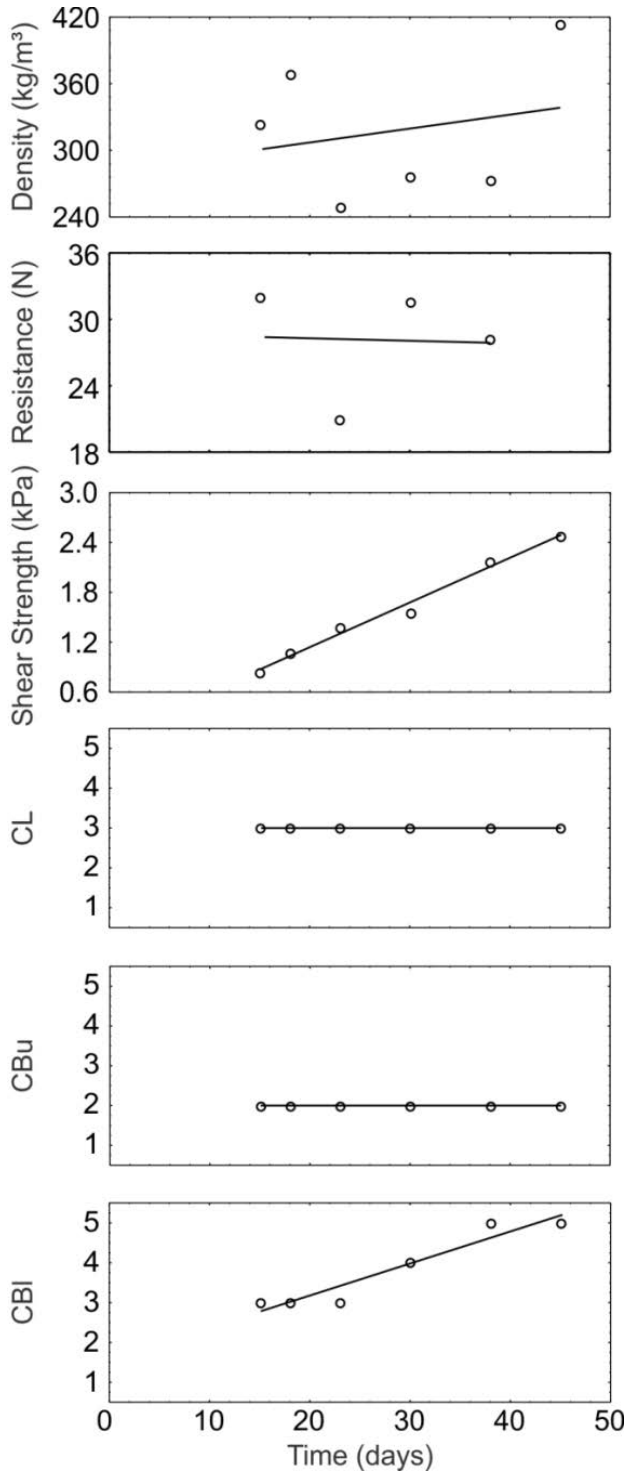

Figure 4.21*: Time series data for the* 12 February 2012 *sun crust at the south study site on Mt. St. Anne near Blue River, BC. In sequence, the plots are density, the thin-blade resistance test, the shear frame test, crust internal lamination index (CL), crust bonding index upper (CBu), and crust bonding index lower (CBl).*

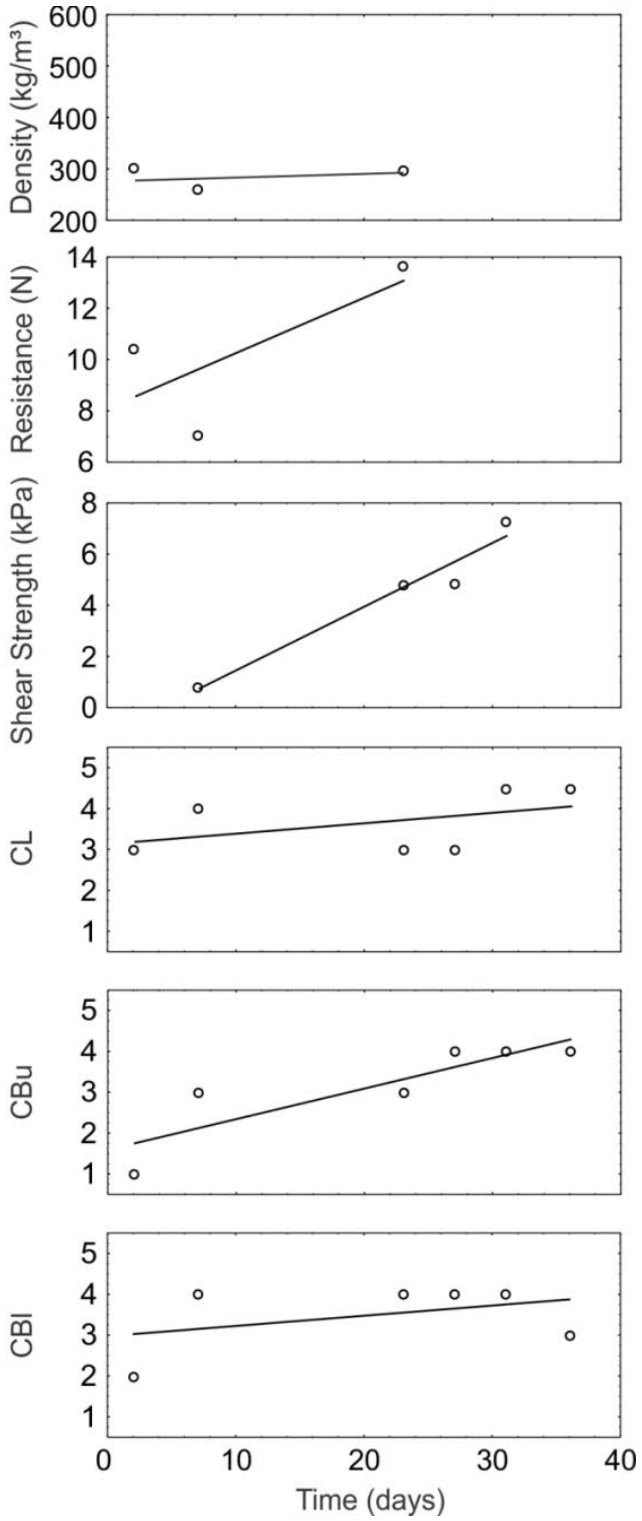

Figure 4.22*: Time series data for the 28 February 2012 sun crust at the south study site on Mt. Fidelity in Glacier National Park. In sequence, the plots are density, the thin-blade resistance test, the shear frame test, crust internal lamination index (CL), crust bonding index upper (CBu), and crust bonding index lower (CBl).*

over the observation period until free water was recorded at which point the density increased to approximately 500 kg m^{-3}. Thin-blade resistance increased slightly over time and shear strength increased at a relatively high rate. The small surface hoar that was initially observed over the crust became rounded grains over time. As a result, the small surface hoar was not considered a persistent weak layer in this analysis. Surface hoar was observed during the first shear strength measurement, but not at the subsequent three observations. Crust lamination increased over time and showed a step from 3 to 4.5 after the presence of free water was recorded. The upper bonding index showed a steady increase as the surface hoar evolved to rounded grains. The lower bonding index was generally high and there was no instability associated with this lower interface based on compression tests performed during field observations.

4.2.2.5 Blue River 5 March 2012 (BR120305) rain crust

On the afternoon of 4 March 2012 the freezing level rose to roughly 1500 meters in the area around Blue River, BC. At the flat, below treeline study site on Mt. St. Anne (1405 m) a rain crust formed. Using the air temperature at the Mt. St. Anne weather station (1900 m) and a wet lapse rate of 6 °C km^{-1} (Ahrens, 2007), the air temperature at the study site was calculated to have reached a high of approximately 0.5 °C. The air temperature at the study site was calculated to have been above 0 °C for seven hours. During this seven hour period, 10.9 mm of precipitation was recorded at the Mt. St. Anne weather station. Because of the extrapolation of meteorological data from the weather station at a different elevation, there was greater uncertainty in the formation conditions of this crust compared with the other crusts in this section. The resulting crust was typically 14 mm thick with knife (K) hand hardness.

The crust was tracked three times until 20 March 2012 for a total period of 15 days. The density increased over time and the thin-blade resistance decreased. This is the only crust in the dataset that showed a decrease in resistance over time. The crust indices did not change substantially over time but the internal lamination dropped from 4 to 3. This may be related to the decrease in resistance. Shear strength was not measured for this crust.

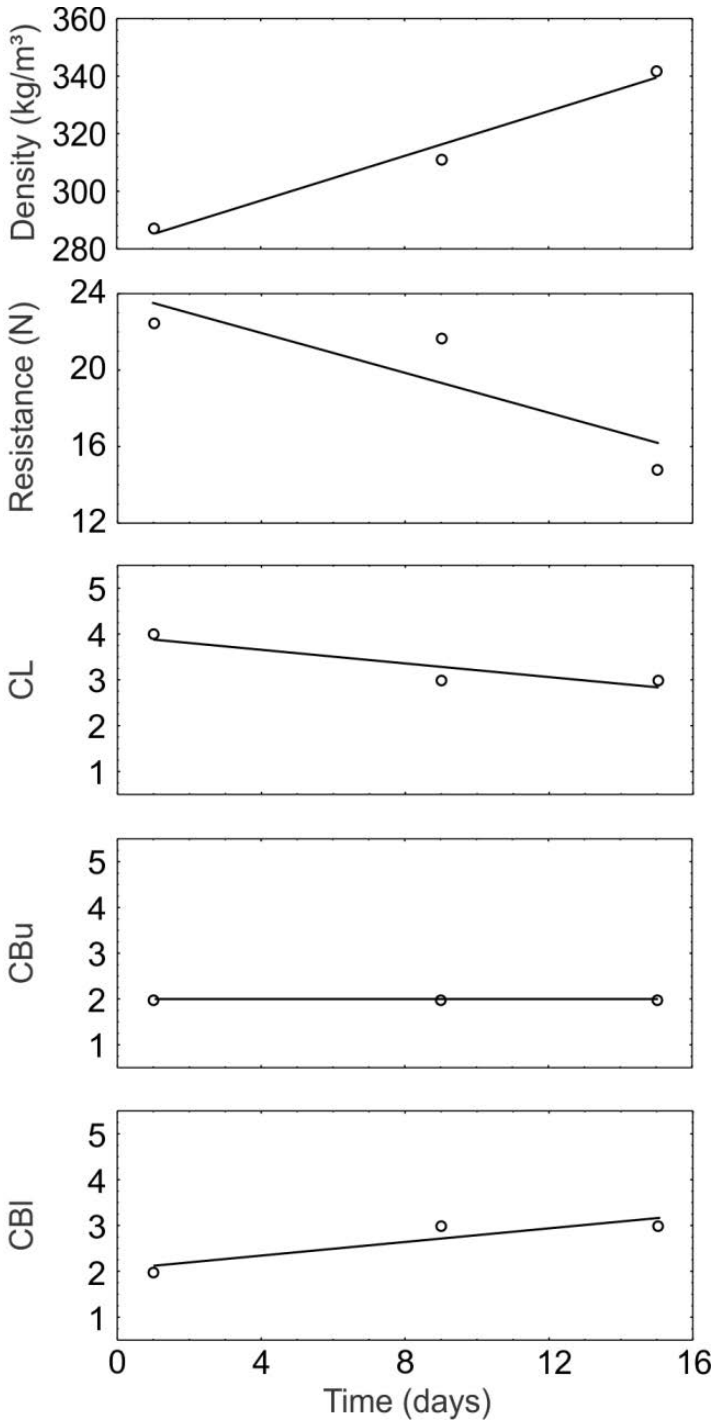

Figure 4.23*: Time series data for the 5 March 2012 rain crust at the flat road-side study site on Mt. St. Anne near Blue River, BC. The study site is below tree-line at 1405 meters elevation. In sequence, the plots are density, the thin-blade resistance test, crust internal lamination index (CL), crust bonding index upper (CBu), and crust bonding index lower (CBl).*

4.2.2.6 Rogers Pass 26 March 2012 (RP120326) sun crust

The RP120326 sun crust formed over four days in late March. The formation conditions are described in Section 4.1.10.2. The crust had a typical thickness of 42 mm and had small facets and surface hoar at the upper interface while the crust was still on the surface. Facets and surface hoar were not observed at subsequent observations.

The crust was observed four times until 4 April 2012. The crust showed an increase in density and resistance over time. Shear frame data were not collected for this crust. The internal lamination, upper bonding, and lower bonding indices did not change substantially over the observation period.

4.2.3 Crust evolution data by physical property

In this section the same data presented Section 4.2.2 are grouped by individual property rather than by the individual crust event. This includes density, shear strength, and thin-blade resistance. Some additional density data were collected during the 2010-11 winter and is included here.

4.2.3.1 Density evolution

Density evolution data were collected for five crusts during the 2011-12 season and an additional two crusts during the 2010-11 season. Figure 4.25 shows the density time series data on the same plot whereas Figures 4.19 through 4.24 show the data for each event separately. Five of the seven crusts were sun crusts at treeline elevation. Two rain crusts were tracked at below treeline elevation. Of the seven crusts tracked, six crusts showed an increasing density trend over time. One of the below treeline rain crusts, BR110127, showed a decreasing density trend over time but this was limited to three observations.

All density observations in which free-water was observed to have influenced the crust after the primary formation event or following substantial burial were excluded from the time series in Figure 4.25. This subsequent free-water influence is recognized by substantial changes from previous observations and may include any or all of the following properties: recently undulated boundaries, varying horizontal hardness and thickness properties, intermittent or

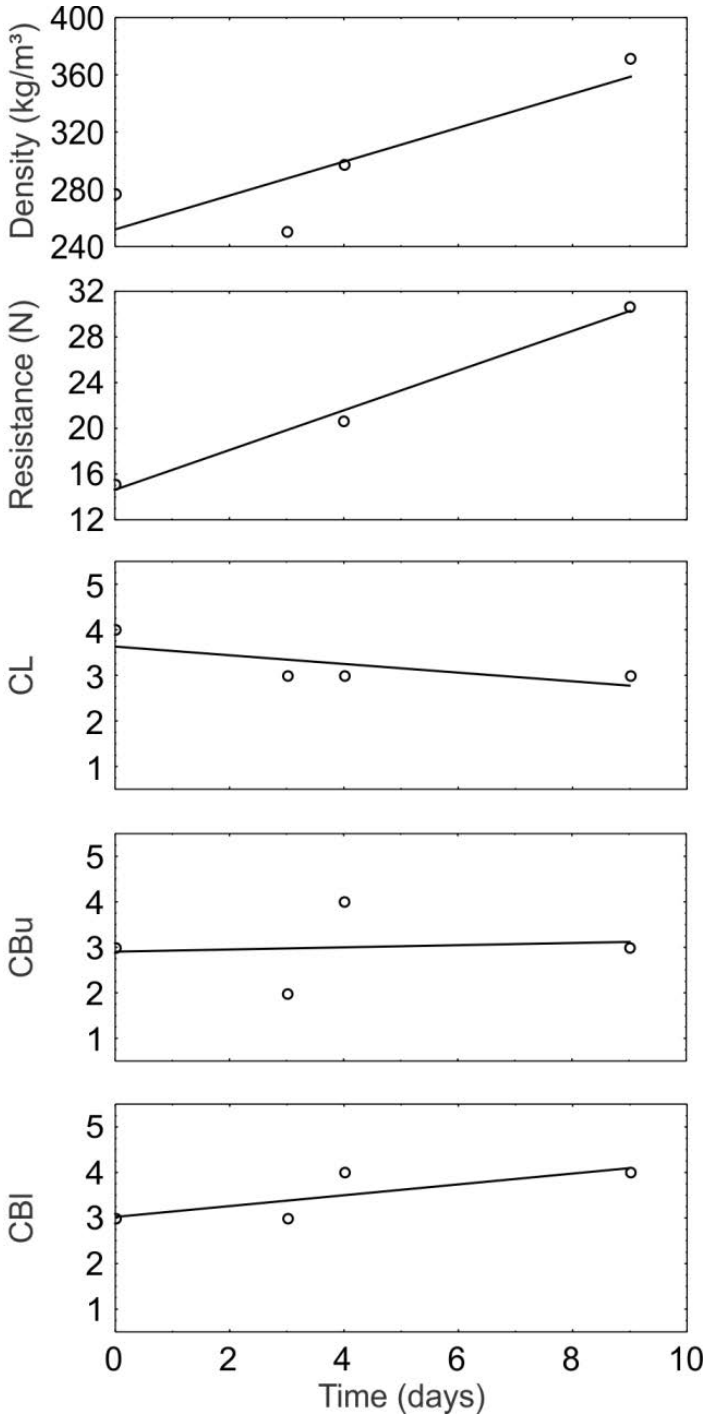

Figure 4.24*: Time series data for the 26 March 2012 sun crust at the south study site on Mt. Fidelity in Glacier National Park. In sequence, the plots are density, the thin-blade resistance test, crust internal lamination index (CL), crust bonding index upper (CBu), and crust bonding index lower (CBl).*

variable ice lens, and vertical percolation channels attached to the crust or observed within the layer above or below the crust. It is likely that this requires the layer to become wet, very wet, or slush as defined by CAA (2007). Figure 4.26 shows the distributions of density values for dry crusts and for crusts influenced by free water. Free water caused a substantial increase in density of melt-freeze crusts.

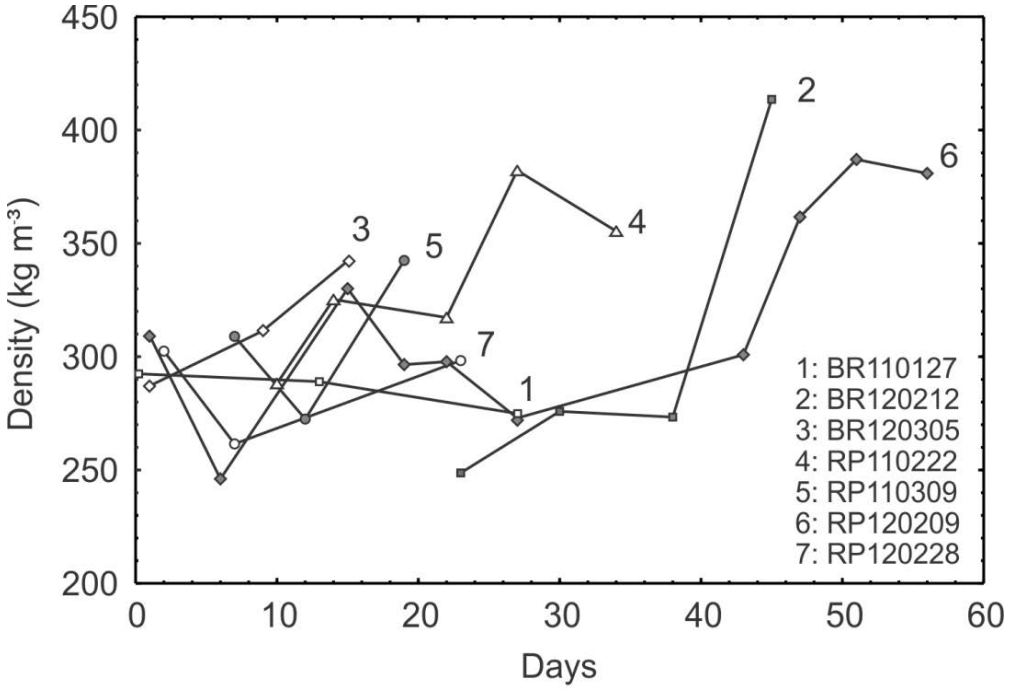

Figure 4.25*: Time series of density evolution for all dry crusts (n = 7). Data were excluded once the presence of free-water was observed.*

4.2.3.2 Shear strength evolution

Shear strength data were collected at the upper interface of four crusts. The data are presented in Figure 4.27. All four crusts showed an increasing trend in shear strength over time. The two cases of crusts with large, persistent surface hoar grains at the upper interface (RP100209 and BR120212) showed a slower increase in shear strength than the two crusts with non-persistent grain types.

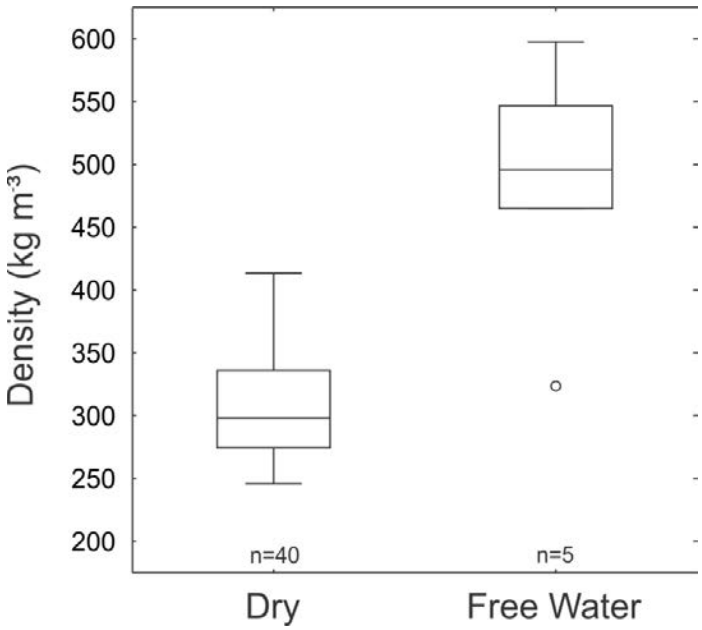

***Figure 4.26**: Range of density values for dry crusts and for crusts after the presence of free water was observed. Box plots as per Figure 4.2.*

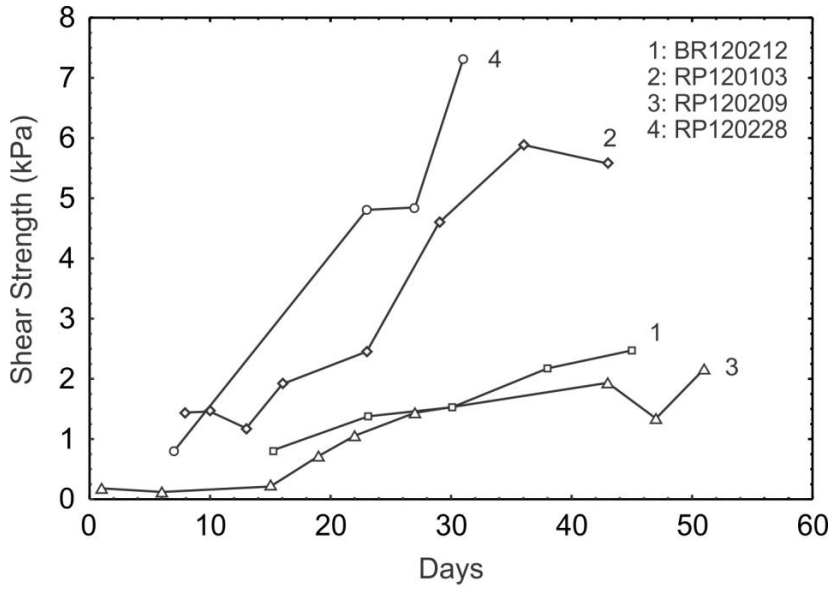

***Figure 4.27**: Time series of shear strength evolution for all upper crust interfaces. Crusts 1 and 3 had persistent surface hoar at the upper interface while crusts 2 and 4 had non-persistent grain types.*

4.2.3.3 Thin-blade resistance evolution

Thin-blade resistance data were collected for six crusts. The data are presented in Figure 4.28. Four of the crusts showed an increasing trend, one showed a decreasing trend, and one a near flat line trend. The crust with the decreasing trend (BR120305) was a below treeline rain crust while the other five were sun crusts at treeline.

Figure 4.29 shows the distribution of thin-blade resistance for each classification of hand hardness. Due to the nature of this research and melt-freeze crusts, hand hardness data with thin-blade resistance data were limited to pencil (P) and knife (K) classifications. Three observations with hand hardness less than pencil hardness were recorded but do not have corresponding thin-blade resistance data. Due to the small dataset, sub-classes of hand hardness (+ or -) were grouped into their primary classification.

A positive correlation existed between thin-blade resistance and density for the crusts measured (Figure 4.30). The Spearman rank order correlation value was 0.62 and the p-value was less than 0.05. This calculation ignored an outlier point at (598 kg m^{-3}, 164 N) which was strongly influenced by free-water.

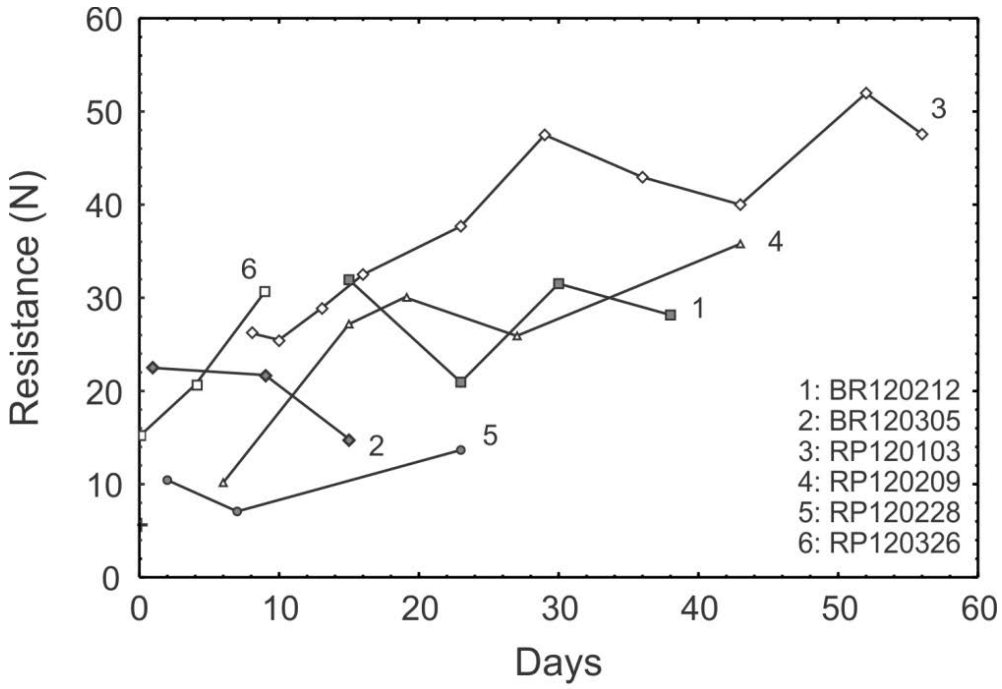

***Figure 4.28**: Time series of thin-blade resistance evolution for all crusts*

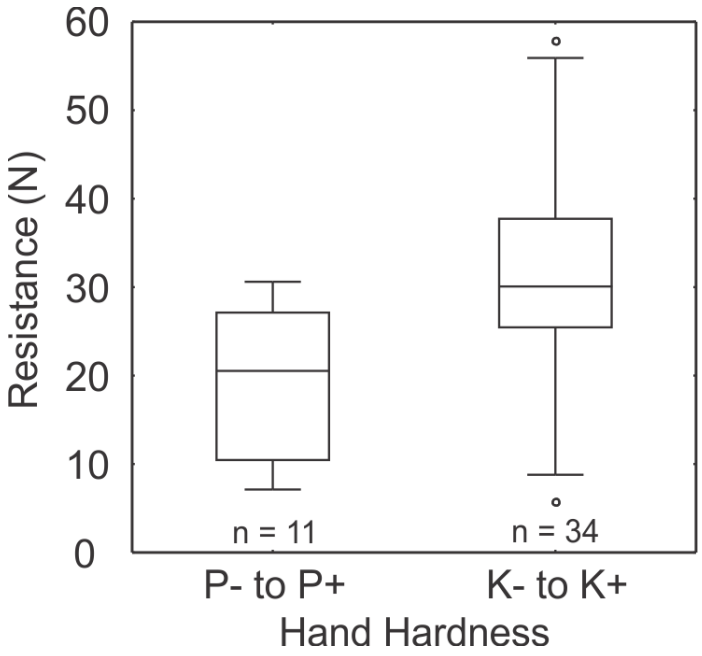

***Figure 4.29**: Range of values of thin-blade resistance for classifications of hand hardness. Sub-classes of hand hardness (+ or -) were grouped into their primary class. Data collected were limited to pencil (P) and knife (K) hand hardness. Box plots properties are defined in Figure 4.2.*

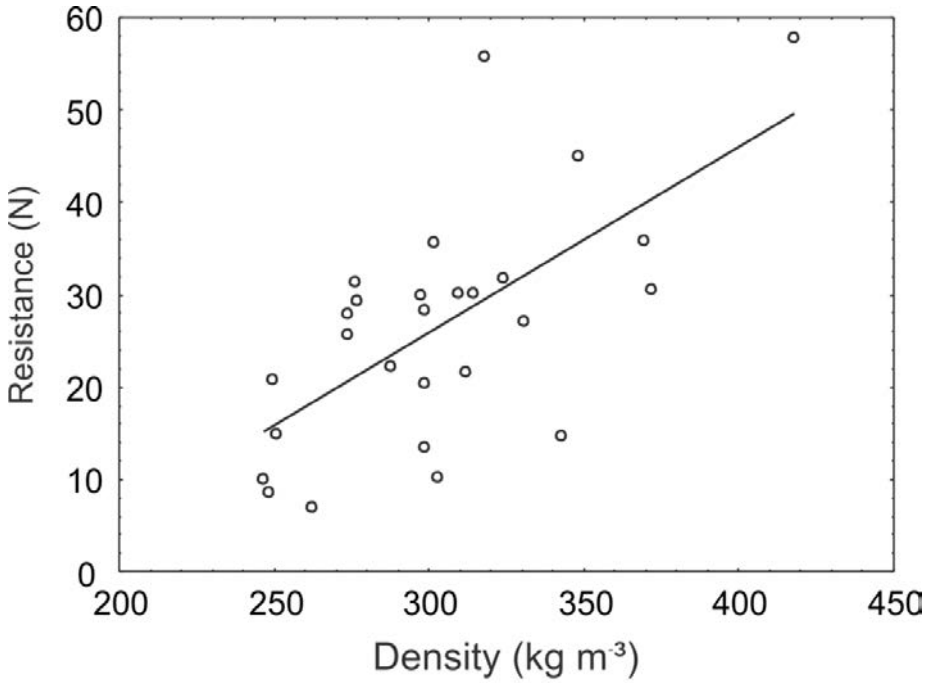

***Figure 4.30**: Relationship between thin-blade resistance and density (n = 27) with Spearman rank order correlation of 0.62 and $p < 0.05$.*

4.2.4 Crust indices data and results

The intention of the crust indices was to create a simple tool to describe the properties of a crust using equipment carried by the average practitioner in the field. The relationship between the interface bonding index and shear strength, grain type, and compression test fracture character were investigated. The relationship between the internal lamination index, crust resistance, and density were also investigated.

4.2.4.1 Crust interface bonding index

Figure 4.31 shows the relationship between the upper bonding index and the measured shear strength. A positive trend exists in the data, especially in the upper range of the bonding index. Large surface hoar crystals at the upper interface of a crust take longer to gain shear strength over time than non-persistent forms as shown in Figure 4.27. Surface hoar also has the tendency to form deep, persistent avalanche problems and produce sudden failure results for long periods of time. This was the case for two crusts, RP120209 and BR120212, which showed smaller increases in shear strength than the other two crusts with non-persistent grain types at the upper interface. Figure 4.32 shows the same data as Figure 4.31, but with surface hoar grain type separated from non-persistent grain types. In this case we see a strong positive trend between the upper bonding index and shear strength for the non-persistent grain types whereas the surface hoar shear strength remains somewhat constant at the lower values of upper bonding index. Surface hoar was typically confined to bonding index 1 and 2 which means that persistent surface hoar is less likely to result in strong layer bonding with crusts than the non-persistent grain types.

The interface bonding index was also related to fracture character observed in compression tests. If a fracture is initiated in a compression test, it can occur at the upper or lower boundary, or, less commonly, within the crust itself. Only results at the upper or lower interface were considered and were coupled with the corresponding upper or lower bonding index. Figure 4.33 shows the relationship between the interface (both upper and lower) bonding index and compression test fracture character. The distribution of the bonding index for each fracture character is shown. While the application of snowpack tests to obtain fracture character can be

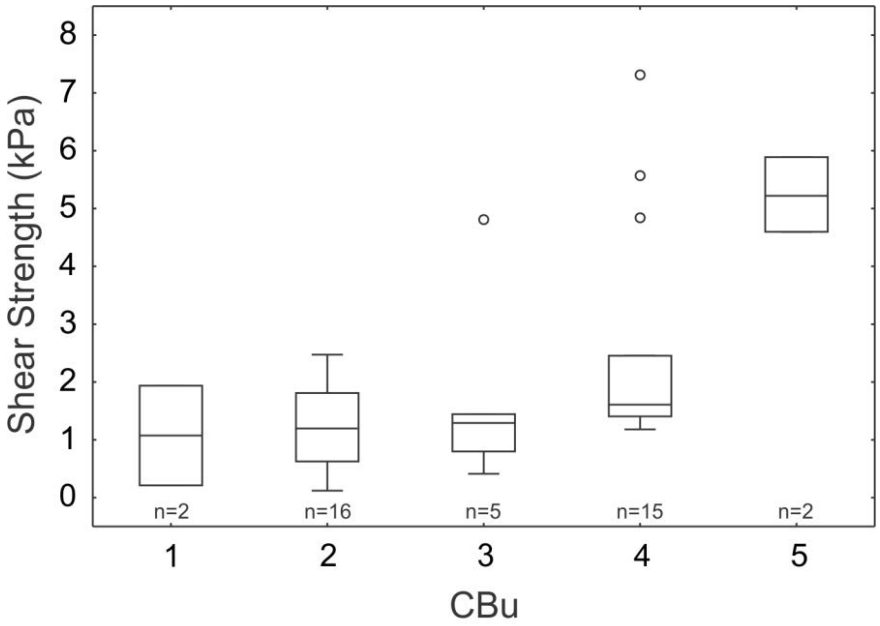

***Figure 4.31**: Relationship between upper crust bonding index (CBu) and shear strength for all data. Box plots properties are defined in Figure 4.2.*

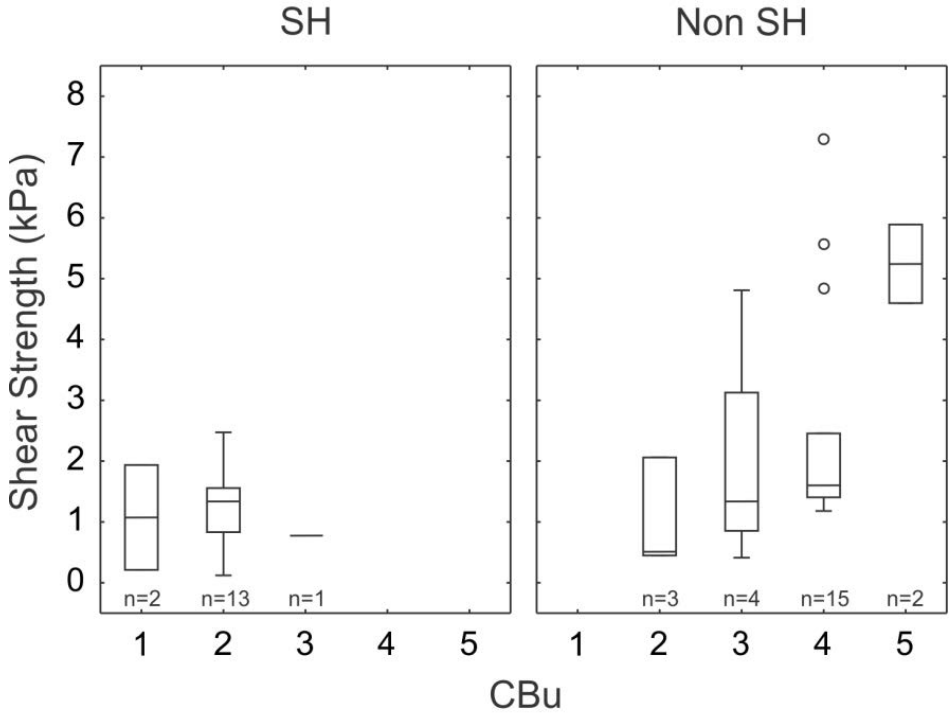

***Figure 4.32**: Relationship between upper crust bonding index (CBu) and shear strength, separating surface hoar (SH) and non-surface hoar grain types at the upper interface. Box plots properties are defined in Figure 4.2.*

done at any depth, the successful initiation of a fracture in the compression test is strongly influenced by depth. For this reason, compression test *No Result* was omitted from the analysis.

Sudden planar (SP) and sudden collapse (SC) are fracture character types in which propagation propensity are likely (van Herwijnen and Jamieson, 2007). The distributions of interface bonding index for these two fracture characters were towards the low end of values with 1 and 2 having the highest frequency. Resistant planar (RP) and break (BRK) fracture character results mean propagation propensity is unlikely. The distribution of the bonding index values for these fracture character was towards the higher values, 3 and 4. The one case of progressive compression (PC), a fracture character also associated with propagation propensity unlikely, was new snow overlying a shallow crust (14 cm depth, 1 day old). This case was not associated with slab avalanche instability but rather new snow that had yet to have time to form bonds with the crust. No occurrences of fracture character exist for results at the value 5 of the bonding index.

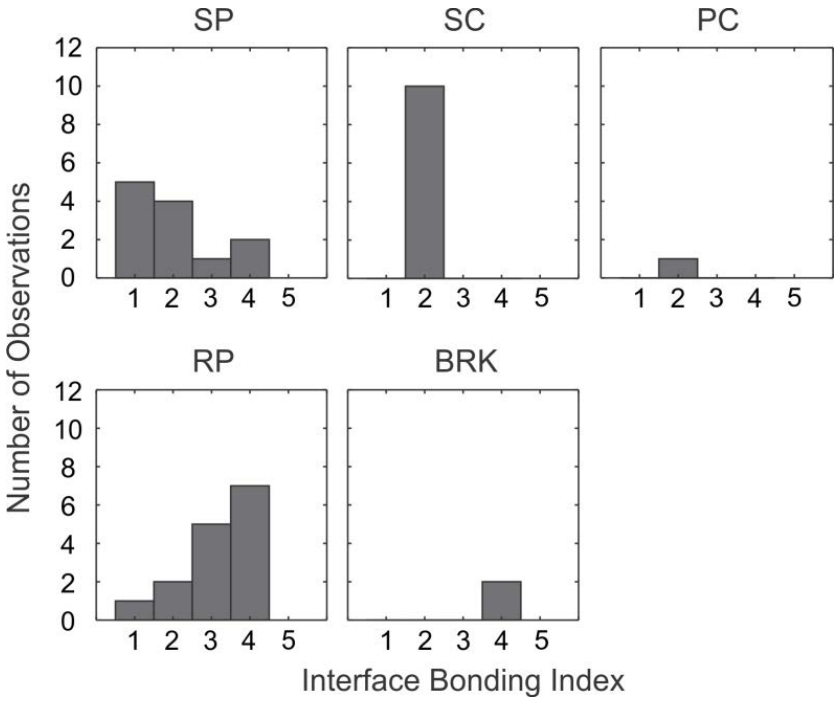

***Figure 4.33**: Distribution of interface bonding index for compression test fracture character results (SP: sudden planar, SC: sudden collapse, PC: progressive compression, RP: resistant planar, BRK: break)*

The interface bonding index was also related to primary grain type adjacent to a crust layer at both the upper and lower interface. Figure 4.34 shows the distribution of the bonding index for each primary grain type. Surface hoar (SH) and facets (FC) are considered to be persistent weak grain and are often associated with avalanche instabilities. The distribution of bonding indices for these persistent grain types was towards the lower end of values. A typical evolution of non-persistent grain types is from new snowfall, which is precipitation particles (PP), to decomposed and fragmented particles (DF) and eventually to rounded grains (RG). This common evolution is typically associated with increasing stability. The distribution of data for these three grain types showed an increase in interface bonding indices. The distribution of values for rounding facets (FCxr) varied due to the nature of this grain type. As a faceted grain evolves towards a rounded grain as is common in the Columbia Mountains, its bonding and stability properties can be representative of either grain type. The 3 January 2012 freezing rain crust had facets develop at the lower interface which were initially associated with instability in the snowpack as indicated by compression test results. Over time, these grains evolved to rounding facets which persisted until the end of the observation period. By the end of the observation period, the rounded facet grains were very well bonded to the crust and the bonding and stability properties were similar to that of rounded grains.

4.2.4.2 Crust lamination index

The relationship between the crust lamination index and thin-blade resistance is shown in Figure 4.35. The distribution of resistance measurements for each lamination classification is shown. There appears to be an increase in thin-blade resistance with increasing crust lamination values. Because of the positive correlation between measured resistance and density shown in Figure 4.30, it might be expected that there is a positive relationship between the crust lamination index and density. Figure 4.36 shows the distribution of density measurements for each lamination class. There was more variability in these data because most of the lamination index data were either 3 or 4 and the other values were not well represented. Initially there does not appear to be a relationship between density and crust lamination. The relationship between density, resistance, and crust lamination index is discussed further in Section 5.2.5.

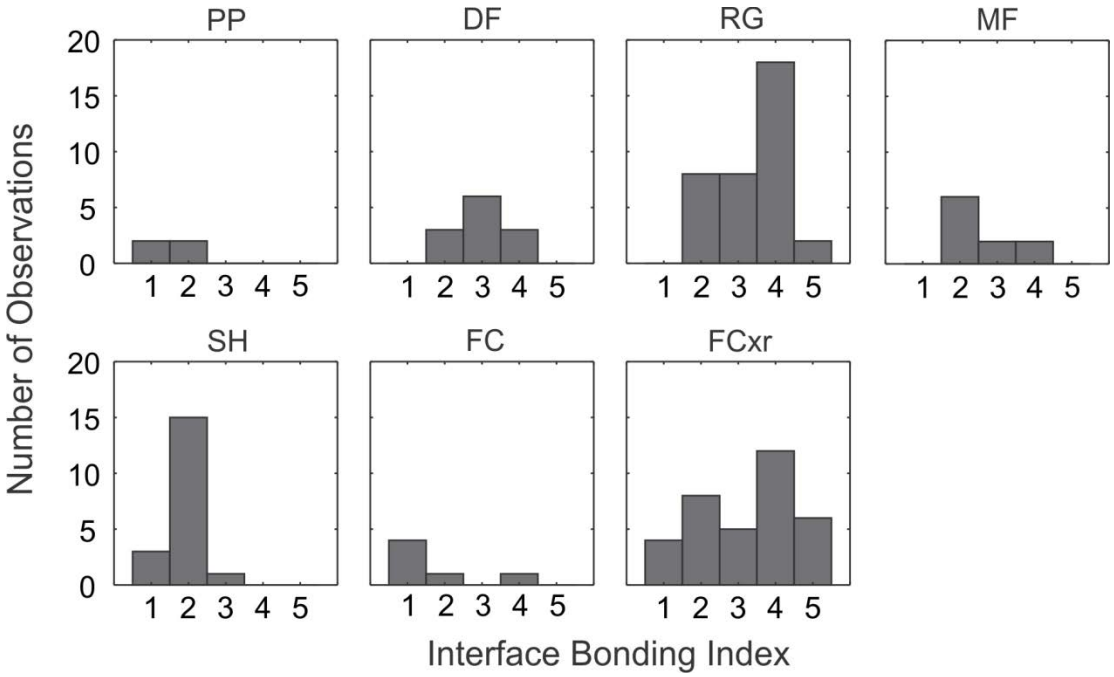

***Figure 4.34**: Distribution of interface bonding index for various primary grain types.*

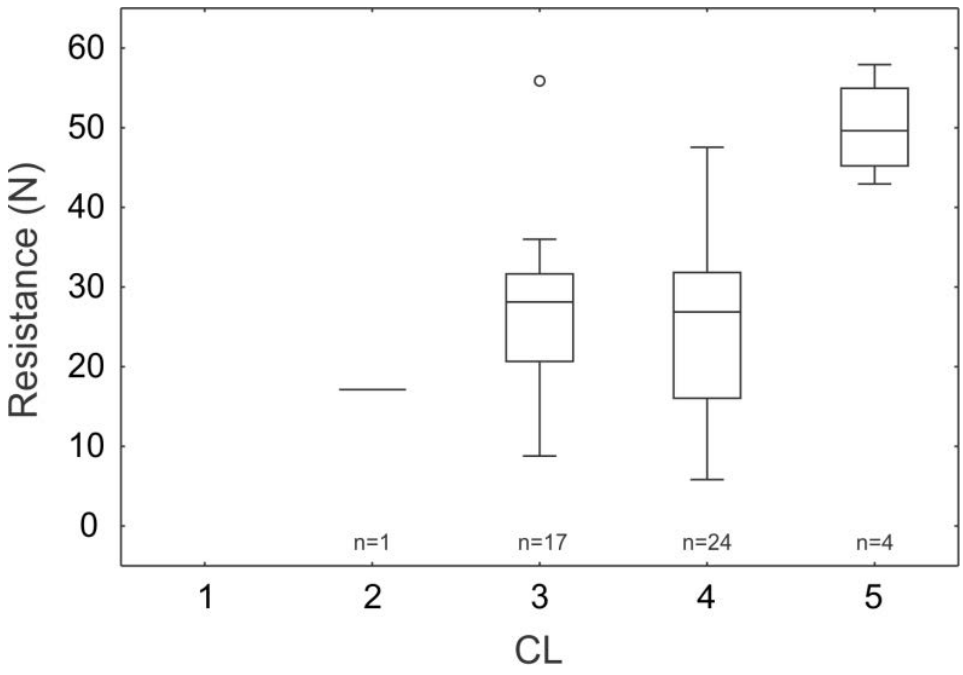

***Figure 4.35**: Relationship between crust lamination index (CL) and thin-blade push gauge resistance. Box plots properties are defined in Figure 4.2.*

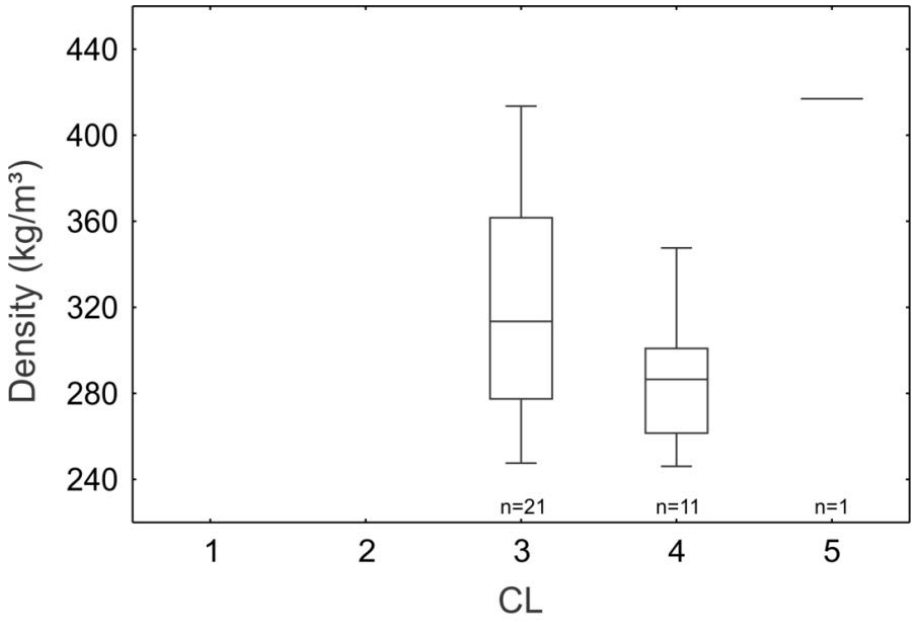

***Figure 4.36**: Relationship between crust lamination index (CL) and density. Box plots properties are defined in Figure 4.2.*

4.2.5 Thermal evolution data and results

Thermal evolution data are presented for three melt-freeze crusts including a freezing rain crust and two sun crusts. As described in Section 3.3.3.7, three variables were obtained from the thermal photos including average upper temperature gradient ($|\nabla T_{Upper}|$), average lower temperature gradient ($|\nabla T_{Lower}|$), and average temperature difference (TD) between the crust and the surrounding snow. The data are presented as box plots on a time series with each box representing the values from the five transects. Additional variables used during the analysis included measured air temperature, crust and snow temperatures obtained from thermal photos, and crust burial depth.

Figure 4.37 shows the thermal data for the freezing rain crust RP120103. This crust initially had strong temperature gradients, the largest observed during this project, with an average value of 211 °C/m at the upper interface. After two weeks the gradients had reduced to roughly 25% of the initial values. Initially the average upper temperature gradient was greater than the average lower temperature gradient. On 16 January this reversed and the average lower gradient became stronger than the upper. The time period following the 16 January

observation was associated with cold air temperatures which reached a low of -26 °C on 18 January, or a mean daily temperature of -23 °C. Following the observation on 16 January and prior to the observation on 19 January, faceting occurred at the lower interface of the crust. Following the 19 January observation, the faceted grains evolved to rounded facets. These subsequent observations also showed smaller average temperature gradients at both interfaces than in previous observations. Table 4.6 shows the progression of grain types above, below, and within the crust, as well the thickness of the crust, for the RP120103 freezing rain crust.

Figure 4.38 shows the data for the RP120209 sun crust. The gradients were initially quite low, but two spikes in the gradients were observed. These spikes in the temperature gradients are related to drops in the air temperature. A third substantial decrease in air temperature occurred on 6 March, but no substantial increase in temperature gradients occurred. The crust was at a depth of 145 cm. This crust did not undergo any faceting during the observation period.

Table 4.6*: Grain type and crust thickness evolution for RP120103 freezing rain crust. Grain types are listed as primary grain type followed by secondary grain type. Grain types as per Table 1.*

	4 Jan	11 Jan	13 Jan	16 Jan	19 Jan	26 Jan	1 Feb	8 Feb	15 Feb	24 Feb	28 Feb	19 Mar
Mean CR Thickness (mm)	4	3	4	4	3.5	4	4	4	2.7	3.5	3	3
Grain Type Above	PP	RG	RG	RG	FCxr	RG	RG FCxr	FCxr	FCxr	FCxr	FCxr	FCxr
CR grain type	MFcr	MFcr	MFcr MFcl	MFcr MFcl	MFcr MFcl	MFcr MFcl	MFcr MFcl	MFcr MFcl	MFcr	MFcr FCxr	MFcr MF	MFcr
Grain Type Below	DF	FCxr	MF RG	RG MFcl	FC	RG FCxr	RG FCxr	FCxr	FCxr	FCxr	FCxr	FCxr

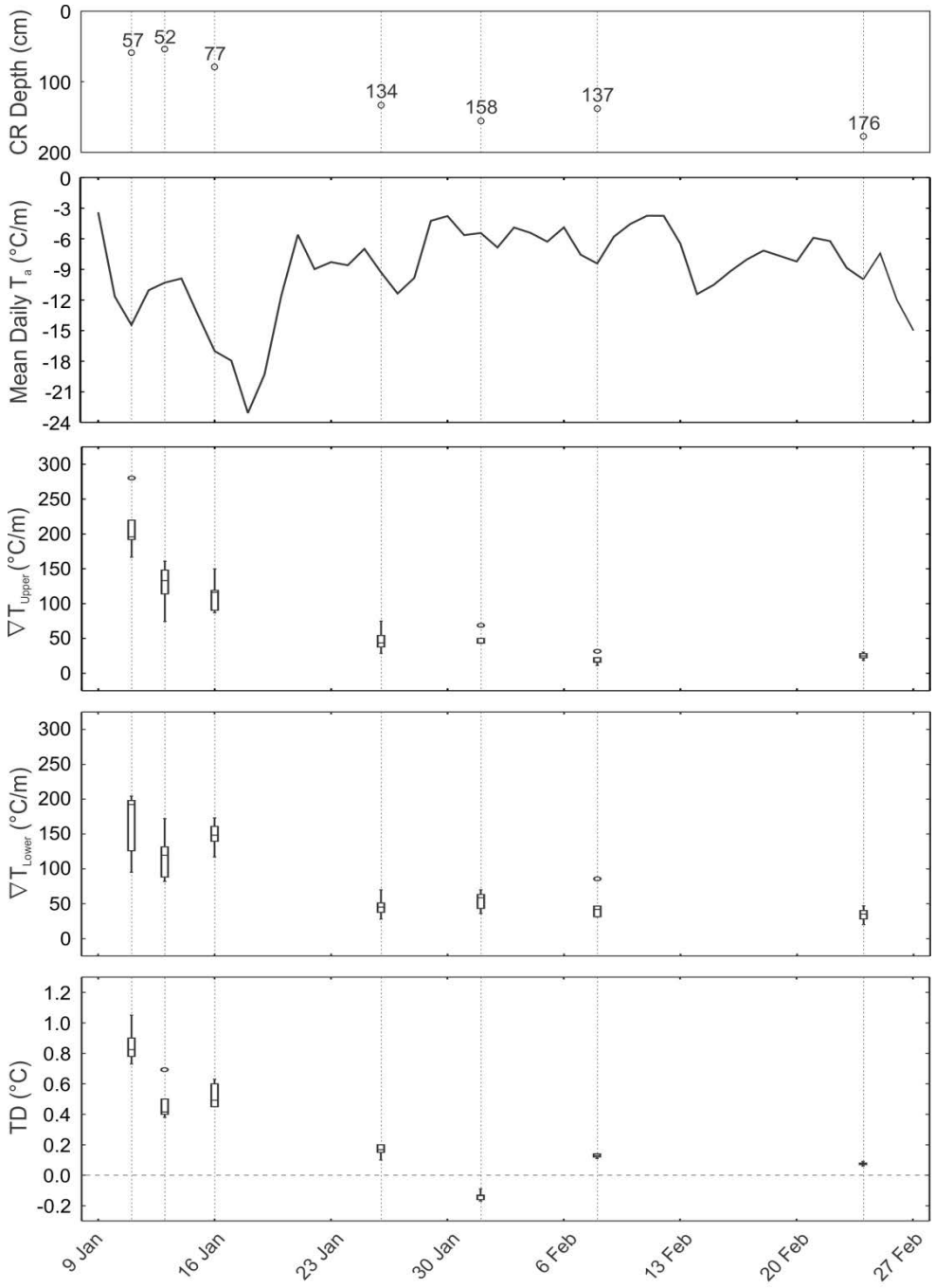

***Figure 4.37**: Thermal evolution for RP120103 freezing rain crust. Crust depth is the measurement from the snow surface to the top of the crust. Mean daily air temperature (T_a) is calculated from data recorded at the Mt. Fidelity weather station. Average upper temperature gradient ($|\nabla T_{Upper}|$), average lower temperature gradient ($|\nabla T_{Lower}|$), and average temperature difference (TD) between the crust and surrounding snow are calculating using the methods described in Section 3.3.3.7. Box plots properties are defined in Figure 4.2.*

Figure 4.39 shows the data for the RP120228 sun crust. This crust had the lowest temperature gradients of the three crusts and the least variance between observations. One increase in temperature gradient was observed on 6 March and is associated with a drop in air temperature. This crust did not undergo faceting during the observation period.

Table 4.7 shows the Spearman correlation matrix for the dataset consisting of crust burial depth, temperature gradients ($|\nabla T_{Upper}|$ and $|\nabla T_{Lower}|$), average crust temperature (T_{cr}), average snow temperature (T_{cr}), measured air temperature (T_a), difference between crust and air temperature (ΔT_{cr-a}), and difference between snow and air temperature (ΔT_{sn-a}). Upper and lower temperature gradients have statistically significantly relationships with measured air temperature, average snow temperature, and average crust temperature.

***Table 4.7**: Spearman correlation matrix (n = 18) for selected variables of thermal evolution including crust depth, upper temperature gradient ($|\nabla TU_{pper}|$), lower temperature gradient ($|\nabla T_{Lower}|$), air temperature (T_a), crust temperature (T_{cr}), snow temperature (T_{sn}), difference between crust and air temperature (ΔT_{cr-a}), and difference between snow and air temperature (ΔT_{sn-a}). Red values indicated $p < 0.05$.*

	ΔT_{sn-a}	ΔT_{cr-a}	T_{sn}	T_{cr}	T_a	$\|\nabla T_{Lower}\|$	$\|\nabla T_{Upper}\|$	Depth
Depth	0.10	0.02	0.25	0.18	0.10	-0.32	-0.46	1.00
$\|\nabla T_{Upper}\|$	0.41	0.46	-0.63	-0.56	-0.75	0.87	1.00	
$\|\nabla T_{Lower}\|$	0.28	0.34	-0.68	-0.65	-0.68	1.00		
T_a	-0.79	-0.81	0.51	0.49	1.00			
T_{cr}	-0.02	-0.01	0.97	1.00				
T_{sn}	0.00	-0.03	1.00					
ΔT_{cr-a}	0.98	1.00						
ΔT_{sn-a}	1.00							

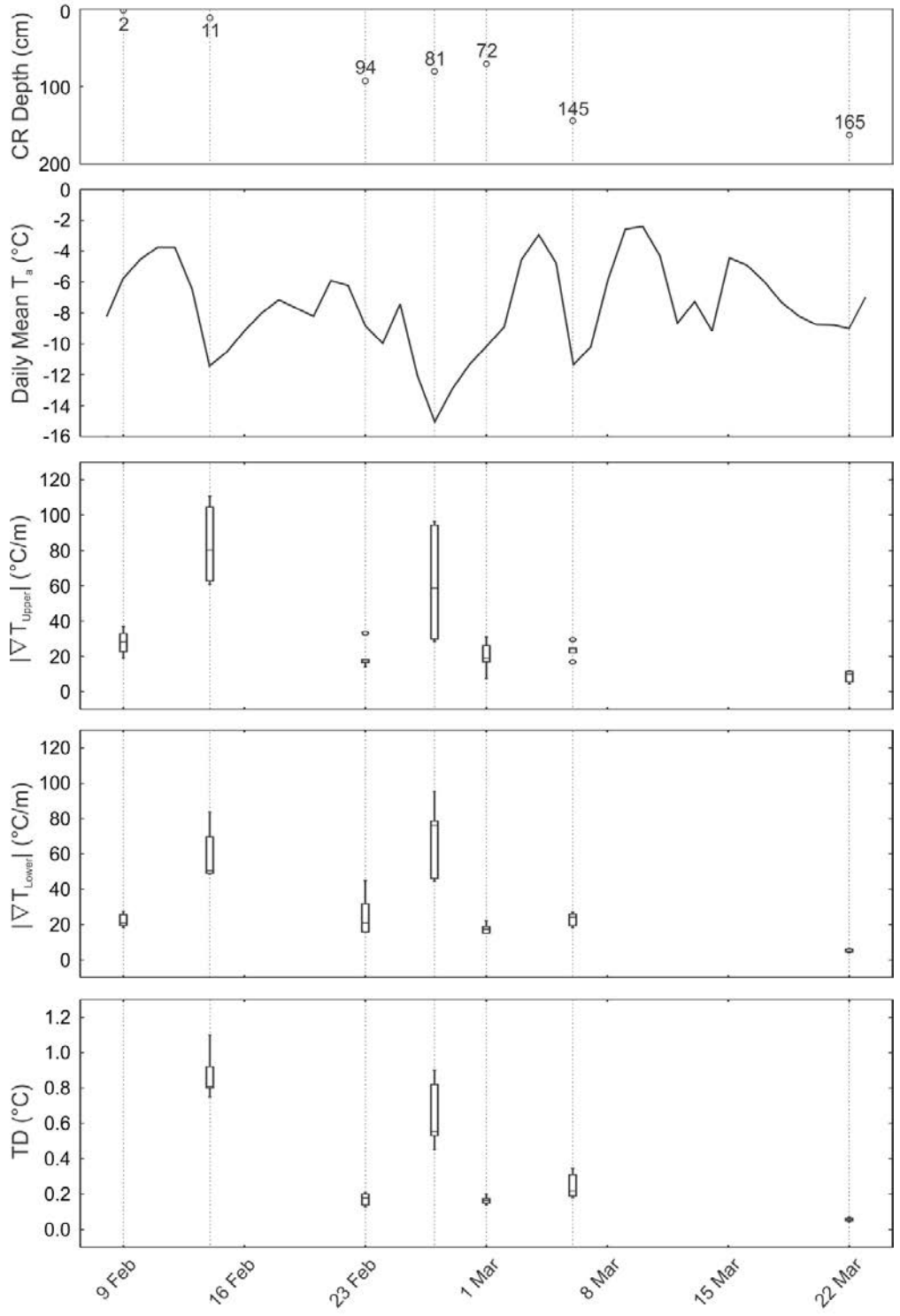

***Figure 4.38**: Thermal evolution for RP120209 sun crust. Crust depth is the measurement from the snow surface to the top of the crust. T_a, $|\nabla T_{Upper}|$, $|\nabla T_{Lower}|$, and TD as per Figure 4.37. Box plots properties are defined in Figure 4.2.*

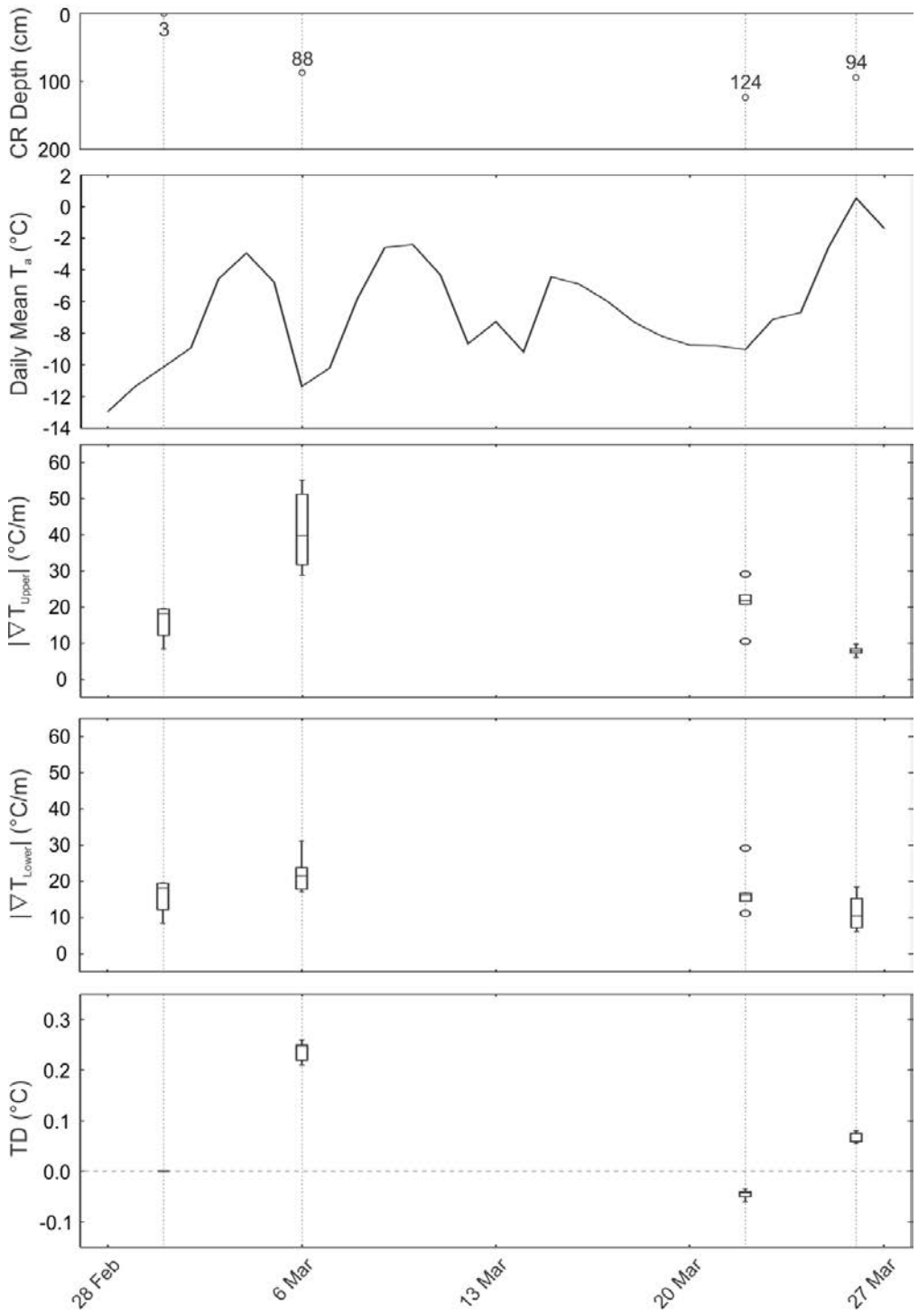

***Figure 4.39**: Thermal evolution for RP120228 freezing rain crust. Crust depth is the measurement from the snow surface to the top of the crust. T_a, $|\nabla T_{Upper}|$, $|\nabla T_{Lower}|$, and TD as per Figure 4.37. Box plots properties are defined in Figure 4.2.*

Based on Figures 4.37 through 4.39, the depth of the crust appears to affect the relationship between air temperature and temperature gradients. Once the crusts were below roughly 1 m, there were no longer substantial increases in the temperature gradients associated with substantial decreases in air temperature. Observations made on 6 March 2012 are a good example. The RP120228 crust was buried 88 cm and showed an increase in temperature gradients associated with the drop in mean daily air temperature to -11.3 °C, which could also be related to the NP_Ta effect. During the same observation, the RP120209 sun crust was buried 145 cm. There does not appear to be a related increase in the temperature gradients compared with the previous observation on 1 March. This same RP120209 crust showed two previous increases in the temperature gradients related to drops in air temperature on 14 February and 27 February. This occurred when the crust was buried 11 cm and 81 cm, respectively.

Using a division threshold of 1 m burial depth based on the observations described above, Spearman correlation values were calculated for each subset of the original dataset. The resulting data are shown in Table 4.8. This table shows an increase in the Spearman rank correlation values for depth < 1 m compared to the complete dataset and a decrease in the Spearman rank correlation values for depth > 1 m.

***Table 4.8**: Spearman correlation values for crust temperature gradients against measured air temperatures based on depth criteria of 1 m. Red values indicate $p < 0.05$.*

Crust Depth	Spearman Value $\lvert\nabla T_{Upper}\rvert$ vs T_{air}	Spearman Value $\lvert\nabla T_{Lower}\rvert$ vs T_{air}
All	-0.75	-0.68
< 1 m	-0.77	-0.82
> 1 m	-0.72	-0.09

CHAPTER 5: DISCUSSION

5.1 Crust formation discussion

This section discusses the conditions during melt-freeze crust formation. In this discussion, the term *formation* generally refers to the melting of snow. The subsequent refreezing of this melted snow can occur during or after the formation periods, which are defined in Section 3.2.2. The refreezing process of melt-freeze crust formation is not investigated in this study. Melting is an important process, especially during the sun crust formation periods lasting longer than one day, and also to our understanding of the near-crust faceting process.

5.1.1 Crust formation period determination and dataset criteria

For crusts to be included in the formation dataset they had to meet several criteria, including the ability to determine the formation period based on the definitions from Section 3.2.2. For sun crusts this was generally straightforward because everything between two periods of precipitation was included. However, this method does not allow for the determination of the specific period of melting. Sun crusts are complicated in this regard because the formation process can include multiple periods of melting and refreezing over multiple days. It has been assumed that each subsequent day has the potential to further contribute to the formation of a crust until it has been buried and is no longer on the surface. The subsequent melting and refreezing of the surface layer has the potential to increase the thickness, hardness, and resistance of the crust. In order to improve the methods to determine specific periods of melting and resulting overnight freezing, a snow surface temperature gauge or a surface energy balance model is likely required.

The criterion for rain crust formation is more inclusive than for sun crusts because it only includes periods of liquid precipitation when there is no snowfall accumulation. However, this requires both a liquid precipitation gauge and a new snowfall gauge. A total snow depth gauge would likely work in the place of a new snowfall gauge but accuracy may be decreased due to the increased influence of snowpack settlement. While the criteria works well for distinct periods of rainfall over several hours, it becomes more difficult to interpret short rain events,

rain events consisting only of small amounts of precipitation, wet snow events, and freezing rain crusts. The melting precipitation gauge has to clearly increase while the snowfall gauge does not increase, and small inherent error in the gauges can increase the uncertainty in interpretation. As a result of these limitations, the dataset becomes biased towards rain crusts that formed with greater amounts of rainfall. Comparing suspected rain crusts that were excluded because of undetermined formation periods to crusts that were included, it is clear that the crusts that were included are generally thicker and/or harder than those that were excluded. While all crusts have the potential to create avalanche problems, it is expected that thicker and/or harder crusts have a greater potential to persist longer in the snowpack. As a result, the bias in the dataset may tend to focus more on rain crusts that have an increased potential to create persistent avalanche problems.

The other criterion, applying to both types of crusts, is that the crust had to appear in at least three snow profiles. This was intended to exclude isolated events. These isolated events may include rain crusts that formed from short periods of isolated rainfall in specific locations or sun crusts that formed on isolated slopes due to the nature of variable cloud cover or additional influence of local pockets of warm air. This project is primarily interested in widespread events that have the potential to cause widespread avalanche problems. It is more difficult to predict localized avalanche problems associated with melt-freeze crusts. The resulting interpretation of isolated avalanche problems associated with spatially variable melt-freeze crusts will continue keep avalanche forecasters busy and employed.

5.1.2 Crust formation by aspect

Figure 4.1 shows that sun crusts tend to form primarily on south aspects at all periods during the winter season. While sun crusts are expected to form more frequently on a wider variety of slopes after the winter solstice, the limited data in this study showed more frequent sun crusts on flat aspects in December/early January and March, than in late January and February.

Typical rain crusts form on all aspects. It is assumed that spatial variability can influence the distribution of this formation from a slope scale to a range scale. Wind patterns, precipitation distribution, and orthographic lifting are sources of rain crust formation variation at range,

region, and basin scales. Local wind and terrain effects are sources of variation at slope and basin scales. Weather systems with precipitation typically arrive from the south-west in the Glacier National Park study area. As a result, it is expected that rain crusts that are not fully widespread would be more likely to form on south aspects than on north aspects if wind is influential. The data in Figure 4.1 appears to support the hypothesis that rain crusts would be more likely to form on south aspects. This is likely affected by error associated with a small dataset and using historical ACS data. The frequency of rain crusts that formed in at least two profiles (dark blue fill) is 11 for south, 10 for flat, and 7 for north. This analysis could be improved by investigating wind conditions during formation, increasing the size of the dataset, and collecting more detailed data on spatial variation of rain crusts shortly after formation.

5.1.3 Crust formation periods

Figure 4.2 shows that rain crusts typically form over short, discrete periods of rainfall. This contrasts to sun crusts which can form over several hours of sun exposure up to several days or even weeks. Note that sun crusts do not form during the entire formation period; rather, they typically go through diurnal cycles of melt and freeze. It is generally assumed in practice that sun crusts will become thicker and/or harder once they undergo subsequent diurnal melt-freeze cycles, at least during the initial few cycles. In Table 4.1 there is statically significant relationship between sun crust formation period and hand hardness. This further adds the common assumption that longer formation periods should result in thicker and/or harder crusts. This is likely due to the contribution of subsequent periods of melting and refreezing that becomes possible when a crust is exposed at the surface for multiple days. Also, as a crust goes through successive melt-freeze cycles, the albedo lowers as grain size increases. This means that more of the incoming short-wave radiation is absorbed by the snowpack.

5.1.4 Air temperature

Air temperature affects whether precipitation falls as snow or rain and appears to be an important predictor variable for rain crust formation. In each case, the local air temperature was above -0.4 °C. Uncertainty is high for this dataset because it is very small (n = 8) and the

formation periods have been defined using historical meteorological data rather than being determined or validated in the field.

The standard deviation of air temperatures in Figure 4.4 shows higher values for sun crusts than rain crusts. This can be attributed primarily to the length of the formation periods and the related diurnal temperature fluctuations. A more interesting comparison is to look at the spread of values between any of the three temperature variables (maximum, average, and minimum) for rain and sun crusts in Figure 4.3. There is a much wider range of values for sun crusts which suggests that sun crust formation showed less dependence on air temperature.

Bellaire and Jamieson (2013) modeled rain and sun crust formation in the Columbia Mountains using the Swiss SNOWPACK model. Snow profiles from Mt. Fidelity north and south aspects, as well as from a flat site, were used for verification. They achieved modeling accuracy of between 65% and 77% depending on aspect and formation type. The SNOWPACK model was developed in an area of Switzerland where the snow climate is classified as continental (Dr. S. Bellaire, personal correspondence) and therefore required adaptation for the Columbia Mountains. One of the primary adaptations was to change the air temperature threshold for rain and rain crust formation from +1.2 °C to -0.5 °C (Bellaire and Jamieson, 2013). This change resulted in the increased inclusion of rain crusts, which would have otherwise been missed by the model. The data from Figure 4.3 has a range of maximum air temperature during rain crust formation of -0.4 to 4.9 °C and therefore shows agreement with this SNOWPACK threshold value of -0.5 °C for the Columbia Mountains.

5.1.5 Short-wave radiation

Several variables of incoming short-wave radiation were considered because of the importance to sun crust formation. Because the availability of incoming short-wave radiation is dependent on the solar zenith angle and therefore time of year, it is difficult to directly compare incoming short-wave radiation data for crusts that form at different times of the year. By plotting the variables of incoming short-wave radiation against the day of year (Figures 4.6 and 4.7), the relationship becomes clear. Both curves have the minima near the middle of December as

would be expected because the solar zenith angle is at a minimum and the days are the shortest.

If we assume maximum daily cumulative incoming short-wave radiation and peak incoming short-wave radiation are representative of sunny periods, then the fit lines can be used to estimate the expected values for sunny periods at any time during the winter season. This has potential applications for remote avalanche forecasting and snowpack modeling. Unfortunately there are many days with values that exist above these two fit lines where sun crusts are assumed to not have formed based on the dataset. There may be a dependency on aspect and slope angle that was not apparent from the methods utilized. It appears that incoming short-wave radiation alone cannot be used to predict sun crust formation and the fit lines cannot be used as threshold values. Further work to investigate how incoming short-wave radiation interacts with other meteorological variables may improve the ability to determine threshold values for sun crust formation. It may be possible to develop a simple surface energy model for the purposes of predicting sun crust formation.

The two fit lines for rain crusts follow the same shape as those for sun crusts but with substantially lower values. If we assume, based on the cloud cover and incoming long-wave radiation data presented in Section 4.1.7, that rain crusts form during periods of overcast cloud cover with intermittent periods of broken sky cover, then these fit lines represent the expected amount of incoming short-wave radiation for overcast or broken sky cover for any day throughout the winter.

5.1.6 Sky cover and incoming long-wave radiation

Incoming long-wave radiation and sky cover are related because increased cloud cover causes more terrestrial radiation to be re-radiated back towards the earth. There is substantial overlap between each step of the box plot in Figure 4.7 because of uncertainty in the input data. There is relatively high confidence in the long-wave radiation entering the atmosphere; the uncertainty comes from the point observation of cloud cover and its interaction with short and long-wave radiation.

Future work to improve the simple relationship between sky cover and incoming long-wave radiation should include making consecutive sky cover observations with a similar sampling frequency to the incoming long-wave radiation data. This way the confidence in the sky cover data could be increased and could be coupled properly with the incoming long-wave radiation data. Once these datasets are coupled properly, less overlap between each sky cover classification would be expected in Figure 4.7. It would also be expected that the standard deviation values for each sky cover classification in Figure 4.8 would decrease. Using these two relationships together, average values and standard deviations of ILWR for each classification of sky cover, it should be possible to predict sky cover at any location where the ILWR is available continually. This has the potential to be useful to avalanche forecasters, especially for remote forecasting, where the sky cover could be estimated in real time at any weather station with remote telemetry and an incoming long-wave radiometer. Further to this, the same method could be used with a weather model such as the numerical weather prediction model GEM (Maillot et al., 2006) to estimate the sky cover from ILWR at any grid point of the weather model.

5.1.7 Crust formation properties

The physical properties of melt-freeze crusts resulting from various formation conditions is an important topic and has the potential to be useful to avalanche forecasters and to improve upon snowpack models. Unfortunately, due to the complicated nature of creating the dataset, there is a lot of uncertainty inherent in the analysis and results. There is more confidence in the crust properties measured by ASRAC field teams between 2010 and 2012 but this dataset is not large enough (n = 5) for confident interpretation of formative effects.

Although uncertainty exists in these datasets, several interesting findings can be made. Using the larger historic dataset for sun crust formation, there is a statistically significant relationship between hand hardness and total incoming short-wave radiation, total incoming long-wave radiation, and formation period duration. It should be noted that total incoming long-wave radiation and formation period duration are effectively auto-correlated because total incoming long-wave radiation is a function of time. The same dataset shows no statistically significant

relationship between thickness and any other variable. The smaller field dataset shows a statistically significant relationship between thickness and maximum air temperature. It also shows a non-statistically significant relationship with a high correlation (0.87) between thickness and total incoming short-wave radiation.

For rain crusts there were only historical data. There were not enough field data collected for rain crusts to create a separate dataset. The historic dataset showed rain crust thickness had statistically significant relationships with precipitation and maximum air temperature. No statistically significant relationships were found for rain crust hand hardness.

While several meteorological variables have been shown to directly influence the resulting crust properties, it is likely that many more variables affect crust properties in conjunction with each other. A surface energy model would likely be required to predict crust properties with any confidence; however, current coupled weather and snowpack models have received little validation for crust formation (Smith, 2009; Bellaire and Jamieson, 2013).

5.1.8 Freezing rain crust formation

Freezing rain occurs when snow or ice particles melt while falling, hit the ground in super-cooled liquid form, and then freeze immediately (Ahrens, 2009). This typically occurs when the snow surface and the air above the surface are well below freezing (Ahrens, 2009). Therefore, this process requires a warm layer in the atmosphere above a cold layer at the surface. The 3 January freezing rain crust was observed to form during a period of temperature inversion as described in the case study in Section 4.1.10.1. The initial crust dataset described in Section 3.2.1 included several crusts that were expected to be freezing rain crusts but it was not possible to determine the formation period with certainty so they were excluded from the subsequent analysis. Freezing rain crusts are often formed over short periods, involve minimal precipitation, and therefore form relatively thin crusts. The methods used to determine the formation period of rain crusts were not adequate for freezing rain crusts. The liquid precipitation involved in the formation of freezing rain crusts is not expected to be great enough to cause the precipitation gauge to consistently show a substantial increase and is often within the margin of error expected from the gauge. Air temperatures are typically

substantially below freezing and therefore are not adequate as a tool for verification as with rain crusts.

The one potential indicator is the radiosonde atmospheric temperature data from the Kelowna airport. In each of the expected cases of freezing rain crust formation there was a layer of warmer air in the atmosphere. This was also the case for all of the eight rain crusts so this variable alone would not be considered adequate for freezing rain crust formation. The Kelowna airport is roughly 200 km southwest of Glacier National Park but is considered the best location for radiosonde data because typical weather systems affecting GNP arrive from the southwest.

5.1.9 Crust formation due to solar radiation and convective heat transfer

Temperature crusts are formed by convective heat transfer. This is often considered a secondary process associated with sun crust formation but can occur on its own. The case study in Section 4.1.10.2 showed how atmospheric warming and convective heat transfer were able to form a temperature crust at our north aspect study site. It is assumed that the sun had not shone directly on the snow surface. The properties of the crust on the South and flat study sites also suggested a contribution of both solar radiation and convective heat transfer in the formation. Based on the hard-soft-hard structure of the crust complex at the south and flat sites, it may be that the incoming short-wave radiation was primarily responsible for the formation of the lower hard layer and convection was primarily responsible for the upper hard layer. Short-wave radiation can penetrate up to 100 mm into the surface of the snowpack (McClung and Schaerer, 2007). On the day with the strongest incoming short-wave radiation, 23 March, the snow surface temperature reached -1.7 °C suggesting that the surface may not have melted initially. On 26 March, the air temperature exceeded 0 °C and the snow surface reached a high of -0.9 °C. While it should have reached closer to 0 °C, it is assumed to be within the margin of error of the sensor. Therefore assuming a threshold of surface melting of -1 °C for the snow surface temperature sensor, it is still possible that the snow surface did not melt on 23 March when the incoming short-wave radiation was the greatest.

Future work distinguishing the contributions of short-wave radiation and convection on crust complexes should focus on the details of snow surface melting. This project primarily focused on crusts following burial and therefore specific details prior to burial were not adequately recorded. Future work should encompass a well calibrated snow surface temperature gauge and a method of estimating the depth of solar radiation penetration beneath the snow surface.

5.1.10 Surface albedo

The case study in Section 4.1.10.2 shows how albedo changes over time during the formation of the 26 March 2012 sun crust complex. Initially during the period of snowfall the mid-day albedo is between 93 % and 95 % which is typical for new snow. Once the initial crust formation occurred on 23 March, the mid-day albedo dropped to 88 %. Over the next three days the albedo dropped to 86 %. With each melt-freeze cycle it is expected that the grain size within the crust increased successively, causing albedo to decrease. As the albedo decreased over subsequent days of sun crust formation, more incoming energy will be absorbed by the snow surface and was available to contribute to the continued formation. Albedo is an important variable for sun crust formation and future work should include regular albedo measurements. An outgoing short-wave radiation sensor should be included in future field work on sun crust formation.

5.2 Crust evolution discussion

Melt-freeze crust evolution data were collected over 2010-11 and 2011-12 winter seasons. Once a crust had formed at any of the study sites, snow pits were dug on a regular basis in order to track changes to the crust layer. Data include density, shear strength, thin-blade resistance, crust indices, and thermal photographs.

5.2.1 Study site selection

Proper site selection is critical to an evolution project. Numerous data were discarded at the early stages of this project due, in hindsight, to spatial variability within the study slopes. Section 3.3.1 describes the methods used for site selection and set-up. While the principles of site selection are described for research applications, they apply directly to operational

settings. Reducing snow pack variability increases confidence in consecutive observations of weak layer evolution.

Many avalanche operations including ski areas, backcountry lodges, and industrial projects utilize a flat study site for taking full snow profiles on a regular basis. These flat site snow profiles are used to track changes to the snowpack over time and these observations form a baseline from which avalanche forecasters can extrapolate data over the terrain at their operation. This is a generally effective method for many types of snow layers but often misses important layers such as sun crusts. As a result, avalanche forecasters typically dig test profiles at other locations in order to determine the stability on various aspects. In order to improve upon these established methods, avalanche operations could establish study sites on south and north aspects in addition to their existing flat site. This allows the direct tracking of weak layers on slopes that better represent the avalanche start zones at their operation. By digging profiles on one uniform study slope for each aspect as opposed to a variety of slopes with different properties, confidence in weak layer evolution can be increased.

5.2.2 Density

Density evolution data was tracked at Mt. Fidelity and Mt. St. Anne for seven crusts. It appears that sun crusts at treeline tend to increase in density over time, even without the introduction of free-water. The RP120228 sun crust density at treeline is the exception and remains almost constant until the presence of free-water was recorded after roughly three weeks. It is assumed that the increase in density of crusts is caused by settlement due to overburden pressure and possibly the deposition of vapour at less permeable layers. The evolution of below treeline rain crusts is less clear and it appears that these crusts can increase or decrease in density over time. This may be related to the evolution process referred to crust disaggregation, which is discussed further is Section 5.2.5. It is important to note that this analysis was based on a small dataset and further crust evolution tracking is required to improve confidence in the findings.

Figure 4.26 compares the range of density values for dry crusts and for crusts which have free-water introduced after melting within the snowpack. It is clear that the addition of free-water increased the density of crust layers. This typically occurred when substantial rainfall or

melting occurred at the surface with subsequent free-water percolation through the snowpack. Water will generally percolate downwards through the soft, permeable snow until it reaches a harder, less permeable crust layer. Once the free-water reaches a crust layer, it tends to run along the crust or within the crust layer. This can also occur when water encounters the boundary of fine grains over coarse grains due to differences in capillary forces (Wankiewicz, 1979). The effects of free-water on a crust layer were easy to recognize. The crust may be undulated at the boundaries and may have varying horizontal hardness and thickness properties. Intermittent or variable ice lens may be present within or above the crust layer. Vertical percolation channels may be attached to the crust or may be observed within the layer above or below the crust.

5.2.3 Shear strength

Shear strength evolution data were collected for four unique crusts. While the data represent the shear strength of the layer directly above the crust rather than the crust itself, it is important to understand how different snow types bond to a crust. It is often the weak layer above or, less commonly, below a crust that creates instability within the snowpack. It is possible for the instability or weakest part of the crust to be internal to the crust but there were no cases of this occurring during the field work for this project. The methods for shear frame test do not allow the testing of the lower interface of a hard crust layer because the weak layer is damaged when the frame is placed. This unfortunately excludes the only case of faceting that was observed during field work because it occurred at the bottom interface of the 3 January 2012 freezing rain crust.

Of the four cases observed, two are classified as persistent weak layers (surface hoar) and two are classified as non-persistent weak layers. From Figure 4.27, it is clear that the non-persistent grain types gain shear strength at a faster rate than the persistent grain types. From these limited data, the non-persistent grain types (0.2 kPa day^{-1}) gain shear strength at an approximate rate 4 times greater than persistent grain types (0.05 kPa day^{-1}). Jamieson (2006) showed the age of a weak layer for various grain types above melt-freeze crusts. Using the median values, surface hoar lasts 5 times longer as a weak layer than precipitation particles (PP)

and decomposed/fragmented particles (DF). Facets (FC) and depth hoar (DH) last almost 8 times longer than PP/DF grain types, and if we assume a linear relationship between age and shear strength, we would expect facets and depth hoar on a crust to have an increase in shear strength of roughly 0.03 kPa day^{-1}.

5.2.4 Thin-blade resistance

Thin-blade resistance proved to be a useful tool for tracking the hardness of a crust. Hand hardness is the industry standard but it tends to be subjective and its usefulness in tracking changes to the hardness of crust layers is limited. Of the 52 observations of crust hand hardness, 47 were at least pencil (P) hardness and 32 were at least knife (K) hardness. At these upper levels of the hand hardness index it was difficult to accurately assess the hand hardness of thin crust layers because the tool tends to slip off the hardest parts such as an ice layer and move towards the less hard areas. By applying the thin-blade vertically through the crust layer, the data were biased in the opposite direction because the most resistance is expected from the hardest part of the layer. For avalanche forecasting, the most interesting parts of a crust are the hardest and the weakest laminations or sub-layers within the crust. The hardest component of a crust represents the layer's ability to bridge stress and also represents the properties of the component of the crust which is likely to persist for the longest within the snowpack. The least hard component of a crust likely represents a weakness within the crust that may have the potential to release avalanches. Any weakness within or adjacent to a crust should become apparent when doing snowpack tests on the layer. Using these new vertical thin-blade methods will represent the hardest part of the crust so it is important that any weaknesses or variability is recorded in the notes.

The original work by Borstad and McClung (2011) showed that as the hand hardness of snow increases, the variability of thin-blade resistance measurements for each class of hand hardness increases. This suggests that the thin-blade resistance will provide greater accuracy when measuring the hardness or resistance of the harder layers compared with the hand hardness test. The data in Figure 4.29 show a similar trend. The distribution of resistance for knife hand hardness has a higher variance than that for pencil hand hardness.

It is unclear how much influence, if any, crust thickness has on thin-blade resistance when applied slope normal. The 3 January 2012 freezing rain crust was the thinnest crust in the dataset, varying between 3 and 4 mm depending on the observation, and all the hand hardness data was knife (K) or knife plus (K+). The distribution of values for the resistance of this crust is similar to the entire dataset in Figure 4.29, with values ranging from 26 N to 52 N. These limited data do not show an effect of thickness on thin-blade resistance measurements applied slope normal.

5.2.5 Crust disaggregation

Crust disaggregation is a termed coined by Smith et al. (2008) used to describe the weakening of a crust without obvious faceting, sometimes called *crust rotting*. The process generally involves a reduction in internal bonding and an increase in grain size and density within the crust, the same as observed for kinetic growth or faceting. The primary differences are the expected temperature gradients during formation and the resulting grain type. Unlike faceting, this process is thought to occur at bulk temperature gradients less than the threshold for kinetic growth (10 °C m^{-1} as measured over 10 cm). While faceting results in large grains with angular corners and square edges, crust disaggregation results in melt forms such as polycrystals or clustered grains. This would also be considered a kinetic growth process because it also results in increased grain size and decreased bonding between grains. This process was only observed by the author at below treeline elevations where the air temperature regularly reached or exceeded 0 °C. There may be a link to availability of free water which would explain why this process was not observed at our treeline study sites but was observed more often at lower elevations. It is possible that typical faceting is occurring at the same time as another process which is depositing moisture more evenly across the grain.

Jamieson (2006) describes cases of crusts faceting at temperatures a few degrees below freezing in the Coast Mountains of North America. The description sounds similar to what is described above. A possible explanation for the faceting within crusts near the freezing point is that below crust faceting and above crust faceting are occurring at the same time (Jamieson, 2006).

It is believed that the Blue River 5 March 2012 rain crust underwent crust disaggregation at the flat study site at 1405 m elevation. The crust saw a decrease in thin-blade resistance, an increase in density, and a small decrease in the internal lamination index. Unfortunately this dataset was limited to three observations made over 15 days and therefore is subject to greater uncertainty than other crusts with more observations.

This is a topic which requires more study. It appears that some crusts at lower elevations undergo this process while other crusts do not. The primary focus of this project was dry crusts at treeline elevation so a focus on lower elevations or warmer sites may achieve different results.

5.2.6 Crust indices

The crust indices were developed as a simple, consistent method for describing the properties of melt-freeze crusts using the basic tools carried by an avalanche technician. Both crust indices, the interface bonding index and the internal lamination index, are qualitative, whereas similar physical properties such as shear strength and thin-blade resistance are quantitative and therefore require more time and specialized tools. The interface bonding index is a proxy for shear strength and can be applied at the lower boundary which is impractical for the shear frame test. The internal lamination index can be a proxy for slope-normal thin-blade resistance when discussing the hardest part of a crust layer, or may also be used to describe a weak lamination within a crust that may be related to potential avalanche instability. It is recommended that both types of internal lamination data be recorded when applicable. The index proved easy to use in the field and was a relatively quick observation when compared with other tools used in this project. The drawbacks are similar to those of the hand hardness test including subjectivity amongst observers and inability to track small scale changes over short time periods. It did prove to be useful in tracking changes over longer periods of time once several observations had been made.

The crust bonding index correlated with the shear strength at the upper crust interface (Figure 4.31). The class 3 is under-represented compared with 2 and 4. 1 and 5 are intended to represent the extremes and therefore the frequency is expected to be lower. Table 5.1

attempts to improve the definitions in order to provide a more even distribution of values when compared against shear strength. This involved widening the definitions of class 3 and narrowing the definitions for classes 2 and 4.

The crust lamination index did a good job representing the thin-blade resistance of crusts as shown in Figure 4.35. However, crust lamination class 4 had a wider distribution of resistance values than the other classes. Also, the bottom end of the class 4 distribution had lower values of resistance than expected. The crust lamination class 1 was not represented and the class 2 was under-represented. This may be due to the nature of the research because we were mainly interested in crusts that we could easily test. Some of the weaker, or less laminated crusts, were omitted from the data collection process. Following use of the index in the field, it became apparent that the definitions can use improvement. Table 5.2 contains suggested changes to the definitions of the crust lamination index.

Table 5.1*: Suggested definition changes to the Crust Bonding Index. Changes to the definitions are underlined*

Class	Description
1	Little to no bonding between layers; clean separation with minimal shear force input
2	Poorly bonded; separates easily <u>in a planar fashion</u>; <u>sudden fracture character type may occur with light pressure</u>; light brushing may be required to isolate crust layer
3	Moderate bonding; <u>planar separation possible</u>, <u>sudden fracture character type may occur with hard pressure;</u> may require hard brushing or light scraping to isolate crust layer
4	Well bonded; <u>may be difficult to get planar separation</u>; requires <u>moderate to hard</u> scraping to isolate crust layer
5	Very well bonded; difficult to separate layers; requires a saw cut or <u>very</u> hard scraping to isolate crust layer

***Table 5.2**: Suggested definition changes to the Crust Lamination Index. Changes to the definitions are underlined*

Class	Description
1	Little to no bonding between grains; very difficult or not possible to handle without breaking / crumbling.
2	Bonds between individual ice grains are discernible, but not strong or extensive. Difficult but possible to isolate a block. Sample crumbles easily and tends to break into individual grains or small clustered grains.
3	Bonding between individual ice grains is moderate. Bonds are discernible and hold the sample together during isolation and handling. Sample tends to break into small pieces or crumble into large clustered grains
4	Well bonded. Sample has strong bonding between individual ice grains. Sample easily maintains shape with handling and cutting. Sample has a tendency to break into large pieces which may have well defined, linear edges.
5	Sample is almost completely bonded. Bonds and grains are difficult to discern as the sample is nearly uniform. Pure ice would be 5+ as it would be entirely bonded. Sample does not crumble, but rather breaks cleanly

During field observations, observers began to use mid-values of the indices (1.5, 2.5, 3.5, and 4.5) in to be more specific with their observations and to increase the number of classifications for the index. This is similar to what happened with the hand hardness index and the avalanche size classifications. Because values 1 and 5 are intended to be extremes and are less likely to be observed during typical conditions, this limits the typical values to three levels. By adding half classifications, we can increase the number of classification values without changing the definitions. In order to use a half-classification, the crust bonding or lamination characteristics should fall between the upper and lower classification.

5.2.7 Thermal evolution

There are several topics of discussion for thermal evolution resulting from use of a thermal imager and therefore this section is divided into five parts.

5.2.7.1 Factors influencing temperature gradients

There are several factors that were expected to influence the temperature gradient around a melt-freeze crust. These factors can be divided into two broad groups including general factors influencing temperature gradients within a typical snowpack and factors specific to temperature gradients around melt-freeze crusts. General factors influencing temperature gradients within the snowpack include total snow depth, layer depth within the snowpack, time of day, snow surface temperature, and rate of change of snow surface temperature. Crust specific factors include density or permeability difference between crust and surrounding snow (Adams and Brown, 1983; Colbeck, 1991), difference in thermal properties of the crust and surrounding snow (Sturm et al., 1997), and difference in grain properties of the crust and surrounding snow (Shea et al., 2012), as well as the NP_Ta effect associated with hardness changes. At this point it is unknown how much each of these factors influences the temperature gradients around melt-freeze crusts.

The temperature gradients initially measured from the RP120103 freezing rain crust were the largest recorded during the project with values exceeding 200 °C m^{-1}. This contrasts to the RP120209 and RP120228 crusts which initially had temperature gradients around 20 °C m^{-1}, or an order of magnitude less. The low permeability of the RP120103 crust likely contributed to the strong temperature gradients initially observed. The low permeability could affect the temperature gradient due to the latent heat flux caused by net water vapour being deposited at the lower interface and/or departing the upper interface (Colbeck, 1991; Greene, 2007). Both the RP120209 and RP120228 crusts were observed to have higher permeability and therefore water vapour may move freely through the crusts, reducing net deposition and departure of water vapour at the crust interface.

5.2.7.2 Thermal evolution of RP120103 freezing rain crust

The evolution of the RP120103 crust showed a continuous decrease in the average upper temperature gradient over time. This general decrease is anticipated because over time the crust was buried deeper within the snowpack and two general changes are expected as a crust becomes buried deeper in the snowpack. First, as the crust becomes deeper in the snowpack, physical properties of the crust including density and hardness become closer to the properties of the surrounding snow. Second, atmospheric influences at the surface are expected to have less effect on the temperature gradient around a crust as it is buried deeper. Both of these points are discussed further below. Between 16 January and 19 January 2012 the RP 120103 crust underwent faceting at the lower interface. During this period the air temperatures reached a low of -26.1°C at the Mt. Fidelity weather station. The lower 2 mm of the 4 mm crust faceted while the top 2 mm appeared relatively unchanged. While thermal photos and temperature gradients were not available during the period of active faceting, it is assumed that the temperature gradient at the lower interface was greater than the values measured on 16 January and 19 January 2012. Between 16 and 19 January 2012 the average lower temperature gradient increased relative to itself and relative to the upper temperature gradient. This increase in the lower temperature gradient relative to the upper temperature gradient likely contributed to the faceting that occurred. Jamieson (2006) explains that faceting can occur below a buried melt-freeze crust at temperature gradients less than the typical threshold bulk temperature gradient for faceting of 10 °C m^{-1} (as measured over 10 cm) whereas the same temperature gradient above the crust will not resulting in faceting.

5.2.7.3 Thermal evolution of RP120209 sun crust

The RP120209 sun crust was initially observed to have a small average upper temperature gradient shortly after burial. While the median temperature gradients remain low, there were two spikes in the temperature gradients as observed in Figure 4.38. The two spikes in upper temperature gradient correlated to substantial drops in the air temperature at Mt. Fidelity. The second spike on 27 February 2012 occurred when the crust was buried 81 cm below the surface. A third substantial drop in air temperature occurred on 6 March 2012 which was

comparable to the first drop in air temperature on 14 February. In this instance, the RP130209 crust did not show an increase in the average temperature gradients from the previous observation. At that point the crust was buried 145 cm below the surface. It is expected that as the crust was buried deeper in the snowpack, the air temperature required to influence the temperature gradients at the crust would have to be increasingly lower. In this case, by 6 March 2012 a drop in the daily mean air temperature to -11 °C was not adequate to influence the temperature gradients of the crust at 145 cm depth. In contrast, also on 6 March 2012, there was a noticeable increase in the average upper temperature gradient of the RP120228 sun crust compared with the previous and subsequent observations as seen in Figure 4.39. At this point the crust was buried 88 cm below the surface. The RP120103 freezing rain crust also showed no substantial increases in temperature gradients related to decreases in air temperature following the observation on 16 January in which the crust was buried 77 cm.

5.2.7.4 Temperature gradients and air temperature

There are two possible explanations for the observed relationship between decreased air temperatures, increased temperature gradients, and crust burial depth, but it likely a combination of both. First, the NP_Ta effect creates artificial temperature gradients around crusts in thermal images during periods of low air temperatures as described above. As the crust is buried deeper in the snowpack two conditions change which would reduce the NP_Ta effect; the hardness of the crust and the surrounding snow become closer to each other making it easier to reduce concavities around the crust and produce a planar pit wall, and the pore space of the crust and the surrounding snow become more similar which reduces the small scale NP_Ta effect at the boundary. Second, low air temperatures result in an increased bulk temperature gradient through the snowpack which is expected to result in increased natural small-scale temperature gradients around melt-freeze crusts.

The crust thermal gradient data was combined with air, crust, and snow temperature data in order to assess the relationships between these variables. Table 4.7 shows the resulting Spearman correlation matrix. The crust temperature gradients had the strongest relationship with the air temperature but are also correlated to the crust and snow temperatures. Because

the crust and snow temperatures were taken from the thermal photos as opposed to measured using thermometers inserted at least 10 cm into the pit wall, the subsequent analysis was done using measured air temperature. There is a strong correlation between air temperature and snow/crust temperatures so this proxy method is considered applicable.

Using 1 m burial depth as a threshold, two sub-groups were created. The crust temperature gradients were compared with the observed air temperature for each sub-group and the Spearman correlation values for each case are presented in Table 4.8. The group for *Depth < 100 cm* had stronger correlations than the complete dataset. For *Depth > 100 cm* the correlations were less and the p-values were no longer significant. Based on these data, it appears that temperature gradients may be a function of air temperature for crusts buried less than 1 m in the snowpack.

5.2.7.5 Natural and artificial temperature gradients

Schirmer and Jamieson (in press) investigated artificial temperature gradients created in thermal photographs by concavities and convexities. Because of the hard, dense nature of melt-freeze crusts, there will inherently be concavities along the length of a crust after snow pit evacuation is completed. Schirmer and Jamieson (in press) showed that artificial concavities made in the snowpack will create artificially stronger temperature gradients in thermal images that would not exist on a planar snow wall. Based on this new research, it is assumed that part of each temperature gradient calculated during the analysis has a component of artificial gradient and a component of natural gradient. At this point it is unknown how much of each component makes up the total temperature gradient. In the future, it would be interesting to combine the two research topics by creating artificial concavities in the snowpack adjacent to natural melt-freeze crusts. If the artificial concavity was created with similar dimensions (depth and thickness) to the melt-freeze crust, than the proportion of artificial gradient could be calculated. At this point we consider the artificial contribution to be part of the overall sources of error which is already assumed to be substantial.

Schirmer and Jamieson (in press) also suggest that the difference between the crust or snow temperature and the air temperature should also affect the apparent temperature gradient

observed with the thermal imager. A larger difference in these temperatures is expected to have a stronger influence on temperature gradients. The data in Table 4.7 show that there is some positive correlation between the variables $\Delta T_{(cr\text{-}air)}$ and $\Delta T_{(sn\text{-}air)}$, and the temperature gradients ($|\nabla T_{Upper}|$ and $|\nabla T_{Lower}|$) at the crust. While the influence of these variables on crust temperature gradients is becoming better understood, it appears to be less than the influence of the actual air temperature in affecting the temperature gradients around a crust, especially when the crust buried less than 1 m. While we do not know how much of role each process contributes, it seems safe to assume that they both play a role in influencing the apparent temperature gradients around a melt-freeze crust in thermal images.

CHAPTER SIX: CONCLUSIONS

This thesis presented research on the formation and evolution of melt-freeze crusts. Historic weather and snow profile data were used to create a dataset of crust formation events. Field data were collected over two winters to track changes to crust properties over time. The finding of each of these topics is presented in the following sections along with a section on recommendations for future research.

One of the main outcomes of this project was the establishment of several new methods for observing and measuring the properties of melt-freeze crusts. Many of the datasets are small and therefore the results may be uncertain. However, with the new methods now established, future research may decrease the uncertainty of these results with increased datasets. These methods could also be applied to different geographic regions to test the reliance of these results on snow climate.

6.1 Crust formation

The objective of crust formation was to better quantify the meteorological conditions during formation of rain and sun crusts using field data. These data may be useful for the validation and refinement of snowpack models. The focus of this section was on the melting of the snow surface and did not specifically address the process of refreezing. Several meteorological variables show promise as indicators of crust formation. The resulting properties of crusts (thickness and hand hardness) were coupled with meteorological variables to determine their dependency.

For rain crusts, the following findings were relevant:

- Formation period: typically short periods (< 1 day) associated with discrete rain events;
- Aspect: generally form on all aspects but the data showed a slight preference for south slopes which was likely due to wind during formation;
- Air temperature: the lowest value of maximum air temperature was -0.4 °C and agrees with the threshold value of -0.5 °C for rain crust formation in the Columbia Mountains used by Bellaire (2013);

- Incoming short-wave radiation (ISWR): the typical values of ISWR for rain crust formation are roughly 2-4 times less than the typical values for sun crust formation, depending on the time of year; and
- Incoming long-wave radiation (ILWR) and sky cover: the coupled dataset of ILWR and sky cover showed that rain crusts typically form under overcast conditions but occasional periods of broken sky cover occurred.

For sun crusts, the following findings were relevant:

- Formation period: length of formation period varied from less than one day to 12 days. Typical values of two to six days;
- Aspect: formed primarily on south aspects but have the potential to form on all aspects including north. It is speculated that the crusts on north aspects were actually formed by convective heat transfer that coincided with periods of strong ISWR;
- Air temperature: did not appear to have directly influenced sun crust formation but likely contributed to convective heat transfer which may indirectly have contributed to sun crust formation;
- Incoming short-wave radiation: varied with time of year due to solar insolation. ISWR alone does not determine sun crust formation but may be used as an indicator variable; and
- Incoming long-wave radiation and sky cover: due to the long overall formation periods, it was assumed that minimum ILWR was representative of the periods of melting. The coupled dataset of minimum ILWR and sky cover showed that sun crusts formed under clear, few, or scattered sky cover, depending on the time of year. In December through mid-February, the sky cover during formation was typically clear. In November and mid-February through to the end of the observation period (mid-March), the sky cover during formation was typically clear or few, with a few cases of scattered sky cover.

Two crust properties, thickness and hand hardness, were obtained from the historic snow profiles and coupled with the historic meteorological data. While there is increased uncertainty with this dataset, there are statistically significantly relationships between rain crust thickness

and precipitation, and rain crust thickness and maximum air temperature. No statistically significant relationships were found for rain crust hand hardness. There are statistically significant increasing relationships between sun crust hand hardness and three variables: total incoming short-wave radiation, total incoming long-wave radiation, and formation period duration. Using a smaller dataset of sun crust thickness collected during field work for this project, there is a statistically significant increasing relationship between sun crust thickness and maximum air temperature. The smaller dataset also showed a non-statistically significant increasing relationship with a high correlation (0.87) between sun crust thickness and total incoming short-wave radiation.

Two cases studies were presented to illustrate important principles that were not evident from the meteorological data. The first shows that freezing rain crust formation occurred during a temperature inversion. The second case study shows the how convective heat transfer can be related to sun crust formation and also how convective heat transfer can form temperature crusts.

6.2 Crust evolution

The objectives of crust evolution were to collect field measurements of the evolution of crust properties following burial and to apply new methods to improve crust evolution tracking. The physical properties measured include density, shear strength, and resistance. A thermal imager was used to measure small-scale temperature gradients around crusts. The new crust indices were also introduced as a simple method of tracking changes to crusts over time.

Dry crusts (excludes data following the observation of free-water) at treeline elevation showed a progressive increase in density over time, likely caused by settlement due to overburden pressure and possibly the deposition of water vapour at less permeable layers. Once free-water was observed at these crusts, the density increased substantially, typically from around 300 kg m^{-3} to around 500 kg m^{-3}.

Shear strength at the upper interface of crusts changes at a rate of about 0.2 kPa day^{-1} for non-persistent grain types and about 0.05 kPa day^{-1} for surface hoar.

Thin-blade methods established by Borstad and McClung (2011) were modified for use with crusts. The vertical thin-blade resistance typically increased over time for crusts at treeline elevation.

Recent work by Schirmer and Jamieson (in press) has shown how non-planar effects create artificial temperature gradients around crusts when observed by a thermal imager. This has increased the uncertainty associated with the thermal image data collected for this project. However, it still appears that substantial decreases in air temperature cause increases in temperature gradients around crusts while they are in the upper 1 m of the snowpack. Of the three crusts tracked, the thin, impermeable freezing rain crust showed the largest temperature gradients. The initial temperature gradients near this crust were roughly ten times the magnitude of the gradients near two more permeable sun crusts, and this impermeability is the expected cause.

The crust indices proved to be a simple and useful tool for tracking changes to crusts. The crust interface bonding index is related to shear strength, grain type, and compression test fracture character. Initial data shows that the crust lamination index is related to thin-blade resistance but not to density. Based on the initial use during the winter of 2011-12, improved definitions were provided for the indices (Section 5.2.6).

6.3 Recommendation for further research

The potential for future research in crust formation and evolution is vast. Some examples were mentioned in the discussion chapter include increasing the size of under-represented datasets, investigating the crust disaggregation process by tracking crust evolution at valley bottom elevations, and quantifying the contributions natural and artificial temperature gradients due to non-planar temperature effects associated with the use of thermal imaging. Some other possible topics are discussed below.

It may be possible to create a simple surface energy model for crust formation based on the SWARM model, which models expected daily increases in the snow temperature 10 cm below the snow surface based on absorbed short-wave radiation (Bakermans, 2006). This may require

assumptions about the snow surface temperature at the beginning of the day, which may be possible using overnight air temperature and long-wave radiation data.

The relationship between meteorological conditions during crust formation and the resulting properties is a topic which needs improvement. Using historical data creates excessive uncertainty and, therefore, the collection of field data may be required. In order to create an adequate size dataset, several years of data should be collected or the geographic study area should be increased.

An important topic for future work is to link the properties of melt-freeze crusts to avalanche activity. This should be possible using a dataset of reported avalanche activity such as the CAA InfoEx database. This relies on the consistent recording of layer identification by the reporting operations. It may also be possible to relate crust properties to a database of snowpack stability or avalanche hazard from a local operation. Crust properties which may be related to weak layer stability may include shear strength, resistance, crust indices, and thermal properties. This may prove useful in improving forecasting for avalanches that release on melt-freeze crusts.

Another potentially interesting area of melt-freeze crust research is the investigation of thermal properties such as thermal conductivity and heat capacity, and the relationship to temperature gradients. Smith (in prep) measured changes to the thermal conductivity of melt-freeze crusts over time. It would be interesting to repeat this research with the use of a thermal imager to measure small scale temperature gradients, although Schirmer and Jamieson (in press) have identified challenges with using thermal imaging on snow pit walls. There is likely a strong relationship between the thermal properties and permeability of crusts and the resulting temperature gradients. This is expected to be important to crust evolution and near-crust faceting. Research would likely involve both field studies and cold-lab work. In the field, it would be possible to measure the thermal properties of the snow layers and the resulting temperature gradients over time in a natural state. In the cold lab, it would be possible to simulate a variety of thermal conditions and measure the resulting temperature gradients. In

the cold lab, it would be interesting to test the difference in evolution between an impermeable crust and a permeable crust, under similar conditions.

REFERENCES

Adams, E. E. and Brown, R. L., 1983. Metamorphism of dry snow as a result of temperature gradient and vapor density differences. Annals of Glaciology, 4, 1–9

Ahrens, C. D., 2009. Meteorology today: an introduction to weather, climate, and the environment. 9th edn. Brooks Cole, Belmont, CA.

Atwater, M. M., 1954. Snow avalanches. Scientific American, 190, 26-31.

Bartelt, P. B. and Lehning, M., 2002. A physical SNOWPACK model for the Swiss avalanche warning, Part I: numerical model. Cold Regions Science and Technology, 35, 123–145.

Bakermans, L., 2006. Near-surface snow temperature changes over terrain. MSc thesis, University of Calgary, Calgary, AB.

Bellaire, S. and Jamieson, B., 2013. Forecasting the formation of critical snow layers using a coupled snow cover and weather model. Cold Regions Science and Technology, 94, 37-44.

Birkeland, K. W., 1998. Terminology and predominant processes associated with the formation of weak layers of near-surface faceted crystals in the mountain snowpack. Arctic and Alpine Research, 30, 193-199.

Borstad, C. P. and McClung, D.M., 2011. Thin-blade penetration resistance and snow strength. Journal of Glaciology, 57, 325-336.

Camponovo, C. and Schweizer, J., 1997. Measurements on skier triggering. Proceedings International Snow Science Workshop, Banff, AB, 100-103.

Campbell, C., Bakermans, L., Jamieson, B., and Stethem, C., 2007. Current and future snow avalanche threats and mitigation measures in Canada. Canadian Avalanche Centre, Revelstoke, BC

Campbell, C., Jamieson, B., and Hägeli, P., 2004. Small-scale mapping of snow stability: If not, why not. Avalanche News, Canadian Avalanche Association, Revelstoke, BC, 71, 45–49.

Campbell Scientific, 2013. SR50A Sonic Ranging Sensor Instruction Manual. https://s.campbellsci.com/documents/ca/manuals/sr50a_man.pdf

Canadian Avalanche Association (CAA), 2007. Observation Guidelines and Recording Standards for Weather, Snowpack, and Avalanche. Canadian Avalanche Association, Revelstoke, BC.

Church, J. E., 1913. Recent studies of snow in the United States. Royal Meteorological Society, Quarterly Journal, January, 43-52.

Colbeck, S. C. 1983. Theory of metamorphism of dry snow. Journal of Geophysical Research, 88, 5475-5482.

Colbeck, S.C., 1991. The layered character of snow covers. Review of Geophysics, 29, 81-96.

Delparte, D., 2008. Avalanche Terrain Modeling in Glacier National Park, Canada. Ph. D. Thesis, University of Calgary, Calgary, AB.

Durand, Y., Giraud, G., Brun, E., Mérindol, L., and Martin, E., 1999. A computer-based system simulating snowpack structures as a tool for regional avalanche forecasting. Journal of Glaciology, 45, 469–484.

Fierz, C., Armstrong, R. L., Durand, Y., Etchevers, P., Greene, E., McClung, D. M., Nishimura, K., Satyawali, P. K., and Sokratov, S. A., 2009. The international classification for seasonal snow on the ground. Tech. Doc. Hydrol. 83, Int. Hydrol. Programme, U.N. Educ., Sci. and Cult. Organ., Paris.

Fukuzawa, T. and Akitaya, E., 1993. Depth-hoar crystal growth in the surface layer under high temperature gradient. Annals of Glaciology, 18, 39-45.

Gauthier, D., 2007. A practical field test for fracture propagation and arrest in weak snowpack layers in relation to slab avalanche release. Ph.D. thesis, University of Calgary, Calgary, AB.

Greene, E., 2007. The Thermophysical and Microstructural Effects of an Artificial Ice Layer in Natural Snow Under Kinetic Growth Metamorphism. Ph.D. Thesis, Colorado State University, Fort Collins, Colorado.

Habermann, M., Schweizer, J., and Jamieson, B.J., 2008. Influence of snowpack layering on human-triggered snow slab avalanche release. Cold Regions Science and Technology, 54, 176– 182.

Haegeli, P. and McClung, D.M., 2003. Avalanche characteristics of a transitional snow climate – Columbia Mountains, British Columbia, Canada. Cold Regions Science and Technology, 37, 255–276.

Haegeli, P. and McClung, D. M., 2007. Expanding the snow climate classification with avalanche-relevant information: initial description of avalanche winter regimes for southwestern Canada. Journal of Glaciology, 53, 266–276.

Horton, R.E., 1915. The melting of snow. Monthly Weather Review, 43, 599-605

Horton, S., Bellaire, S., and Jamieson, B., 2012. Modelling surface hoar formation and evolution on mountain slopes. Proceedings International Snow Science Workshop, Anchorage, AK.

Jamieson, B., 2001. Snow avalanches. A Synthesis of Geological Hazards in Canada. 548, 81-100.

Jamieson, B., 2004 (a). Between a slab and a hard layer: Part 1— Formation of poorly bonded crusts in the Columbia Mountains. Avalanche News, 70, 48–54.

Jamieson, B., 2004 (b). Between a slab and a hard layer: Part 2— The persistence of poorly bonded crusts in the Columbia Mountains. Avalanche News, Canadian Avalanche Association, 71, 34–37.

Jamieson, B., 2006. Formation of refrozen snowpack layers and their role in slab avalanche release. Review of Geophysics, 44, RG2001.

Jamieson, B. and Geldsetzer, T., 1996. Avalanche Accidents in Canada, Volume 4 1984 – 1996. Canadian Avalanche Association, Revelstoke, BC.

Jamieson, B., Geldsetzer, T., and Stethem, C., 2001. Forecasting for deep slab avalanches. Cold Regions Science and Technology, 33, 275 –290.

Jamieson, J.B. and Johnston, C.D., 1997. The facet layer of November 1996. Avalanche News, Canadian Avalanche Association, 52, 10-15.

Jamieson, J.B. and Johnston, C.D., 2001. Evaluation of the shear frame test for weak snowpack layers. Annals of Glaciology, 32, 59-68.

Jamieson, B., and Langevin, P., 2004. Between a slab and a hard layer: Part 3—Two field studies of facets growing above wet layers. Avalanche News, Canadian Avalanche Association, 72, 48–51.

Jamieson, J.B. and van Herwijnen, A., 2002. Preliminary results from controlled experiments on the growth of faceted crystals above a wet snow layer. Proceedings International Snow Science Workshop, Penticton, BC.

LaChapelle, E.R, 1980. The fundamental processes in conventional avalanche forecasting. Journal of Glaciology, 26, 75-84.

Lehning, M., Bartelt, P., Brown, B., Fierz, C., and Satyawali, P., 2002 (a). A physical SNOWPACK model for the Swiss avalanche warning: Part II. Snow Microstructure. Cold Regions Science and Technology, 35, 147–167.

Lehning, M., Bartelt, P., Brown, B., and Fierz, C., 2002 (b). A physical SNOWPACK model for the Swiss avalanche warning: Part III. Meteorological forcing, thin layer formation and evaluation. Cold Regions Science and Technology, 35, 169–184.

McClung, D. and Schaerer, P., 2006. The Avalanche Handbook. The Mountaineers Books, Seattle, Washington.

Mailhot, J., Bélair, S., Lefaivre, L., Bilodeau, B., Desgagné, M., Girard, C., Glazer, A., Leduc, A. M., Méthot, A., Patoine, A., and others, 2006. The 15-km version of the Canadian regional forecast system. Atmosphere-Ocean, Taylor & Francis, 44, 133-149.

Marshall, S., 2012. The Cryosphere. Princeton Primers in Climate, Princeton University Press, Princeton, New Jersey.

Moore, M., 1982. Temperature gradient weakening of snowpacks near rain crusts or melt-freeze layers. Presented at the 1982 International Snow Science Workshop in Bozeman, Montana. Unpublished.

Ross, C., 2010. Testing fracture propagation propensity for slab avalanche forecasting. MSc thesis, University of Calgary, Calgary, AB.

Schirmer, M. and Jamieson, B., 2013 (in preparation). Limitations of an Infrared Camera to Measure Snow Pit-Wall Temperatures

Schweizer, J., 1993. The influence of the layered character of snow cover on the triggering of slab avalanches. Annals of Glaciology, 18, 193-198.

Schweizer, J. and Jamieson, B., 2007. A threshold sum approach to stability evaluation of manual snow profiles. Cold Regions Science and Technology, 47, 50-59.

Schweizer, J., Jamieson, B., and Schneebeli, M., 2003. Snow avalanche formation. Review of Geophysics, 41.

Schweizer, J. and Kronholm, K., 2007. Snow cover spatial variability at multiple scales: characteristics of a layer of buried surface hoar. Cold Regions Science and Technology, 47, 207-223.

Schweizer, J., Kronholm, K., Jamieson, J.B., and Birkeland, K.W., 2008. Review of spatial variability of snowpack properties and its importance for avalanche formation. Cold Regions Science and Technology, 51, 253–272.

Seligman, G., 1936. Snow Structures and Ski Fields. MacMillan and Co., London, UK.

Shea, C. and Jamieson, B., 2011. Some fundamentals of handheld snow surface thermography. The Cryosphere, 5, 55–66.

Shea, C., Jamieson, B., and Birkeland, K., 2012. Use of a thermal imager for snow pit temperatures. The Cryosphere, 6, 287-299.

Smith, M., in preparation. Tracking changes in buried melt freeze crusts in the seasonal snowpack. Ph.D. thesis, University of Calgary, Calgary, AB.

Smith, M., Jamieson, B., and Fierz, C., 2008. Observation and modeling of a buried melt-freeze crust. 2008 International Snow Science Workshop, Whistler, B.C., 170– 178.

Smith, M. and Jamieson, B., 2009. Tracking changes in buried melt freeze crusts. International Snow Science Workshop, Davos, Switzerland.

Smith, M. and Jamieson, B., 2010. Near-infrared photography to quantify temporal changes in melt-freeze crusts. International Snow Science Workshop, Squaw Valley, California, 409-414.

Sommerfeld, R. A., 1984. Instructions for using the 250 cm^2 shear frame to evaluate the strength of a buried snow surface. USDA Forest Service Research Note, Fort Collins, Colorado, RM-446.

Stull, R. B., 2000. Meteorology for Scientists and Engineers, Second Edition. Brooks/Cole, Pacific Grove, CA.

Sturm, M., Holmgren, J., nig, M., and Morris, K., 1997. The thermal conductivity of seasonal snow. Journal of Glaciology. 43, 26–42.

van Herwijnen, A. and Jamieson, J.B., 2007. Fracture character in compression tests. Cold Regions Science and Technology, 47, 60-68.

Wankiewicz, A., 1979. A review of water movement in snow. Modeling of Snow Cover Runoff. U.S. Army Cold Regions Research and Engineering Laboratory, Hanover, NH, 222–252.

APPENDIX A: 2011-12 crust evolution field book page

Crust Observations					
Crust ID:	CR Type:		Loc. Name:		
Opr		Latitude			
Date *yymmdd*		Longitude			
Time *2400*		Map datum			
Elev. Band	A T BT	Aspect (°)			
Elev. (m)		Slope Angle (°)			
$T_{present}$ (°C)		Pcp type/rate	nil R S RS G ZR ___		
Sky	○◔◑◍⊕⊗	$Wind_{site}$ Spd/Dir	C L M S X ___		
$Depth_{Top}$ (cm)	T ↕ (mm)	1	2	3	
Grain F/E↑	1	2	HH↑		
Grain F/E CR	1	2	HH CR		
Grain F/E↓	1	2	HH↓		
ρ_{calc} block size (cm^3)		ρ_{calc} wt (g)			
ρ_{calc} block size (cm^3)		ρ_{calc} wt (g)			
ρ_{calc} block size (cm^3)		ρ_{calc} wt (g)			
Push gauge result (kg)	1	2	3	4	5	6
Gauge capacity (kg)		7	8	9	10	
Disc type/size (cm^2)		11	12	13	14	
CT_1 Score / Char / depth(cm)*		SP SC PC RP BRK			
CT_2 Score / Char / depth(cm)*		SP SC PC RP BRK			
CT_3 Score / Char / depth(cm)*		SP SC PC RP BRK			
DH_1 score (cm)/Char/depth(cm)*		SP SC PC RP BRK			
DH_2 score (cm)/Char/depth(cm)*		SP SC PC RP BRK			
DH_3 score (cm)/Char/depth(cm)*		SP SC PC RP BRK			
Strong/weak lamination	1 2 3 4 5				
Bonding to upper layer	1 2 3 4 5				
Bonding to lower layer	1 2 3 4 5				
Uniform Vertically?	Y N _____				
Uniform Horizontally?	Y N _____				
Well defined upper boundary, planer?	Y N _____				
Well defined lower boundary, planer?	Y N _____				
Near Crust Faceting?	Y N _____				
Ice Lens?	N cont int top mid bot planer n. planer				
*depth propotional to crust depth					

APPENDIX B: Parks Canada Avalanche Control Section snow profile example

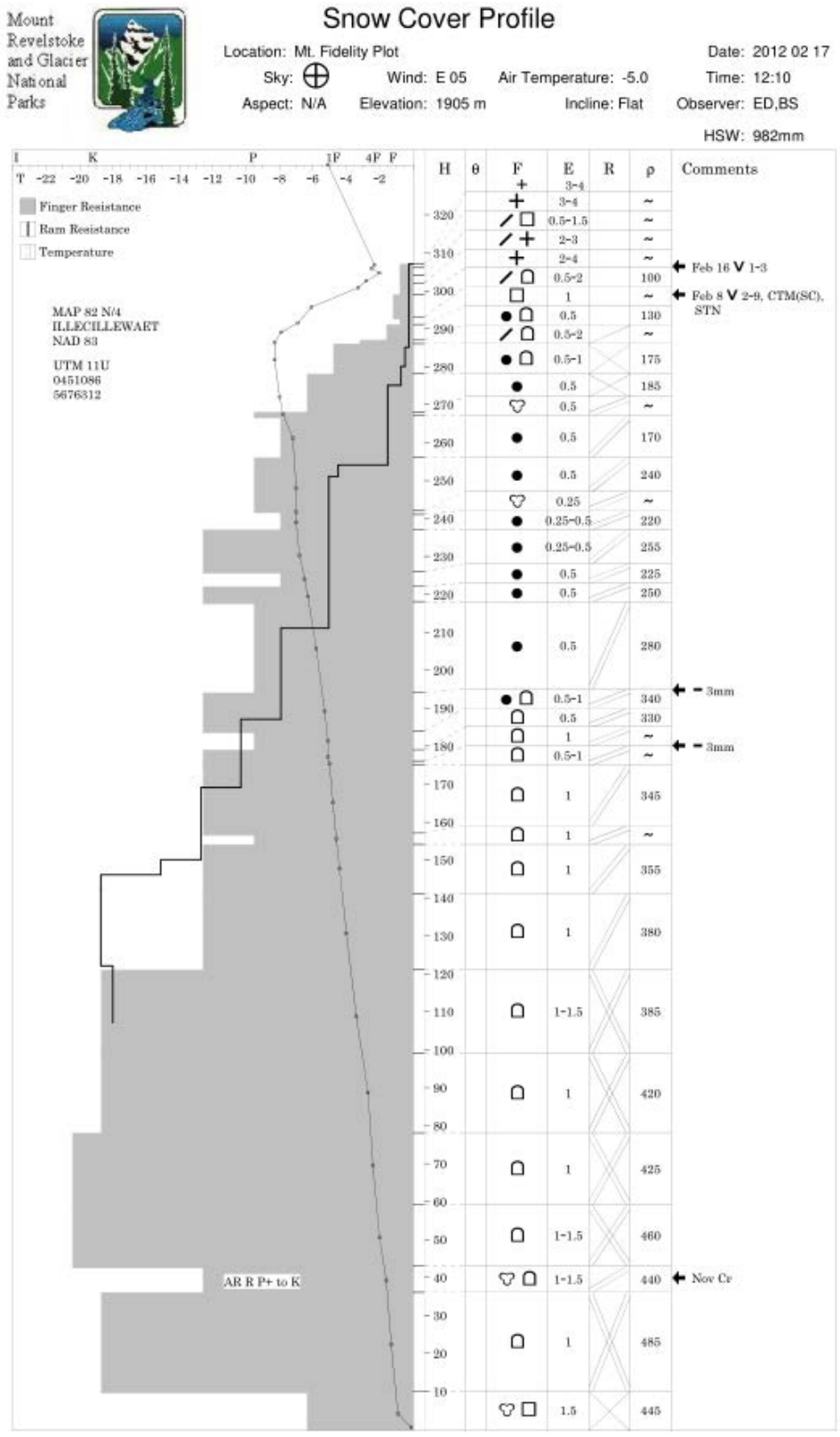

APPENDIX C: University of Calgary snow profile example